Lectures on nonlinear finite element analysis of concrete shells

Eugenio Oñate

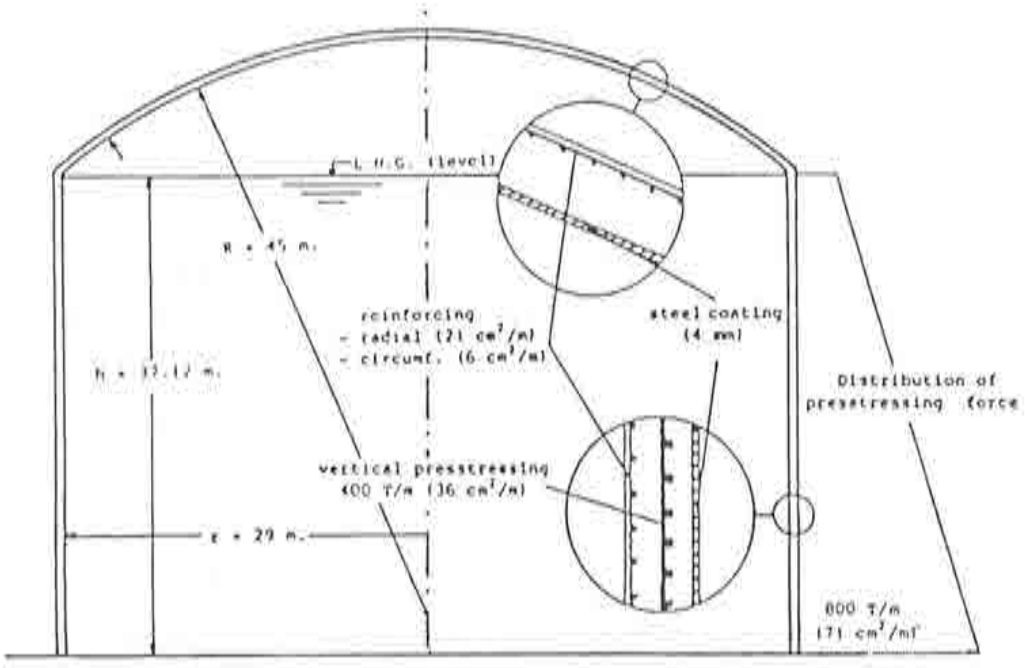

Monografía CIMNE Nº 7, Febrero 1992

INDEX

pag.

INTRODUCTION

Lecture 1: CONCRETE SHELLS. BASIC FINITE ELEMENT FORMULATION 1

Summary 1
Introduction 1
Formulation of flat shell elements for analysis of reinforced concrete shells 3
Formulation of curved degenerate shell elements for analysis of reinforced concrete shells 15
The inclusion of non linear behaviour 24
Nonlinear finite element solution 29
References 33

Lecture 2: MATERIAL MODELLING OF CONCRETE AND STEEL FOR ANALYSIS OR REINFORCED/PRESTRESSED CONCRETE SHELLS 37

Summary 37
Introduction 37
Elasto-plastic-brittle concrete model 38
A plastic damage model for nonlinear analysis of concrete 47
Definition of the yield surface 51
Evolution law for the internal friction angle ϕ 56
Plastic potential function and dilatancy angle ψ 57
Behaviour of reinforcing steel in tension and compression 61
References 61

Lecture 3: STIFFENED SHELLS. MODELLING OF ECCENTRIC BEAM STIFFENERS 65

Summary 65
Introduction 65
Curved Timoshenko beam elements 66
Formulation of eccentric beam stiffener elements 73
Non linear analysis of shells with eccentric beam stiffness 77
References 79

Lecture 4: SOME EXAMPLES OF FINITE ELEMENT NON LINEAR ANALYSIS OF CONCRETE SHELLS 81

Summary 81
Example 1. Bending test of a simple supported notched beam under central point load (Fracture mode I) 81
Example 2. Analysis of a notched beam (mixed fracture mode) 83
Example 3. Prestressed cantilever beam 89
Example 4. Simply supported mixed beam-slab bridge 89
Example 5. Cylindrical concrete shell with edge beams 96
Example 6. Parabolic cylindrical reinforced concrete shell 96
Example 7. Cylindrical criogenic reinforced concrete tank 103
References 108

INTRODUCCION

This monograph presents 4 lectures on non linear analysis of concrete shells by the finite element method. The lectures were prepared by the author for the course on "Non linear analysis of shells by finite elements" held at the International Center for Mechanical Sciences in Udine, Italy on June 24th-28th 1991.

The content of the lectures presents an overview of the different aspects involved in the analysis of concrete shells by finite elements. Thus, lecture 1 introduces the basic concepts of the analysis of reinforced concrete shell structures using flat shell and curved degenerated layered shell finite elements. Both the geometric and kinematic assumptions are described in detail together with the respective finite element formulation and the numerical algorithm for non linear elasto-plastic analysis including the effect of moderately large displacements.

Lecture 2 presents an overview of the constitutive behaviour of concrete and steel in a form suitable for numerical computations using the finite element models described in previous lecture. The reinforcing steel bars are modelled with a simple elasto-plastic model. Hovewer, two conceptualy different concrete models are presented. The first model is based on elasto-plastic theory to describe the compressive behaviour of concrete, whereas a linear orthotropic elasto-brittle model is used for modelling the cracking behaviour under tensile conditions. This "elasto-platic-brittle" model has been extensively used by Owen and Figueiras and most of the concepts presented emanate from reference [18] of this chapter.

The second model is based on the assumptions that both the tensile and compressive behaviour of concrete can be treated under the unified framework of elasto-plasticity theory. This model termed "plastic-damage model" has ben proposed by Lubliner, Oller, Oliver and Oñate in different publications which main concepts are summarized in the lecture (see refs. [33-38] of this chapter).

In lecture 3 the basic finite element formulation for the analysis of

stiffened concrete shells via the use of eccentric beams is described.

Finally, in lecture 4 some examples of applications of the finite element formulations presented to the non-linear analysis of different reinforced concrete shell structures analyzed by different authors are described. Examples included range from the analysis of plain and pre-stressed concrete deep beams, to more sophisticated shell type structures including the nonlinear behaviour of a composite steel-concrete girder bridge and a cryogenic concrete liquid gas tank under severe thermal conditions.

This monograph has been written exclusively with didactic purposes. Most of the ideas included in the text have been extracted from research publications by the author and many others. The interested reader will be able to find details on the different subjects treated in the many references included at the end of each chapter.

LECTURE 1

CONCRETE SHELLS. BASIC FINITE ELEMENT FORMULATION

SUMMARY

This lecture describes the basis of the analysis of reinforced concrete shell structures using flat shell and curved degenerated layered shell finite elements. Both the geometric and kinematic assumptions are described together with the respective finite element formulations for small and moderately large displacement analysis.

INTRODUCTION

Concrete shell structures are very common in civil engineering practice. Typical examples are reinforced and pre–stressed slabs, bridges, shell roofs, water tanks, nuclear reactors cylindrical walls and buildings, etc. Some examples of these structures are shown in Figure 1.1. The importance of all these structures requires an adequate design based on an accurate evaluation of the structural response both at service and ultimate loading levels.

The analysis and design of reinforced and prestressed concrete structures has been based on simple equilibrium conditions and empirical rules for almost a century. The traditional methods generally result in safe designs, but they frecuently contain inherent inconsistencies and often do not reflect a clear understanding of the actual composite action of the material. Present–day design codes continue, in many respects, to be based on empirical approaches and rely heavily on the results of a considerable amount of experimental data. This situation is largely attributable to the complex behaviour of reinforced concrete components and structures. Concrete cracking, tension stiffening, nonlinear multiaxial material properties and complex interface behaviours were previously ignored or treated in a very approximate manner. Numerical methods, and particularly the finite element technique, now permits a more rational analysis of these complexities.

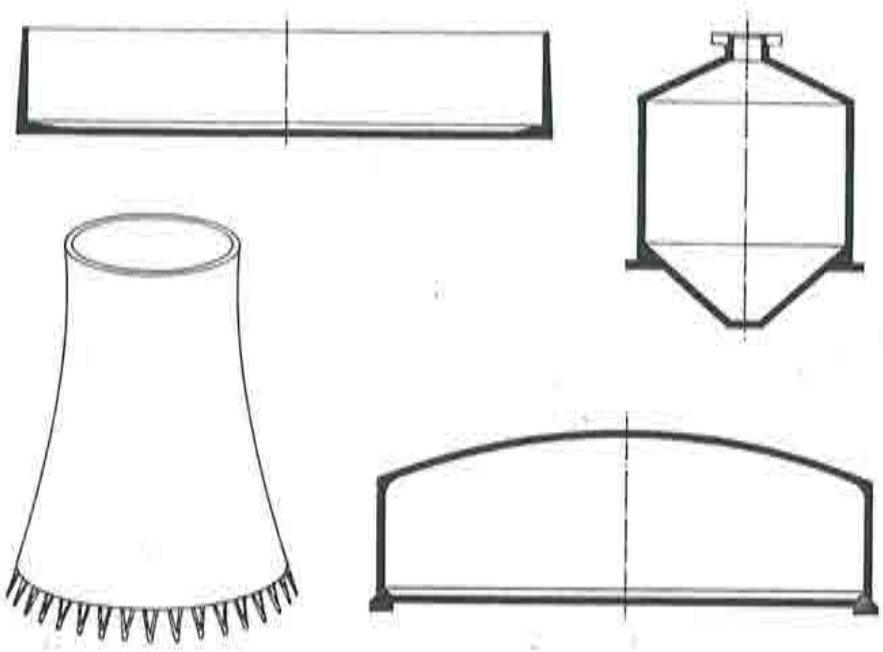

Figure 1.1 Some concrete shell structures.

The last two decades have witnessed rapid advances in the use of finite element methods for the analysis of reinforced concrete structures as reported in several comprehensive review articles [1–5]. Some numerical approaches have been developed to mainly study local behaviours, such as bond effects craking, interface shear, and dowel action [6–9], while other numerical studies have been directed at the analysis and design of components and structures [10–13]. The primary objectives in the latter case are the accurate prediction of the overall deformation characteristics and limit loads. A layered approach is generally employed to simulate steel reinforcement with the crack effects being assumed to be distributed (smeared) within each concrete layer. Full bond is assumed at the steel–concrete interfaces.

In this lecture we present the basis of the finite element formulation for the analysis of reinforced concrete shells using layered shell theory and two different finite element formulations: (a) Flat shell elements and (b)Degenerate shell elements. Both small and moderately large displacements will be considered.

The description of the linear and non linear material models for concrete and reinforcement steel *is not included* here and will be treated in detail in Lecture 2 .

FORMULATION OF FLAT SHELL ELEMENTS FOR ANALYSIS OF REINFORCED CONCRETE SHELLS

Basic theory

The simplest approach for deriving finite elements for shell analysis is to assume that the mid–surface of each shell element is flat. It is well known that in this case membrane and bending kinematics are uncoupled at element level. We will assume the standard hypothesis of Reissner-Mindlin thick plate theory [22], [23], i.e. the normals to the element mid–surface before deformation remain straight but not necessarily normal to the mid–surface after deformation. Therefore the displacement field can be written as (Figure 1.2)

$$\begin{aligned} u'(x',y',z') &= u'_o(x',y') - z'\theta_{x'}(x',y') \\ v'(x',y',z') &= v'_o(x',y') - z'\theta_{y'}(x',y') \\ w'(x',y',z') &= w'_o(x',y') \end{aligned} \tag{1.1}$$

The local displacement vector is then defined as

$$\mathbf{u}' = \left[u'_o, v'_o, w'_o, \theta_{x'}, \theta_{y'}\right]^T \tag{1.2}$$

where u'_o, v'_o are the in–plane (membrane) displacements and $w'_o, \theta_{x'}$ and $\theta_{y'}$ are the transverse displacements and local rotations of the normal (flexural displacements)

Assuming now the standard plane stress hypothesis ($\sigma_{z'} = 0$) allows to elliminate the thickness strain in local axes. The local strain vector is thus obtained using (1.1) as

$$\boldsymbol{\varepsilon}' = \left\{ \begin{array}{c} \varepsilon_{x'} \\ \varepsilon_{y'} \\ \gamma_{x'y'} \\ \cdots\cdots \\ \gamma_{x'z'} \\ \gamma_{y'z'} \end{array} \right\} = \left\{ \begin{array}{c} \frac{\partial u'}{\partial x'} \\ \frac{\partial v'}{\partial y'} \\ \frac{\partial u'}{\partial y'} + \frac{\partial v'}{\partial x'} \\ \cdots\cdots \\ \frac{\partial u'}{\partial z'} + \frac{\partial w'}{\partial x'} \\ \frac{\partial v'}{\partial z'} + \frac{\partial w'}{\partial y'} \end{array} \right\} = \left\{ \begin{array}{c} \frac{\partial u'_o}{\partial x'} \\ \frac{\partial v'_o}{\partial y'} \\ \frac{\partial u'_o}{\partial y'} + \frac{\partial v'_o}{\partial x'} \\ \cdots\cdots\cdots \\ 0 \\ 0 \end{array} \right\} + \left\{ \begin{array}{c} -z'\frac{\partial \theta_{x'}}{\partial x'} \\ -z'\frac{\partial \theta_{y'}}{\partial y'} \\ -z'\left(\frac{\partial \theta_{x'}}{\partial y'} + \frac{\partial \theta_{y'}}{\partial x'}\right) \\ \cdots\cdots\cdots \\ \frac{\partial w'_o}{\partial x'} - \theta_{x'} \\ \frac{\partial w'_o}{\partial y'} - \theta_{y'} \end{array} \right\} \tag{1.3}$$

Eq. (1.3) can be rewritten as

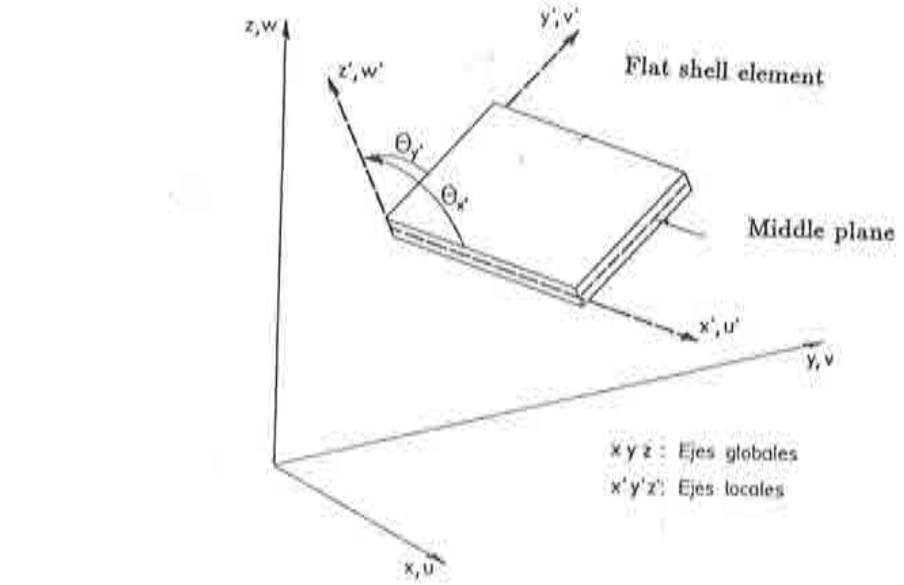

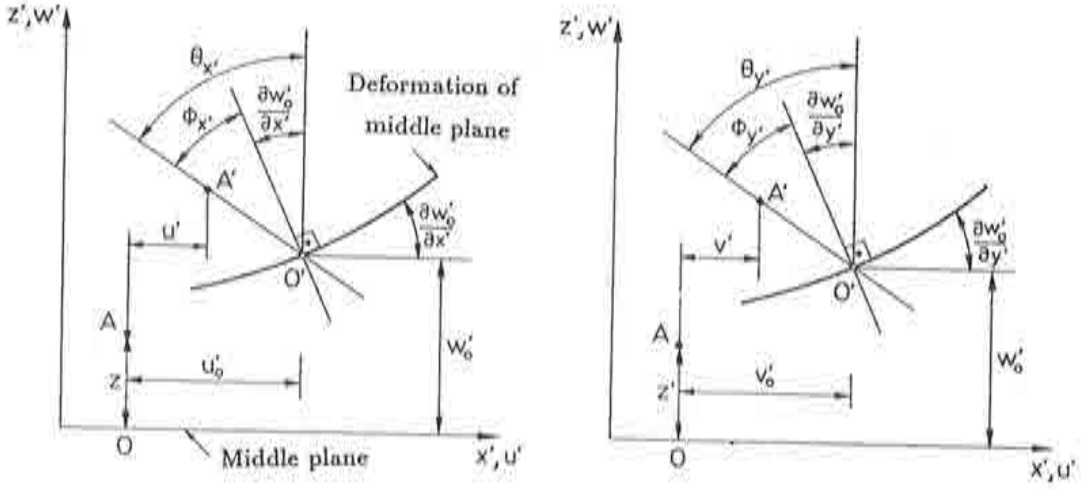

Figure 1.2 Definition of local displacements and rotations in flat shell theory.

$$\boldsymbol{\varepsilon}' = \begin{Bmatrix} \hat{\boldsymbol{\varepsilon}}'_m \\ \cdots\cdots \\ 0 \end{Bmatrix} + \begin{Bmatrix} z'\hat{\boldsymbol{\varepsilon}}'_b \\ \cdots\cdots \\ \hat{\boldsymbol{\varepsilon}}'_s \end{Bmatrix} \tag{1.4}$$

where

$$\hat{\boldsymbol{\varepsilon}}'_m = \left[\frac{\partial u'_o}{\partial x'}, \frac{\partial v'_o}{\partial y'}, \left(\frac{\partial u'_o}{\partial y'} + \frac{\partial v'_o}{\partial x'} \right) \right]^T \tag{1.5a}$$

$$\hat{\boldsymbol{\varepsilon}}'_b = \left[-\frac{\partial\theta_{x'}}{\partial x'}, -\frac{\partial\theta_{y'}}{\partial y'}, -\left(\frac{\partial\theta_{x'}}{\partial y'} + \frac{\partial\theta_{y'}}{\partial x'}\right)\right]^T \tag{1.5b}$$

$$\hat{\boldsymbol{\varepsilon}}'_s = \left[\left(\frac{\partial w'_o}{\partial x'} - \theta_{x'}\right), \left(\frac{\partial w'_o}{\partial y'} - \theta_{y'}\right)\right]^T \tag{1.5c}$$

are respectively the generalized *membrane*, ***bending*** and *shear* local strain vectors.

For linear elastic analysis the local stresses are related to the local strains in the standard manner by

$$\boldsymbol{\sigma}' = \begin{Bmatrix} \sigma_{x'} \\ \sigma_{y'} \\ \tau_{x'y'} \\ \cdots\cdots \\ \tau_{x'z'} \\ \tau_{y'z'} \end{Bmatrix} = \begin{Bmatrix} \boldsymbol{\sigma}'_f \\ \cdots \\ \boldsymbol{\sigma}'_s \end{Bmatrix} = \begin{bmatrix} \mathbf{D}'_f & \vdots & \mathbf{0} \\ \cdots & \cdots & \cdots \\ \mathbf{0} & \vdots & \mathbf{D}'_s \end{bmatrix} \begin{Bmatrix} \varepsilon_{x'} \\ \varepsilon_{y'} \\ \gamma_{x'y'} \\ \cdots\cdots \\ \gamma_{x'z'} \\ \gamma_{y'z'} \end{Bmatrix} = \mathbf{D}'\boldsymbol{\varepsilon}' \tag{1.6}$$

where for orthotropic material

$$\mathbf{D}'_f = \frac{1}{1-\nu_{x'y'}\nu_{y'x'}} \begin{bmatrix} E_{x'} & \nu_{x'y'}E'_x & 0 \\ \nu_{y'x'}E'_x & E'_y & 0 \\ 0 & 0 & (1-\nu_{x'y'}\nu_{y'x'})G_{x'y'} \end{bmatrix}$$

$$\mathbf{D}'_s = \begin{bmatrix} \alpha G_{x'z'} & 0 \\ 0 & \alpha G_{y'z'} \end{bmatrix} \tag{1.7}$$

and for isotropic material

$$E_{x'} = E_{y'} = E \;;\; \nu_{x'y'} = \nu_{y'x'} = \nu \;;\; G_{x'y'} = G_{x'z'} = G_{y'z'} = \frac{E}{2(1+\nu)} \tag{1.8}$$

In (1.6) and (1.8) $(\cdot)_f$ and $(\cdot)_s$ stand for *flexural* and transverse *shear* terms, respectively.
From (1.4) and (1.6) it can be obtained

$$\begin{aligned} \boldsymbol{\sigma}'_f &= \mathbf{D}'_f(\hat{\boldsymbol{\varepsilon}}'_m + z'\hat{\boldsymbol{\varepsilon}}'_b) \\ \boldsymbol{\sigma}'_s &= \mathbf{D}'_s\hat{\boldsymbol{\varepsilon}}'_s \end{aligned} \tag{1.9}$$

The *resultant stress* vector is now defined as

$$\hat{\boldsymbol{\sigma}}' = \begin{Bmatrix} \hat{\boldsymbol{\sigma}}'_m \\ \cdots \\ \hat{\boldsymbol{\sigma}}'_b \\ \cdots \\ \hat{\boldsymbol{\sigma}}'_s \end{Bmatrix} = \begin{Bmatrix} N_{x'} \\ N_{y'} \\ N_{x'y'} \\ \cdots \\ M_{x'} \\ M_{y'} \\ M_{x'y'} \\ \cdots \\ Q_{x'} \\ Q_{y'} \end{Bmatrix} = \int_{-\frac{t}{2}}^{+\frac{t}{2}} \begin{Bmatrix} \sigma_{x'} \\ \sigma_{y'} \\ \tau_{x'y'} \\ \cdots \\ z'\sigma_{x'} \\ z'\sigma_{y'} \\ z'\tau_{x'y'} \\ \cdots \\ \tau_{x'z'} \\ \tau_{y'z'} \end{Bmatrix} dz' = \int_{-\frac{t}{2}}^{+\frac{t}{2}} \begin{Bmatrix} \boldsymbol{\sigma}'_m \\ \cdots \\ z'\boldsymbol{\sigma}'_b \\ \cdots \\ \boldsymbol{\sigma}'_s \end{Bmatrix} dz' \quad (1.10)$$

where $\hat{\boldsymbol{\sigma}}'_m$, $\hat{\boldsymbol{\sigma}}'_b$, $\hat{\boldsymbol{\sigma}}'_s$ are respectively the local membrane, bending and shear resultant stress vectors. For sign convention see Figure 1.3.

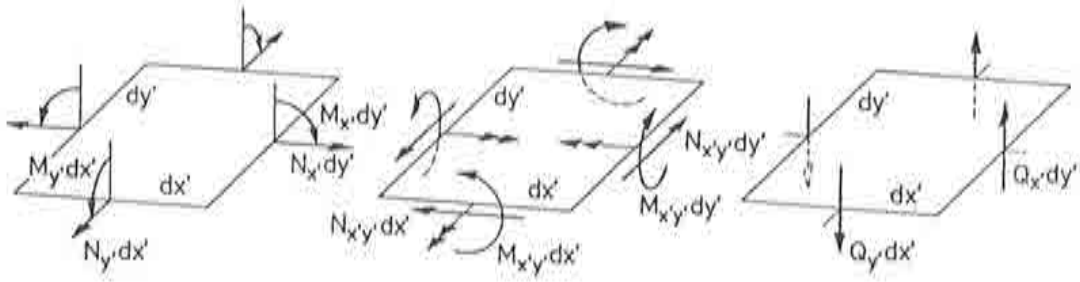

Figure 1.3 Sign convention for local resultant stresses in flat shell elements.

The relationship between resultant stresses and generalized strains in local axes can be obtained by combining (1.10) and (1.9) as

$$\hat{\boldsymbol{\sigma}}' = \begin{Bmatrix} \hat{\boldsymbol{\sigma}}'_m \\ \cdots \\ \hat{\boldsymbol{\sigma}}'_b \\ \cdots \\ \hat{\boldsymbol{\sigma}}'_s \end{Bmatrix} = \int_{-\frac{t}{2}}^{+\frac{t}{2}} \begin{Bmatrix} \boldsymbol{\sigma}'_m \\ \cdots \\ z'\boldsymbol{\sigma}'_b \\ \cdots \\ \boldsymbol{\sigma}'_s \end{Bmatrix} dz' =$$

$$= \int_{-\frac{t}{2}}^{+\frac{t}{2}} \begin{Bmatrix} \mathbf{D}'_b(\hat{\boldsymbol{\varepsilon}}'_m + z'\hat{\boldsymbol{\varepsilon}}'_b) \\ \cdots\cdots\cdots\cdots \\ z'\mathbf{D}'_f(\hat{\boldsymbol{\varepsilon}}'_m + z'\hat{\boldsymbol{\varepsilon}}'_b) \\ \cdots\cdots\cdots\cdots \\ \mathbf{D}'_s\hat{\boldsymbol{\varepsilon}}'_s \end{Bmatrix} dz' = \hat{\mathbf{D}}' \begin{Bmatrix} \hat{\boldsymbol{\varepsilon}}'_m \\ \cdots \\ \hat{\boldsymbol{\varepsilon}}'_b \\ \cdots \\ \hat{\boldsymbol{\varepsilon}}'_s \end{Bmatrix} = \hat{\mathbf{D}}'\hat{\boldsymbol{\varepsilon}}' \quad (1.11)$$

where $\hat{\mathbf{D}}'$ is given by

$$\hat{\mathbf{D}}' = \int_{-\frac{t}{2}}^{+\frac{t}{2}} \begin{bmatrix} \mathbf{D}'_f & z'\mathbf{D}'_f & \mathbf{0} \\ z'\mathbf{D}'_f & z'^2\mathbf{D}'_f & \mathbf{0} \\ \mathbf{0} & \mathbf{0} & \mathbf{D}'_s \end{bmatrix} dz' = \begin{bmatrix} \hat{\mathbf{D}}'_m & \hat{\mathbf{D}}'_{mb} & \mathbf{0} \\ \hat{\mathbf{D}}'_{mb} & \hat{\mathbf{D}}'_b & \mathbf{0} \\ \mathbf{0} & \mathbf{0} & \hat{\mathbf{D}}'_s \end{bmatrix} \tag{1.12a}$$

with
$$\hat{\mathbf{D}}'_m = \int_{-\frac{t}{2}}^{+\frac{t}{2}} \mathbf{D}'_f dz' \quad ; \quad \hat{\mathbf{D}}'_{mb} = \int_{-\frac{t}{2}}^{+\frac{t}{2}} z'\mathbf{D}'_f dz'$$
$$\hat{\mathbf{D}}'_b = \int_{-\frac{t}{2}}^{+\frac{t}{2}} z'^2\mathbf{D}'_f dz' \quad ; \quad \hat{\mathbf{D}}'_s = \int_{-\frac{t}{2}}^{+\frac{t}{2}} \mathbf{D}'_s dz' \tag{1.12b}$$

where $\hat{\mathbf{D}}'_m$, $\hat{\mathbf{D}}'_b$ and $\hat{\mathbf{D}}'_s$ are respectively the generalized membrane, bending and shear constitutive matrices, and $\hat{\mathbf{D}}'_{mb}$ is the coupled bending–membrane constitutive matrix. Note that $\hat{\mathbf{D}}'_{mb} = 0$ in the case of homogeneous material, or if the material properties are symmetricaly distributed with respect to the element mid–surface. However, in the analysis of general reinforced concrete shells material heterogenity prevails and $\hat{\mathbf{D}}'_{mb}$ must be appropiately computed.

If an elasto–plastic material model is considered eq.(6) is defined in an incremental form as

$$d\boldsymbol{\sigma}' = \mathbf{D}'_{ep} d\boldsymbol{\varepsilon}' \tag{1.13a}$$

where $\mathbf{D}'_{ep}$ is the tangent elasto–plastic constitutive matrix which will be defined in a latter section and more specifically in Lecture 2. Integration of $\mathbf{D}'_{ep}$ across the element thickness allows to write eq.(1.11) also in an incremental form as

$$d\hat{\boldsymbol{\sigma}}' = \hat{\mathbf{D}}'_{ep} d\hat{\boldsymbol{\varepsilon}}' \tag{1.13b}$$

Layered model

In reinforced concrete shell problems a convenient representation of concrete and steel behaviour across the shell thickness is needed. This is of particular importance if the non linear behaviour of compressive concrete, concrete cracking and reinforcement response are to be appropiately modelled. The most popular computational approach is to use a layered model in which the shell thickness is divided into a series of plain (unreinforced) concrete layers and of reinforcing steel layers. (Figure 1.4) Plain concrete layers can be either elastic, (singly or doubly) cracked, and yielded or crushed. Appropiate stress–strain relations must be used for each of these states of behaviour (see Lecture 2). On the other hand, the reinforcing steel is replaced by an equivalent smeared uniformly

distributed steel layer with stiffness only in the direction of the reinforcement. The equivalent thickness of the steel layer is determined such that the corresponding area of reinforcement in the layer remains unchanged. Ordinarly, a concrete shell is reinforced by at least two sets of reinforcing bars. It is also usualy assumed that the reinforcing steel is arranged in layers forming grids intersecting each other at arbitrary angles. Any number of such layers can be accounted for and each layer is to be located exactly in space for the purpose of generating its stiffness properties. Perfect bond is assumed to exist between the reinforcing steel and the surrounding concrete. However, appropiate bond slip laws can also be incoporated into the analysis.

Layers are numbered sequentially, starting at the bottom surface of the shell element, and each layer contains stress points on its mid-surface. The stress components of the layer are computed at these stress points and are assumed to be constant over the thickness of each layer, so that the actual stress distribution over the shell thickness is modelled by a piecewise constant approximation [6] (Figure 1.4).

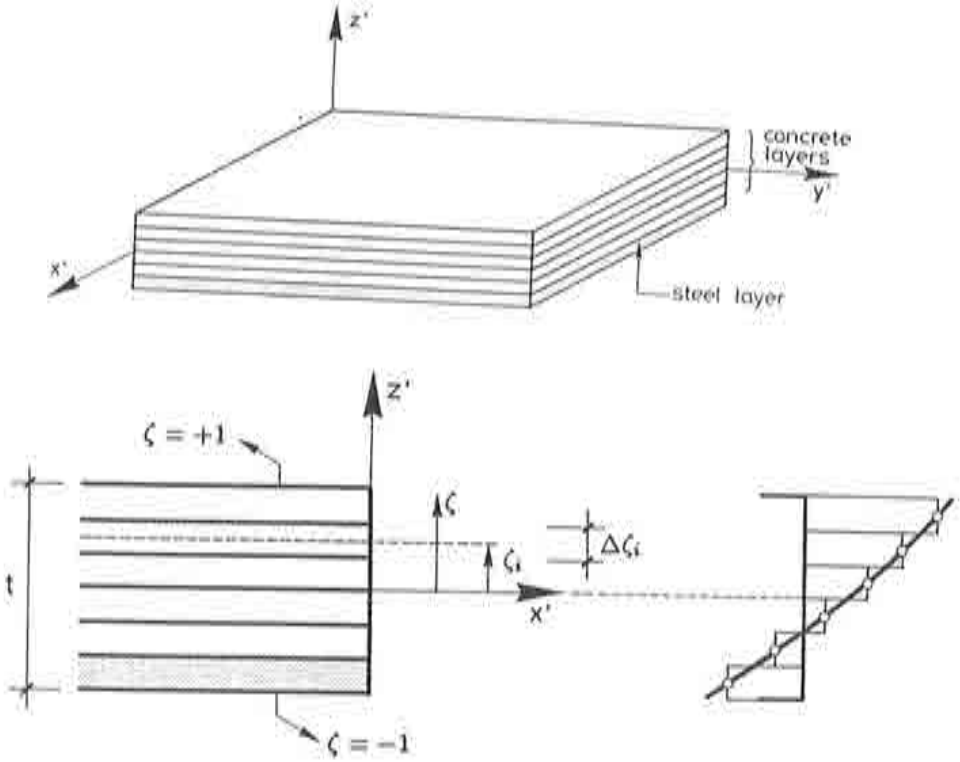

Figure 1.4 Layered discretization of reinforced concrete slab.

Layers of different thickness can be employed, as well as different number of layers per element. The specification of the layer thickness in terms of a normalized thickness coordinate $\zeta = \frac{2}{t}z'$, permits the variation of the layer thickness as the shell thickness varies [6] [7].

The stress resultants are obtained from eq.(1.11) by adequately integrating the constitutive matrices (1.12) across the element layers as

$$\begin{aligned}
\hat{\mathbf{D}}'_m &= \frac{t}{2}\sum_{i=1}^{l}\hat{\mathbf{D}}'_{f_i}\Delta\zeta_i \\
\hat{\mathbf{D}}'_b &= \frac{t^3}{8}\sum_{i=1}^{l}\hat{\mathbf{D}}'_{f_i}\Delta\zeta_i^2\zeta_i \\
\hat{\mathbf{D}}'_s &= \frac{t}{2}\sum_{i=1}^{l}\hat{\mathbf{D}}'_{s_i}\Delta\zeta_i \\
\hat{\mathbf{D}}'_{m_b} &= \frac{t^2}{4}\sum_{i=1}^{l}\hat{\mathbf{D}}'_{f_i}\zeta_i\Delta\zeta_i
\end{aligned} \tag{1.14}$$

where $\zeta_i = \frac{2z'_i}{t}$, l is the number of layers and $(\cdot)_i$ denotes values in the ith layer. For the non linear material case the elastic matrices in (1.14) will be substituted by the corresponding non linear operators via eq.(1.13b).

Finite element discretization

We will consider the discretization of the shell mid–surface in a mesh of isoparametric flat finite elements of n nodes (Figure 1.5). The local displacement field can be interpolated in the standard form

$$\mathbf{u}' = \sum_{i=1}^{n}\mathbf{N}_i\mathbf{a}_i'^{(e)} = [\mathbf{N}_1, \mathbf{N}_2, \cdots, \mathbf{N}_n]\begin{Bmatrix}\mathbf{a}_1'^{(e)}\\ \mathbf{a}_2'^{(e)}\\ \vdots\\ \mathbf{a}_n'^{(e)}\end{Bmatrix} = \mathbf{N}\mathbf{a}'^{(e)} \tag{1.15}$$

where

$$\mathbf{N}_i = \begin{bmatrix} N_i & 0 & 0 & 0 & 0\\ 0 & N_i & 0 & 0 & 0\\ 0 & 0 & N_i & 0 & 0\\ 0 & 0 & 0 & N_i & 0\\ 0 & 0 & 0 & 0 & N_i\end{bmatrix}; \quad \mathbf{a}_i'^{(e)} = \left[u'_{o_i}, v'_{o_i}, w'_{o_i}, \theta_{x'_i}, \theta_{y'_i}\right]^T \tag{1.16}$$

are the shape function matrix and the local displacement vector of a node i.

From (1.5) and (1.15) the local generalized strains can be obtained as

$$\hat{\boldsymbol{\varepsilon}}' = \mathbf{B}'\mathbf{a}'^{(e)} \tag{1.17}$$

with $\mathbf{B}' = [\mathbf{B}'_1, \mathbf{B}'_2, \cdots, \mathbf{B}'_m]$

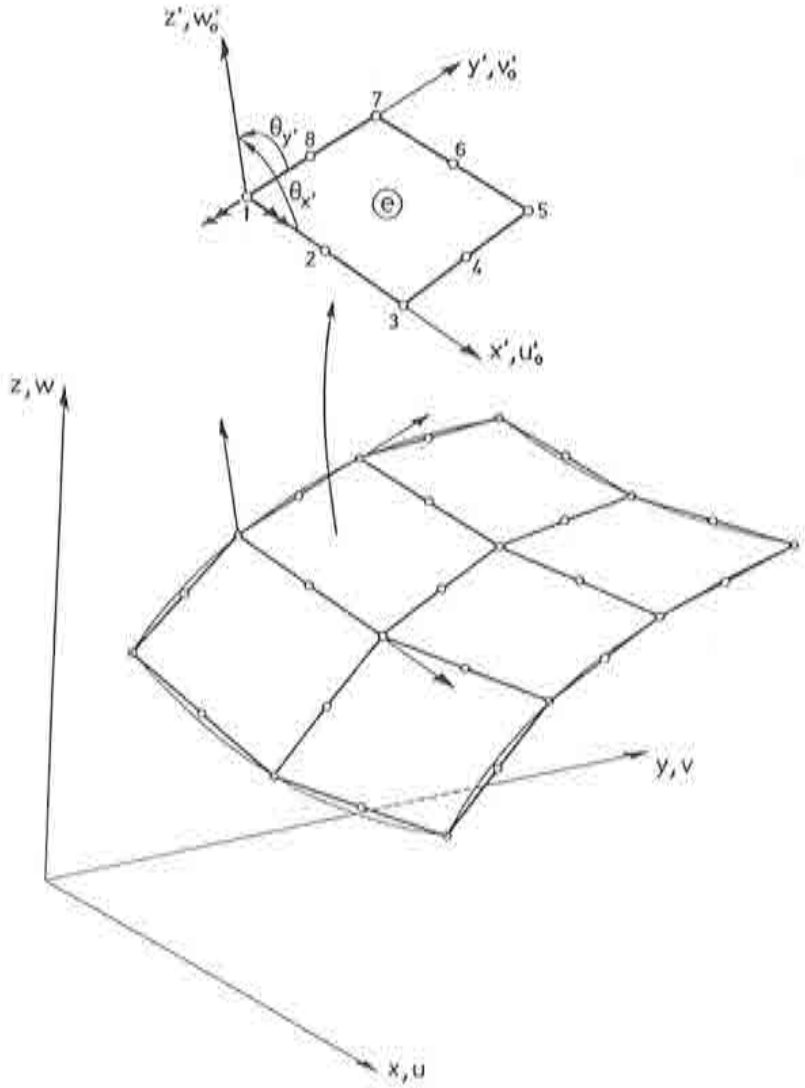

Figure 1.5 Discretization of a shell into flat shell finite elements.

and

$$\mathbf{B}'_i = \begin{Bmatrix} \mathbf{B}'_{mi} \\ \mathbf{B}'_{bi} \\ \mathbf{B}'_{si} \end{Bmatrix} \tag{1.18}$$

where $\mathbf{B}'_{mi}$, $\mathbf{B}'_{bi}$ and $\mathbf{B}'_{si}$ are respectively the local membrane, bending and shear generalized strain matrices of a node i, given by

$$\mathbf{B}'_{m_i} = \begin{bmatrix} \frac{\partial N_i}{\partial x'} & 0 & 0 & 0 & 0 \\ 0 & \frac{\partial N_i}{\partial y'} & 0 & 0 & 0 \\ \frac{\partial N_i}{\partial y'} & \frac{\partial N_i}{\partial x'} & 0 & 0 & 0 \end{bmatrix} \tag{1.19}$$

$$\mathbf{B}'_{b_i} = \begin{bmatrix} 0 & 0 & 0 & -\frac{\partial N_i}{\partial x'} & 0 \\ 0 & 0 & 0 & 0 & -\frac{\partial N_i}{\partial y'} \\ 0 & 0 & 0 & -\frac{\partial N_i}{\partial y'} & -\frac{\partial N_i}{\partial x'} \end{bmatrix} \tag{1.20}$$

$$\mathbf{B}'_{s_i} = \begin{bmatrix} 0 & 0 & \frac{\partial N_i}{\partial x'} & -N_i & 0 \\ 0 & 0 & \frac{\partial N_i}{\partial y'} & 0 & -N_i \end{bmatrix} \tag{1.21}$$

The virtual work principle for a single element can be written as

$$\int\int_{A^{(e)}} \delta\hat{\boldsymbol{\varepsilon}}'^T \hat{\boldsymbol{\sigma}}' dA = \int\int_{A^{(e)}} \delta\mathbf{u}'^T \mathbf{t}' dA + \left[\delta\mathbf{a}'^{(e)}\right]^T \mathbf{q}'^{(e)} \tag{1.22}$$

where $\mathbf{t}'$ and $\mathbf{q}'^{(e)}$ are the distributed local vector and nodal point load vector, respectively.

Substituting eqs.(1.11), (1.15) and (1.17) in (1.22) the standard stiffness equilibrium equations for a single element can be obtained as

$$\mathbf{q}'^{(e)} = \mathbf{K}'^{(e)}\mathbf{a}'^{(e)} - \mathbf{f}'^{(e)} \tag{1.23}$$

where

$$\mathbf{K}'^{(e)}_{ij} = \int\int_{A^{(e)}} \mathbf{B}'^T_i \hat{\mathbf{D}}' \mathbf{B}'_j dx' dy' \tag{1.24}$$

$$\mathbf{f}'^{(e)}_i = \int\int_{A^{(e)}} \mathbf{N}^T_i \mathbf{t}' dx' dy' \tag{1.25}$$

are the element stiffness matrix and equivalent nodal load vector, respectively.

Matrix $\mathbf{K}'^{(e)}_{ij}$ can be rewritten using (1.12) and (1.18) as

$$\mathbf{K}'^{(e)}_{ij} = \mathbf{K}'^{(e)}_{m_{ij}} + \mathbf{K}'^{(e)}_{b_{ij}} + \mathbf{K}'^{(e)}_{s_{ij}} + \mathbf{K}'^{(e)}_{mb_{ij}} + \mathbf{K}'^{(e)}_{bm_{ij}} \tag{1.26}$$

where

$$
\begin{aligned}
\mathbf{K}^{\prime(e)}_{m_{ij}} &= \int\int_{A^{(e)}} \mathbf{B}^{\prime T}_{m_i} \hat{\mathbf{D}}^{\prime}_{m} \mathbf{B}^{\prime}_{m_j} dx' dy' \\
\mathbf{K}^{\prime(e)}_{b_{ij}} &= \int\int_{A^{(e)}} \mathbf{B}^{\prime T}_{b_i} \hat{\mathbf{D}}^{\prime}_{b} \mathbf{B}^{\prime}_{b_j} dx' dy' \\
\mathbf{K}^{\prime(e)}_{s_{ij}} &= \int\int_{A^{(e)}} \mathbf{B}^{\prime T}_{s_i} \hat{\mathbf{D}}^{\prime}_{s} \mathbf{B}^{\prime}_{s_j} dx' dy' \\
\mathbf{K}^{\prime(e)}_{mb_{ij}} &= \int\int_{A^{(e)}} \mathbf{B}^{\prime T}_{m_i} \hat{\mathbf{D}}^{\prime}_{mb} \mathbf{B}^{\prime}_{b_j} dx' dy' = \left[\mathbf{K}^{\prime(e)}_{bm_{ij}}\right]^T
\end{aligned}
\tag{1.27}
$$

are respectively the membrane, bending, shear and membrane-bending coupling local stiffness mattrices. Note that if $\hat{\mathbf{D}}^{\prime}_{mb}$ is zero (which is the case for homogeneous material or when there is material symmetry with respect to the mid–plane) $\mathbf{K}^{\prime(e)}_{mb}$ and $\mathbf{K}^{\prime(e)}_{bm}$ are also zero and the *local* stiffness matrix can be directly obtained by simple addition of the membrane, bending and shear uncoupled contributions.

Note that in (1.23)–(1.27) we have assumed elastic material behaviour. The non linear case will be treated in a later section.

The global stiffness matrix and the global equivalent nodal load vector for the whole mesh are obtained by assembly of the individual element contributions in the standard manner [14]. This involves first a transformation of local degrees of freedom and forces to a common global cartesian coordinate system as

$$
\mathbf{a}^{\prime(e)} = \mathbf{T}\mathbf{a}^{(e)} \quad \text{and} \quad \mathbf{f}^{\prime(e)} = \mathbf{T}\mathbf{f}^{(e)} \tag{1.28}
$$

where $\mathbf{T}$ is the transformation matrix relating local and global nodal degrees of freedom and forces at element level [14], [15]. The global element stiffness matrix is then computed by the well known transformation

$$
\mathbf{K}^{(e)} = \mathbf{T}^T \mathbf{K}^{\prime(e)} \mathbf{T} \tag{1.29}
$$

If the shell has folds or kinks the transformations (1.28)–(1.29) involve and additional global rotation θ_z which plays the role of a sixth degree of freedom at each non-coplanar node, whereas the standard five degrees of freedom (three global displacements and two local rotations) can be kept at the coplanar nodes (Figure 1.6). Details of the treatment of co-planar and non coplanar nodes can be found in [14], [15].

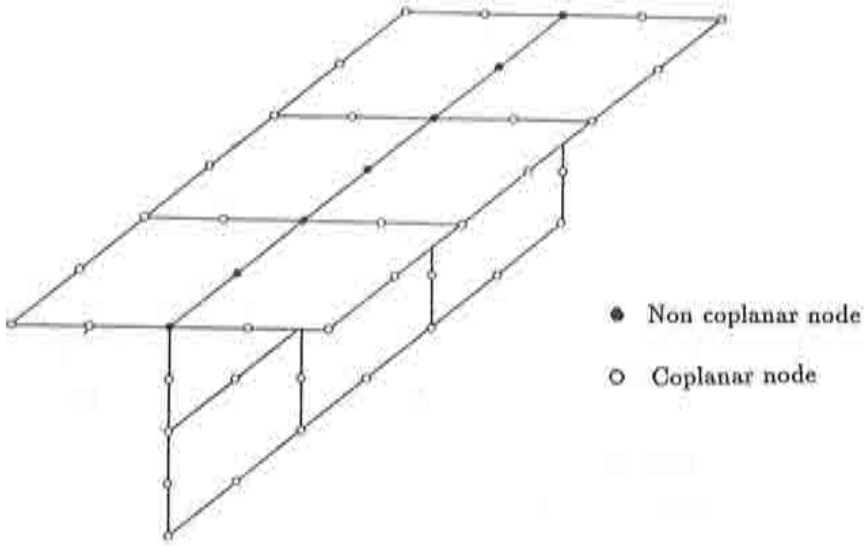

Figure 1.6 Definition of coplanar and non–coplanar nodes.

Numerical integration. Shear locking and element typology

Numerical integration across the thickness is performed via the layered model as described previously. In the shell plane the normal (full) integration rule consists of $m \times m$ Gauss points where m is the number of nodes along each element side. Nevertheless when flat shell elements are fully integrated they exhibit shear locking and over–stiff solutions are obtained in the majority of applications [14], [15].

The simplest procedure to overcome shear locking behaviour is to use a reduced integration quadrature for the shear stiffness [14], [15] whereas the rest of the stiffness terms can be exactly integrated. However it has been proved that this procedure may occasionally lead to spurious zero–energy modes appearing in the global equations

An alternative approach for derivation of *robust* shell elements is based on the use of an assumed shear strain field. In this method a shear strain field is "a priori" assumed over the element in the natural coordinate system.

$$\gamma_\xi = \mathbf{N}_\gamma \bar{\gamma}_\xi \tag{1.30}$$

where $\bar{\gamma}_\xi$ contains the values of the shear strains at some prescribed points within the element and $\mathbf{N}_\gamma$ are appropiate shear interpolating functions. The displacement and rotations are interpolated in the standard manner. However, a different interpolation for each displacement field must sometimes be used to satisfy the the requirements for the existence of the solution [14], [18].

By relating $\bar{\gamma}_\xi$ with the cartesian shear strains and these with the element

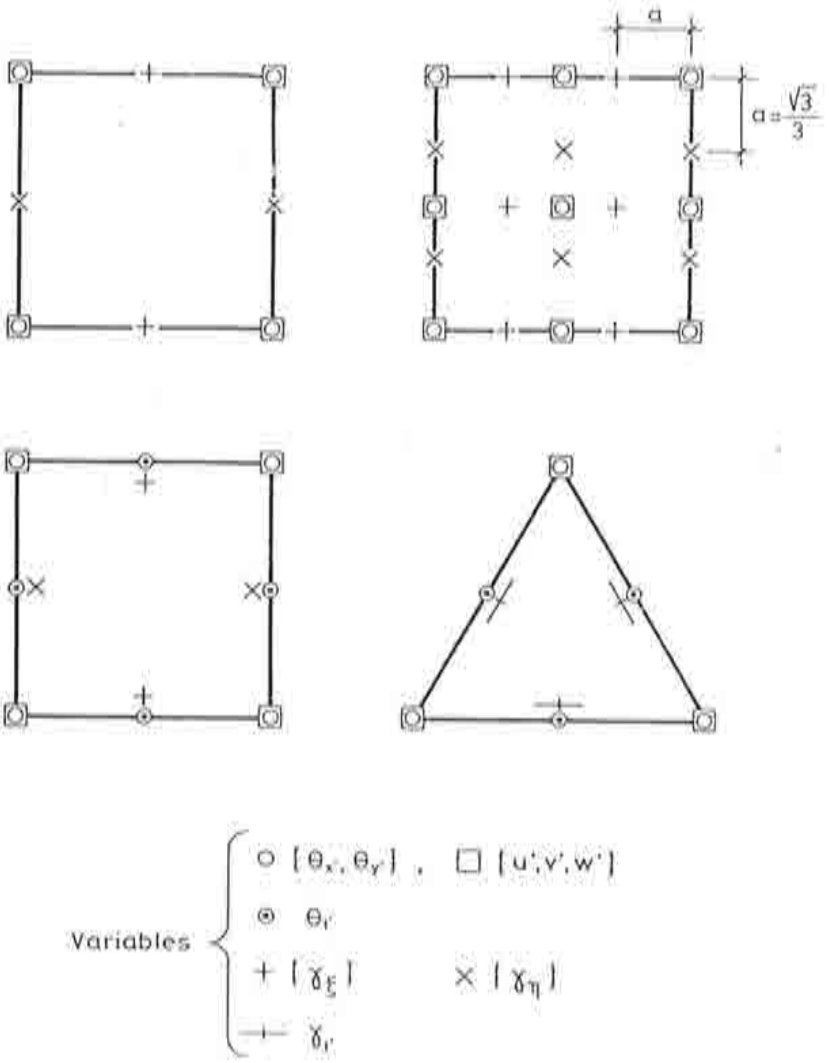

Figure 1.7 Some quadrilateral and triangular assumed shear strain shell elements [19–21], [24].

nodal displacements $\mathbf{a}^{(e)}$ through eq.(1.17) a final relationship beteween $\boldsymbol{\gamma}'_s$ and $\mathbf{a}^{(e)}$ can be found in the form

$$\boldsymbol{\gamma}'_s = \hat{\mathbf{B}}'_s \mathbf{a}^{(e)} \tag{1.31}$$

where $\hat{\mathbf{B}}'_s$ is termed *substitute shear strain* matrix (or shear **B**-bar matrix). Matrix $\mathbf{K}'_s$ is computed by eq.(1.27) using $\hat{\mathbf{B}}'_s$ instead of the original shear strain matrix $\mathbf{B}'_s$, whereas the rest of the stiffness matrix terms are computed as shown in (1.27). Full integration is now used for the computation of *all* the element matrices.

Figure 1.7 shows some of the most popular rectangular and triangular flat shell elements based on this approach. The interested reader can found further information in [14], [19], [20], [24].

FORMULATION OF CURVED DEGENERATE SHELL ELEMENTS FOR ANALYSIS OF REINFORCED CONCRETE SHELLS

General

Figure 1.8 shows a solid three–dimensional element based on a quadratic displacement field and the corresponding quadratic degenerate shell element. Two basic assumptions are adopted in this process: Firstly it is assumed that, even for thick shells, *normals* to the middle surface remain practically straight after deformation. Secondly, the strain energy corresponding to stresses perpendicular to the surface is disregarded, i.e. the stress component normal to the shell mid–surface is constrained to be zero in the constitutive equations.

Five degrees of freedom are specified at each point, corresponding to its three displacements and the two rotations of the *normal* at the node. The definition of independent rotational and displacement degrees of fredom permits transverse shear deformation to be taken into account, since rotations are not tied to the slope of the mid–surface. This approach is equivalent to using a general shell theory and reduces to the hypotheses of Reissner [22] and Mindlin [23] when applied to plates, and it has also been used in the the flat shell theory described in previous sections.

Coordinate systems

1 *Global coordinate set* x, y, z

This is a Cartesian coordinate system freely chosen in relation to which the geometry of the structure is defined in space. Nodal displacements as well as the stiffness matrix and applied load vector are referred to this system.

2 *Nodal coordinate set* $\vec{v}_{1i}, \vec{v}_{2i}, \vec{v}_{3i}$

A nodal coordinate system is defined at each nodal point with origin at the reference (mid) surface (Figure 1.8). The vector $\vec{v}_{3i}$ defines the direction of the "normal" at node i, and it can be defined from the nodal coordinates of the top and bottom surfaces at node i, so that it is not necessarily perpendicular to the mid surface at i. The vector $\vec{v}_{1i}$ is perpendicular to $\vec{v}_{3i}$ and parallel to the global $x - z$ plane and the vector $\vec{v}_{2i}$ is perpendicular to the plane defined by $\vec{v}_{1i}$ and $\vec{v}_{3i}$. Vectors $\vec{v}_{1i}$ and $\vec{v}_{2i}$ define the local rotations (θ_{1i} and θ_{2i}) of the corresponding normal.

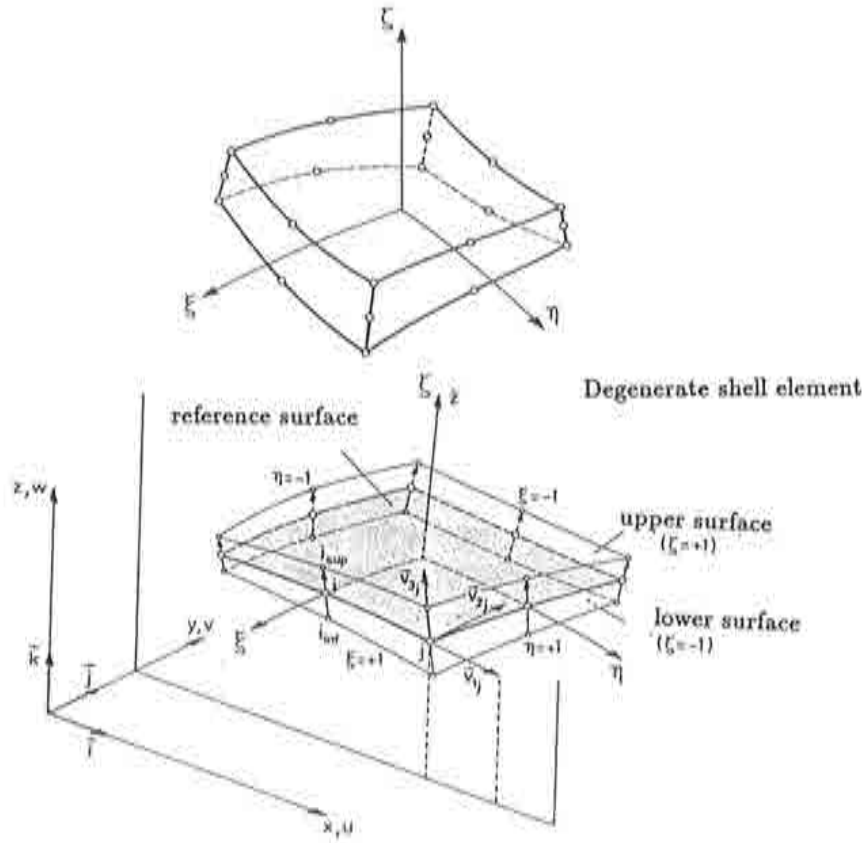

Figure 1.8 Degenerate shell element (a) Parent quadratic solid element, (b)Degenerate shell element. global, nodal and curvilinear coordinate systems.

3 *Curvilinear coordinate set* ξ, η, ζ

In this system ξ, η are two curvilinear coordinates in the middle surface of the shell element and ζ is a linear coordinate in the thickness direction. (Figure 1.8). It is assumed that ξ, η and ζ vary between -1 $+1$ on the respective element faces.

4 *Local coordinate set* x', y', z'

This is a Cartesian coordinate system defined at the sampling points wherein stresses and strains are to be calculated. The direction $\mathbf{z}'$ is taken perpendicular to the surface ζ =constant, being obtained by the cross product $\mathbf{z}' = \left(\frac{\partial \mathbf{r}}{\partial \xi}\right) \wedge \left(\frac{\partial \mathbf{r}}{\partial \eta}\right)$. The direction $\mathbf{x}'$ can be taken tangent to the $\xi-$direction at the sampling point, or else defined similarly as the direction of $\vec{v}_{1i}$. Finally $\mathbf{y}'$ is obtained as cross product of $\mathbf{z}'$ and $\mathbf{x}'$.

Unit vectors $\mathbf{l}, \mathbf{m}$ and $\mathbf{n}$ can now be associated to the local directions $\mathbf{x}'$, $\mathbf{y}'$ and $\mathbf{z}'$ so that the transformation matrix $\mathbf{S}$ is defined as

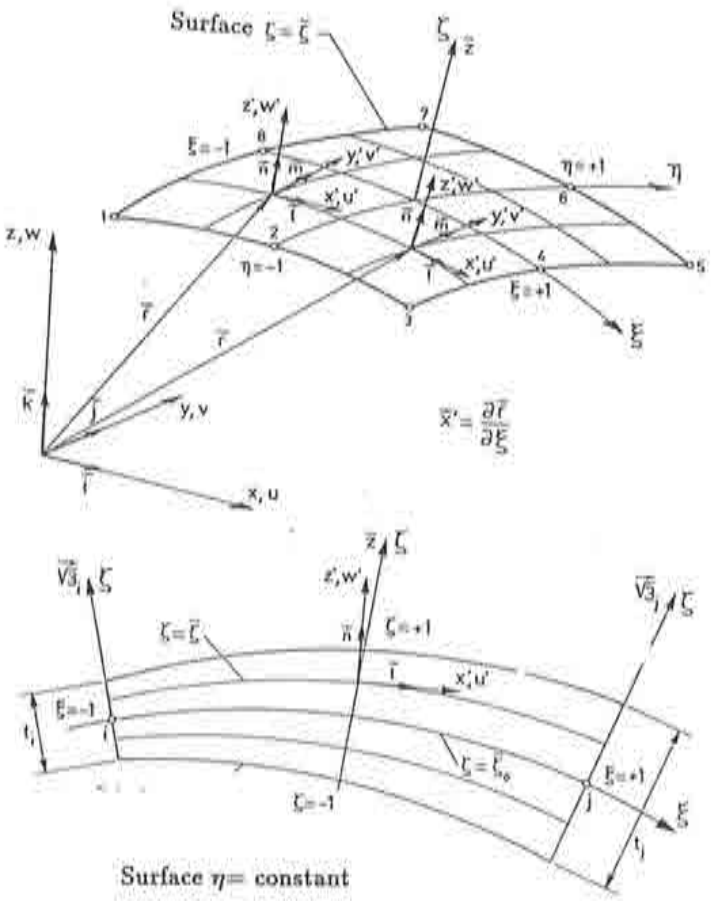

Figure 1.9 Degenerate shell element. Local coordinate system.

$$\mathbf{S} = [\mathbf{l}, \mathbf{m}, \mathbf{n}] \tag{1.32}$$

Element geometry

The geometry of the element can be expressed in terms of the coordinates of the mid surface nodes, $\mathbf{r}_{0_i} = [x_{0_i}, y_{0_i}, z_{0_i}]^T$, and the unit normal at each node, $\mathbf{v}_{3_i}$, as

$$\mathbf{r} = [x, y, z]^T = \sum_{i=1}^{n} N_i(\xi, \eta) \left[\mathbf{r}_{0_i} + \frac{t_i}{2} \zeta \mathbf{v}_{3_i} \right] \tag{1.33}$$

where t_i is the shell thickness of node i.

Displacement field

Taking into account the assumptions of the degeneration process, the displacement field is described by the five degrees of freedom of a "normal"; the three global displacements of its mid–point $\mathbf{u}_{o_i}$ and the two *local* rotations θ_{2_i} and θ_{2_i} (Figure 1.10) as

$$\mathbf{u} = \sum_{i-1}^{n} N_i \left[\mathbf{u}_{o_i}^{(e)} + \frac{t_i}{2} \zeta [-\mathbf{v}_{1_i},\ -\mathbf{v}_{2_i}] \left\{ \begin{matrix} \theta_{1_i} \\ \theta_{2_i} \end{matrix} \right\} \right] = \sum_{i=1}^{n} \mathbf{N}_i \mathbf{a}_i^{(e)} \tag{1.34}$$

with

$$\begin{aligned} \mathbf{N}_i &= [\mathbf{I}_3, \frac{t_i}{2} \zeta \mathbf{C}_i] \\ \mathbf{C}_i &= \left[-\mathbf{v}_{1_i},\ -\mathbf{v}_{2_i} \right] \end{aligned} \qquad \mathbf{a}_i^{(e)} = \left\{ \begin{matrix} u_{o_i} \\ v_{o_i} \\ w_{o_i} \\ \theta_{1_i} \\ \theta_{2_i} \end{matrix} \right\} \tag{1.35}$$

Definition of strains

In order to more easily deal with the shell assumption of zero normal stress in the local z' =direction ($\sigma_{z'} = 0$) the strain components should be defined in the local system of axes x', y', z'. The local system of axes is also the most convenient system for expressing the stress components (and their resultants) for shell analysis and design. The five significant strain components are

$$\boldsymbol{\varepsilon}' = \left\{ \begin{matrix} \varepsilon_{x'} \\ \varepsilon_{y'} \\ \gamma_{x'y'} \\ \cdots\cdots \\ \gamma_{x'z'} \\ \gamma_{y'z'} \end{matrix} \right\} = \left\{ \begin{matrix} \frac{\partial u'}{\partial x'} \\ \frac{\partial v'}{\partial y'} \\ \frac{\partial u'}{\partial y'} + \frac{\partial v'}{\partial x'} \\ \cdots\cdots\cdots\cdots \\ \frac{\partial u'}{\partial z'} + \frac{\partial w'}{\partial x'} \\ \frac{\partial v'}{\partial z'} + \frac{\partial w'}{\partial y'} \end{matrix} \right\} = \left\{ \begin{matrix} \boldsymbol{\varepsilon}'_f \\ \cdots\cdots \\ \boldsymbol{\varepsilon}'_s \end{matrix} \right\} \tag{1.36}$$

where u', v', and w' are the displacement components in the local system x', y', z'. These local derivatives are obtained from the global derivatives of the displacements u, v and w by the following operation

$$\begin{bmatrix} \frac{\partial u'}{\partial x'} & \frac{\partial v'}{\partial x'} & \frac{\partial w'}{\partial x'} \\ \frac{\partial u'}{\partial y'} & \frac{\partial v'}{\partial y'} & \frac{\partial w'}{\partial y'} \\ \frac{\partial u'}{\partial z'} & \frac{\partial v'}{\partial z'} & \frac{\partial w'}{\partial z'} \end{bmatrix} = \mathbf{S}^T \begin{bmatrix} \frac{\partial u}{\partial x} & \frac{\partial v}{\partial x} & \frac{\partial w}{\partial x} \\ \frac{\partial u}{\partial y} & \frac{\partial v}{\partial y} & \frac{\partial w}{\partial y} \\ \frac{\partial u}{\partial z} & \frac{\partial v}{\partial z} & \frac{\partial w}{\partial z} \end{bmatrix} \mathbf{S} \tag{1.37}$$

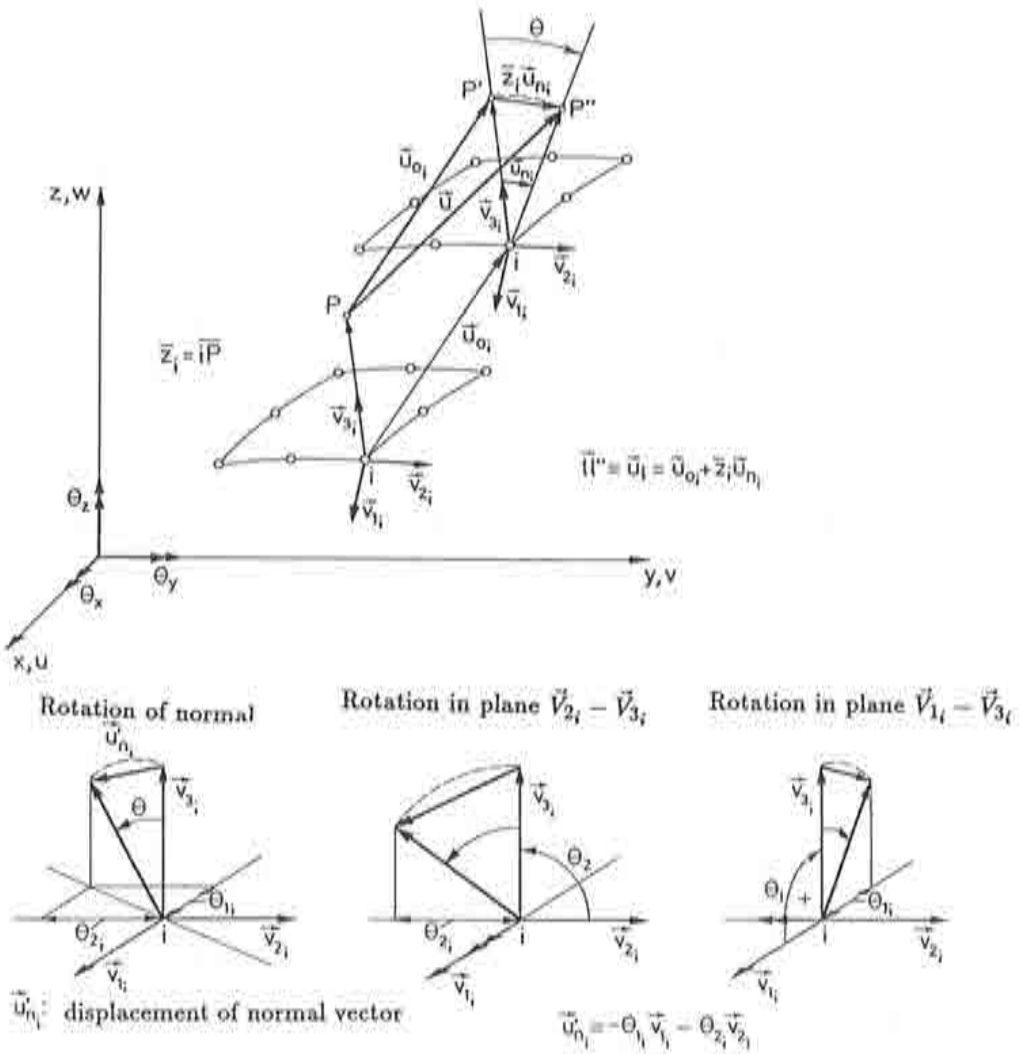

Figure 1.10 Displacement vector. Definitions of local nodal rotations.

where **S** is the transformation matrix defined by (1.32). The derivatives of the displacements with respect the global coordinates are given by

$$\begin{bmatrix} \frac{\partial u}{\partial x} & \frac{\partial v}{\partial x} & \frac{\partial w}{\partial x} \\ \frac{\partial u}{\partial y} & \frac{\partial v}{\partial y} & \frac{\partial w}{\partial y} \\ \frac{\partial u}{\partial z} & \frac{\partial v}{\partial z} & \frac{\partial w}{\partial z} \end{bmatrix} = \mathbf{J}^{-1} \begin{bmatrix} \frac{\partial u}{\partial \xi} & \frac{\partial v}{\partial \xi} & \frac{\partial w}{\partial \xi} \\ \frac{\partial u}{\partial \eta} & \frac{\partial v}{\partial \eta} & \frac{\partial w}{\partial \eta} \\ \frac{\partial u}{\partial \zeta} & \frac{\partial v}{\partial \zeta} & \frac{\partial w}{\partial \zeta} \end{bmatrix} \tag{1.38}$$

where **J** is the jacobian matrix

$$\mathbf{J} = \begin{bmatrix} \frac{\partial x}{\partial \xi} & \frac{\partial y}{\partial \xi} & \frac{\partial z}{\partial \xi} \\ \frac{\partial x}{\partial \eta} & \frac{\partial y}{\partial \eta} & \frac{\partial z}{\partial \eta} \\ \frac{\partial x}{\partial \zeta} & \frac{\partial y}{\partial \zeta} & \frac{\partial z}{\partial \zeta} \end{bmatrix} \tag{1.39}$$

The local strains can therefore be obtained in the following steps.

1) Computation of derivatives of global displacements with respect to coordinates ξ, η, ζ. Using eq.(1.34) we obtain

$$\begin{aligned} \frac{\partial \mathbf{u}}{\partial \xi} &= \left[\frac{\partial u}{\partial \xi}, \frac{\partial v}{\partial \xi}, \frac{\partial w}{\partial \xi}\right]^T = \sum_{i=1}^{n} \frac{\partial N_i}{\partial \xi} \left[\mathbf{I}_3, \ \frac{t_i}{2}\zeta \mathbf{C}_i\right] \mathbf{a}_i^{(e)} \\ \frac{\partial \mathbf{u}}{\partial \eta} &= \left[\frac{\partial u}{\partial \eta}, \frac{\partial v}{\partial \eta}, \frac{\partial w}{\partial \eta}\right]^T = \sum_{i=1}^{n} \frac{\partial N_i}{\partial \eta} \left[\mathbf{I}_3, \ \frac{t_i}{2}\zeta \mathbf{C}_i\right] \mathbf{a}_i^{(e)} \\ \frac{\partial \mathbf{u}}{\partial \zeta} &= \left[\frac{\partial u}{\partial \zeta}, \frac{\partial v}{\partial \zeta}, \frac{\partial w}{\partial \zeta}\right]^T = \sum_{i=1}^{n} N_i \left[\mathbf{0}, \ \frac{t_i}{2}\mathbf{C}_i\right] \mathbf{a}_i^{(e)} \end{aligned} \tag{1.40}$$

2) Computation of $\mathbf{J}^{(e)}$. From (1.39) and (1.33)

$$\begin{aligned} \frac{\partial \mathbf{r}}{\partial \xi} &= \left[\frac{\partial x}{\partial \xi}, \frac{\partial y}{\partial \xi}, \frac{\partial z}{\partial \xi}\right]^T = \sum_{i=1}^{n} \frac{\partial N_i}{\partial \xi} \left[\mathbf{r}_{o_i} + \frac{t_i}{2}\zeta \mathbf{v}_{3_i}\right] \\ \frac{\partial \mathbf{r}}{\partial \eta} &= \left[\frac{\partial x}{\partial \eta}, \frac{\partial y}{\partial \eta}, \frac{\partial z}{\partial \eta}\right]^T = \sum_{i=1}^{n} \frac{\partial N_i}{\partial \eta} \left[\mathbf{r}_{o_i} + \frac{t_i}{2}\zeta \mathbf{v}_{3_i}\right] \\ \frac{\partial \mathbf{r}}{\partial \zeta} &= \left[\frac{\partial x}{\partial \zeta}, \frac{\partial y}{\partial \zeta}, \frac{\partial z}{\partial \zeta}\right]^T = \sum_{i=1}^{n} N_i \frac{t_i}{2} \mathbf{v}_{3_i} \end{aligned} \tag{1.41}$$

3) Computation of $\frac{\partial u}{\partial x}$, $\frac{\partial u}{\partial y}$, etc. by (1.38).

4) Computation of local strain components by (1.37). The strain matrix $\mathbf{B}'$, relating the local strain components to the element nodal variables can then be constructed as

$$\boldsymbol{\varepsilon}' = \mathbf{B}' \mathbf{a}^{(e)} \tag{1.42a}$$

with

$$\mathbf{B}' = \begin{bmatrix} \mathbf{B}'_f \\ \mathbf{B}'_s \end{bmatrix} \tag{1.42b}$$

where as always $(\cdot)_f$ and $(\cdot)_s$ denotes flexural and transverse shear contributions. The form of $\mathbf{B}'$ can be found in [30].

Definition of stresses

Taking into account the assumption of zero normal local stress the five stress components in the local system are (see Figure 1.11)

$$\boldsymbol{\sigma}' = [\sigma_{x'}, \sigma_{y'}, \tau_{x'y'} | \tau_{x'z'}, \tau_{y'z'}]^T = \begin{Bmatrix} \boldsymbol{\sigma}'_f \\ \boldsymbol{\sigma}'_s \end{Bmatrix} \tag{1.43}$$

For elastic analysis a standard constitutive relationship relating stresses and strains can be written in the form [14]

$$\boldsymbol{\sigma}' = \mathbf{D}'(\boldsymbol{\varepsilon}' - \boldsymbol{\varepsilon}'_0) = \mathbf{D}'\mathbf{B}'\mathbf{a}^{(e)} - \mathbf{D}'\boldsymbol{\varepsilon}'_o \tag{1.44}$$

where $\boldsymbol{\varepsilon}'_0$ is an initial strain vector which may represent, for instance, the expansion due to thermal loading. The elasticity matrix $\mathbf{D}'$ is given in eq.(1.7)

If non linear elastoplastic material models are considered the stress-strain relationship is obtained in an incremental form as

$$\mathbf{d}\boldsymbol{\sigma}' = \mathbf{D}'_{ep} d\boldsymbol{\varepsilon}' \tag{1.45}$$

Details of the non linear incremental constitutive matrix $\mathbf{D}'_{ep}$ are given in a latter section and also in Lecture 2.

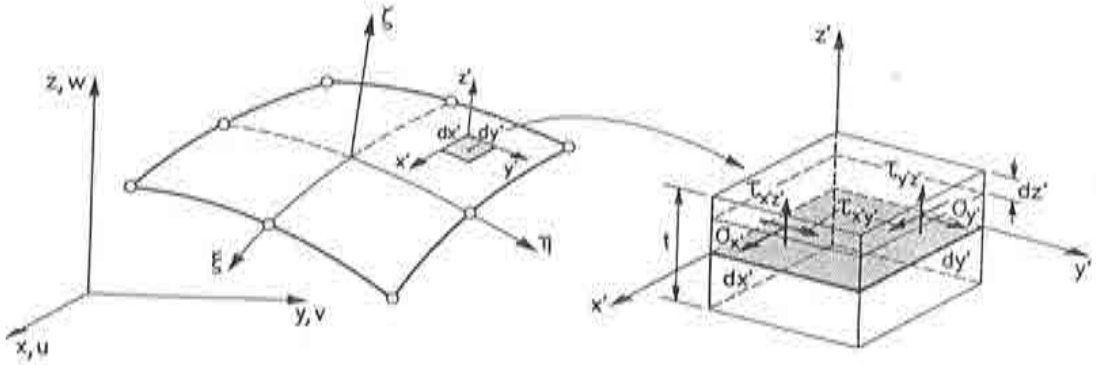

Figure 1.11 Definition of local stresses.

Discretized equilibrium equation

The virtual work expression for a shell element can be written as

$$\int\int\int_{V^{(e)}} \delta\boldsymbol{\varepsilon}'^{T}\boldsymbol{\sigma}' dV = \int\int\int_{V^{(e)}} \delta\mathbf{u}^{T}\mathbf{b} dV + \int\int_{S^{(e)}} \delta\mathbf{u}^{T}\mathbf{t} dS + \sum_{i=1}^{n} \left[\delta\mathbf{a}_i^{(e)}\right]^{T} \mathbf{q}^{(e)} \tag{1.46}$$

where $\mathbf{b}$, $\mathbf{t}$ and $\mathbf{q}$ represent body force surface load and point load vectors respectively. Note that the components of all these vectors are now expressed in global axes.

By adequate substitution of the discretized expressions of displacement and strains the following equation can be obtained, after assembly of all element contributions

$$\boldsymbol{\Psi}' = \int\int\int_{V} \mathbf{B}'^{T}\boldsymbol{\sigma}' dV - \mathbf{f} = \mathbf{0} \tag{1.47}$$

where $\boldsymbol{\Psi}$ is the standard residual force vector, the integral represents the internal force vector and $\mathbf{f}$ is the vector of external loads, which expression for an individual element is given by

$$\mathbf{f}_i^{(e)} = \int\int\int_{V^{(e)}} \mathbf{N}_i^{T}\mathbf{b} dV + \int\int_{S^{(e)}} \mathbf{N}_i^{T}\mathbf{t} dS + \mathbf{q}_i^{(e)} \tag{1.48}$$

For linear elastic analysis eq.(1.47) leads after substituting the constitutive equation (1.44), to the standard expression

$$\mathbf{K}\mathbf{a} = \mathbf{f} \tag{1.49}$$

where $\mathbf{K}$ is the global stiffness matrix obtained by assembly of the individual element contributions given by

$$\mathbf{K}'^{(e)} = \int\int\int_{V^{(e)}} \mathbf{B}'^{T}\mathbf{D}'\mathbf{B}' dV \tag{1.50}$$

The element stiffness matrix can be written using (1.6) and (1.42b) as

$$\mathbf{K}^{(e)} = \int\int\int_{V^{(e)}} \mathbf{B}_f'^{T}\mathbf{D}_f'\mathbf{B}_f' dV + \int\int_{V^{(e)}} \mathbf{B}_s'^{T}\mathbf{D}_s'\mathbf{B}_s' dV = \mathbf{K}_f'^{(e)} + \mathbf{K}_s'^{(e)} \tag{1.51}$$

where $\mathbf{K}_f'$ and $\mathbf{K}_s'$ account respectively for flexural and shear contributions.

Numerical integration, shear and membrane locking and element typology

The computation of the element stiffness matrix involves an integration over the element volume. In the through thickness direction an integration across the element layers is used following the lines previously explained for flat elements.

Shear locking can be eliminated by using an assumed shear strain formulation, similarly as explained for the flat element case [14], [20]. The same element typologies shown in Figure 1.7, could be successfully used for the degenerated shell problem. Amongst those elements the most popular is the 4 node quadrilateral element with an assumed linear shear strain field [20].

It is clearly noticed in the flat shell case that both shear and membrane stiffness are of same order of magnitude. This leads in some curved shell problems to a tendency of the membrane stiffness to dominate the total stiffness yielding wrong results. This deficiency, termed membrane locking, can also be overcome by the same techniques used for the treatement of shear locking i.e. reduced integration of membrane stiffness terms or the use of assumed membrane strains. More information can be found in [19], [20].

Computation of resultant stresses

In degenerate shell elements the stress resultants are obtained "a posteriori" by integrating the corresponding local stress components with respect to the thickness coordinate. By assuming a layer discretization we have

- *Normal forces*

$$[N_{x'}, N_{y'}, N_{x'y'}]^T = \int_{-t/2}^{+t/2} \boldsymbol{\sigma}'_s dz' = \frac{t}{2} \sum_{i=1}^{l} \boldsymbol{\sigma}'_{s_i} \Delta\zeta_i \tag{1.52}$$

- *Bending moments*

$$[M_{x'}, M_{y'}, M_{x'y'}]^T = \int_{-t/2}^{+t/2} z' \boldsymbol{\sigma}'_s dz' = \frac{t^2}{4} \sum_{i=1}^{l} \boldsymbol{\sigma}'_{s_i} \zeta_i \Delta\zeta_i \tag{1.53}$$

- *Shear forces*

$$[Q_{x'}, Q_{y'}]^T = \int_{-t/2}^{+t/2} \boldsymbol{\sigma}'_t dz' = \frac{t}{2} \sum_{i=1}^{l} \boldsymbol{\sigma}'_{t_i} \Delta\zeta_i \tag{1.54}$$

where l is the number of layers, $\boldsymbol{\sigma}'_s = [\sigma_{x'}, \sigma_{y'}, \tau_{x'y'}]^T$ and $\boldsymbol{\sigma}'_t = [\tau_{x'z'}, \tau_{y'z'}]^T$.

THE INCLUSION OF NON LINEAR BEHAVIOUR

Two types of non linear behaviour will be accounted for here. Firstly material non-linearity of concrete (i.e. tensile cracking, compressive crushing, etc.) and reinforced steel (elasto–plastic behaviour) is dealt with on the basis of a general elasto–plastic model. Details of this model are given in next lecture. The second source of non linearity considered is that brought about by changes in the geometrical configuration of the structure.

General numerical procedure for nonlinear analysis

During the general stage of the incremental/iterative solution of a finite element elasto–plastic problem, the equilibrium equations will not be exactly satisfed and a system of residual forces Ψ will exist such that

$$\Psi_i^n = \mathbf{p}_i^n - \mathbf{f}_i^n = \int_V \mathbf{B}'^T \boldsymbol{\sigma}_i'^n dV - \mathbf{f}_i^n \neq 0 \tag{1.55}$$

in which $\mathbf{f}^n$ and $\mathbf{p}^n$ are respectively the external applied force and internal equivalent force vectores, $\mathbf{B}'$ is the strain/displacement matrix (constant for infinitesimal deformation problems). $\boldsymbol{\sigma}'^n$ is the current (local) stress field satisfying the yield condition, V denotes the volume of the shell, the superscript n denotes the load increment number, and subscript i the iteration cycle number within that increment.

An iteration sequence must be performed for each load increment in order to obtain a displacement fiel, $\mathbf{a}_i^n$, which provides a stress field $\boldsymbol{\sigma}_i'^n$ in (1.55) such that the residuals Ψ_i^n vanish. In particular, the displacements are updated at the end of each iteration according to

$$\mathbf{a}_i^n = \mathbf{a}_{i-1}^n + \Delta\mathbf{a}_i^n \tag{1.56}$$

where $\Delta\mathbf{a}_i^n$ denotes the displacement change occuring during the iteration. Several options exist for the choice of the displacement search directions. If the tangential stiffness approach is employed the iterative displacement change is evaluated according to [14], [25]

$$\Delta\mathbf{a}_i^n = -\left[\mathbf{K}_{T_{i-1}}^n\right]^{-1} \Psi_{i-1}^n \tag{1.57}$$

in which $\mathbf{K}_{T_{i-1}}^n$ is the tangential stiffness matrix of the structure evaluated at the beginning of the ith iteration. The updated displacements $\mathbf{a}_i^n$ obtained from (1.56) are used to evaluate the current stresses $\boldsymbol{\sigma}_i'^n$ and hence the residual forces by (1.55). The iteration process is repeated until these residual forces are deemed to be sufficiently close to zero.

It should be noted that assembly and inversion of the full equation system is required for each iteraton. A variant on the above algorithm is offered by

the initial stiffness scheme in which the original structural stiffness matrix $\mathbf{K}^o_{T_o}$ is employed at each stage of the iteration process. This reduces the computational cost per iteration but unfortunately also reduces the rate of convergence of the process. In practice the optimum algorithm is generally provided by updating the stiffnesses at selected iterative intervals only. As an example we could consider two typical possibilities (a) the structural stiffness matrix is updated at the beginning of a load increment and maintained constant during iteration to equilibrium, so that $\mathbf{K}^n_{T_i}$ in (1.57) is replaced by $\mathbf{K}^n_{T_o}$. (b) the stiffnesses are updated after the first iteration of each load incement only (i.e. $\mathbf{K}^n_{T_1}$ is used in (1.57)).

Elasto–plastic stress/strain relations

We will assume here that the behaviour of both concrete and reinforcement steel can be adequately model using elasto–plasticity theory. A discussion on the validity of this assumption is given in Lecture 2.

The yield criterium defines the onset of plasticity and can be written in the general form

$$F(\boldsymbol{\sigma}', \chi) = f(\boldsymbol{\sigma}') - \chi = 0 \tag{1.58}$$

in which χ is a hardening parameter.

The total local strain increment $d\boldsymbol{\varepsilon}'$ is the sum of the elastic and plastic components, so that

$$d\boldsymbol{\varepsilon}' = d\boldsymbol{\varepsilon}'^e + d\boldsymbol{\varepsilon}'^p \tag{1.59}$$

The elastic strains increment $d\boldsymbol{\varepsilon}'^e$ is given by the incremental form of (1.6) and the plastic strain increment by the flow rule

$$d\boldsymbol{\varepsilon}'^p = d\lambda \frac{dQ}{d\boldsymbol{\sigma}'} \tag{1.60}$$

where Q is termed the plastic potencial and $d\lambda$ is a proportional constant. Different forms of the yield criterion and of the form of Q for concrete and reinforcement steel are discussed in next lecture.

The assumption $Q \equiv f$ gives rise to an associated plasticity theory, in which case expression (1.60) is termed the normality (since $\partial f/\partial \boldsymbol{\sigma}$ is a vector directed normal to the yield surface in a stress space)

The differential form of (1.58) can be written

$$\mathbf{a}^T d\boldsymbol{\sigma}' - A d\lambda = 0 \tag{1.61}$$

in which the flow vector a defined by

$$\mathbf{a}^T = \frac{\partial F}{\partial \boldsymbol{\sigma}'} \tag{1.62a}$$

and

$$A = -\frac{1}{d\lambda}\frac{\partial F}{\partial \chi}d\chi \tag{1.62b}$$

Manipulation of (59)–(62) leads to the following elasto–plastic incremental stress–strain relationship, [14]

$$d\boldsymbol{\sigma}' = \mathbf{D}'_{ep}d\boldsymbol{\varepsilon}' \tag{1.63a}$$

with the elastoplastic constitutive matrix given by [14], [25]

$$\mathbf{D}'_{ep} = \mathbf{D}' - \frac{\mathbf{D}'\mathbf{a}\mathbf{a}^T\mathbf{D}'}{A + \mathbf{a}^T\mathbf{D}'\mathbf{a}} \tag{1.63b}$$

The hardening parameter A can be deduced from uniaxial conditions to be

$$A = H' = \frac{d\bar{\sigma}}{d\bar{\varepsilon}_p} \tag{1.64}$$

Thus A is the tangent to the effective stress–plastic strain curve and is a function of the accumulated effective plastic strain $\bar{\varepsilon}_p$ [14], [25].

The tangential stiffness matrix of the material for use in (1.57) can be obtained on use of (1.55) and (1.63a) to be

$$\mathbf{K}_T = \frac{d\mathbf{p}}{d\mathbf{a}} = \int_V \mathbf{B}'^T \frac{d\boldsymbol{\sigma}'}{d\boldsymbol{\varepsilon}'}\frac{d\boldsymbol{\varepsilon}'}{d\mathbf{a}}dV = \int_V \mathbf{B}'^T\mathbf{D}'_{ep}\mathbf{B}'dV \tag{1.65}$$

Further details on the treatment of material non linearity in reinforced concrete structures are given in next lecture.

Geometric nonlinearity

Two basically different formulations can be employed for the description of large deformation problems: (a) A total Lagrangian approach in which the current (2nd Piola Kirchhoff) stress and (Green–Lagrange) strain fields are referred to the original geometric configuration and the displacement field gives the current configuration of the system in relation to its initial position, (b) An updated Lagrangian approach in which the current configuration of the system is used to define the current (Cauchy) stress and (Almansi) strain state. The geometry of the structure is successively updated during the incremental process and the stress and strain fields are referred to the last evaluated configuration. The stress and strain measures employed above are defined in such a way as to be energy conjugates. Both the Green–Lagrange and Almasi strains reduce to the usual definition of engineering strains for

infinitesimal deformation problems. The Cauchy stresses have the usual meaning (i.e. force/unit area in the deformed configuration) but the physical meaning of the Piola–Kirchoff stresses may be lost if significant changes in the original geometry occurs. Transformation of all quantities from a Total Lagrangian formulation to an Updated Lagrangian formulation, and vice–versa, can be perfomed by considering the displacement and strectching of two natural systems of axes [25[, [26].

The most appropiate formulation for numerical solution depends on the type of analysis being considered. For the shell elements defined earlier a specific (and appropiate) total Lagrangian is adopted in which large deflections and moderate rotations (in the sense of the Von Karman hypothesis) are accounted for. Reference of the problem variables to the original configuration is advantageous for quadratic shell elements, since the computationally expensive transfer of quantities between local and global axes need then be performed only one. The strain–displacement matrix is calculated once during the nonlinear process and its nonlinear part is updated using the current displacements by a simple matrix product. The constitutive relations defined previously in terms of engineering stresses and strains are considered valid for the new stress–strain quantities measured in the original configuration.

Taking the variation on (1.55) with respect to a displacement variation $d\mathbf{a}$ gives the tangential stiffness matrix for a geometrically nonlinear problem to be

$$\mathbf{K}_T d\mathbf{a} = d\mathbf{p} = \int_V \mathbf{B}'^T d\boldsymbol{\sigma}' dV + \int_V d\mathbf{B}'^T \boldsymbol{\sigma}' dV \tag{1.66}$$

The strain–displacements matrix $\mathbf{B}'$ may be separated into the usual infinitesimal part $\mathbf{B}'_o$ and nonlinear contributions $\mathbf{B}'_L$ so that

$$\mathbf{B}' = \mathbf{B}'_o + \mathbf{B}'_L \tag{1.67}$$

Consequently $d\mathbf{B}'^T = d\mathbf{B}'^T_L$. Defining the initial stress or geometric stiffness matrix, $\mathbf{K}_\sigma$, as

$$\mathbf{K}_\sigma d\mathbf{a} = \int_V d\mathbf{B}'^T_L \boldsymbol{\sigma}' dV \tag{1.68}$$

then use of (1.6) and (1.68) in (1.66) results in

$$\mathbf{K}_T = \bar{\mathbf{K}} + \mathbf{K}_\sigma \tag{1.69}$$

in which $\bar{\mathbf{K}}$ is given by the usual expression

$$\bar{\mathbf{K}} = \int_V \mathbf{B}'^T \mathbf{D}' \mathbf{B}' dV \tag{1.70}$$

For elasto plastic problems, use of (1.63) in place on (1.6) results in $\mathbf{D}'$ being replaced by $\mathbf{D}'_{ep}$ in (1.70).

Introducing the Von Karman assumptions, which imply that derivatives of u' and v' with respect to x', y' and z' are small, and noting that variation of w' with z' may be negleted, the Green–Lagrange strains may be expressed in local coordinates as

$$\boldsymbol{\varepsilon}' = \begin{bmatrix} \varepsilon_{x'} \\ \varepsilon_{y'} \\ \gamma_{x'y'} \\ \gamma_{x'z'} \\ \gamma_{y'z'} \end{bmatrix} = \begin{bmatrix} \frac{\partial u'}{\partial x'} \\ \frac{\partial v'}{\partial y'} \\ \frac{\partial u'}{\partial y'} + \frac{\partial v'}{\partial x'} \\ \frac{\partial u'}{\partial z'} + \frac{\partial w'}{\partial x'} \\ \frac{\partial v'}{\partial z'} + \frac{\partial w'}{\partial y'} \end{bmatrix} + \begin{bmatrix} \frac{1}{2}\left(\frac{\partial w'}{\partial x'}\right)^2 \\ \frac{1}{2}\left(\frac{\partial w'}{\partial y'}\right)^2 \\ \frac{\partial w'}{\partial x'}\frac{\partial w'}{\partial y'} \\ 0 \\ 0 \end{bmatrix} = \boldsymbol{\varepsilon}'_o + \boldsymbol{\varepsilon}'_L \tag{1.71}$$

The components of the Piola–Kirchhoff stress vector are again given by relation (1.6) but in which the current strains are now taken to be Green–Lagrange strains.

From (1.71), the nonlinear contribution to the strain vector can be written

$$\boldsymbol{\varepsilon}'_L = \frac{1}{2}\mathbf{L}\mathbf{R} \tag{1.72}$$

where

$$\mathbf{L}^T = \begin{bmatrix} \frac{\partial w'}{\partial x'} & 0 & \frac{\partial w'}{\partial x'} & 0 & 0 \\ 0 & \frac{\partial w'}{\partial y'} & \frac{\partial w'}{\partial y'} & 0 & 0 \end{bmatrix} \tag{1.73}$$

and

$$\mathbf{R} = \begin{bmatrix} \frac{\partial w'}{\partial x'} \\ \frac{\partial w'}{\partial y'} \end{bmatrix} = \mathbf{G}\mathbf{a} \tag{1.74}$$

The term $\mathbf{G}$ is a matrix with two rows and a number of columns equal to the total number of element nodal variables. The first row contains the contribution of each nodal variable to the local derivative $\frac{\partial w'}{\partial x'}$ (corresponding shape function derivatives) and the second row contains similar contributions for $\frac{\partial w'}{\partial y'}$.

Taking the variation of (1.72) gives

$$d\boldsymbol{\varepsilon}'_L = \frac{1}{2}d\mathbf{L}\mathbf{R} + \frac{1}{2}\mathbf{L}d\mathbf{R} = \mathbf{L}\mathbf{G}d\mathbf{a} \tag{1.75}$$

and then by definition we have

$$\mathbf{B}'_L = \mathbf{LG} \tag{1.76}$$

In order to determine the tangential stiffness matrix given by (1.69), for use in the nonlinear solution algorithm, it only now remains to explicitly evaluate the geometric matrix, $\mathbf{K}_\sigma$. Substituting from (1.76) in (1.68) results in

$$\mathbf{K}_\sigma d\mathbf{a} = \int_V \mathbf{G}^T d\mathbf{L}^T \boldsymbol{\sigma}' dV \tag{1.77}$$

The term $d\mathbf{L}^T\boldsymbol{\sigma}'$ can be written, with the aid of (1.73) and (1.74), as

$$d\mathbf{L}^T\boldsymbol{\sigma}' = [\boldsymbol{\sigma}']\mathbf{G}d\mathbf{a} \tag{1.78}$$

in which

$$[\boldsymbol{\sigma}'] = \begin{bmatrix} \sigma_{x'} & \tau_{x'y'} \\ \tau_{x'y'} & \sigma_{x'} \end{bmatrix} \tag{1.79}$$

Substituting (1.78) into (1.77) gives the geometric stiffness matrix to be a symmetric matrix of the form

$$\mathbf{K}_\sigma = \int_V \mathbf{G}^T[\boldsymbol{\sigma}']\mathbf{G}dV \tag{1.80}$$

Matrix $\mathbf{G}$ was previously defined in (1.74) and $[\boldsymbol{\sigma}']$ is seen from (1.79) to be composed of components of the current Piola–Kirchhoff stress vector.

Further details of the geometrically non linear solution can be found in [14], [16], [17] and [25]

NONLINEAR FINITE ELEMENT SOLUTION

The flat shell and degenerate shell elements described in previous sections can be effectively employed in the analysis of reinforced concrete shell structures. A layered approach is employed to represent steel reinforcement and to discretize the concrete behaviour through the thickness. Reinforcing steel is represented as a smeared layer of equivalent thickness with (anisotropic) uniaxial strength and rigidity properties. The progress of cracked zones, as well as the compressive behaviour of the concrete is analysed and monitored for each layer and for each element Gauss point. To simplify the data input and also to deal with variable thickness of the structure the layer thickness is defined in terms of the normalised ζ coordinate.

Geometric nonlinearities may play an important role in the behaviour of reinforced concrete beams, plates and shells [27–29]. Even for relatively

small deflections (0.05* thickness) the consideration of nonlinear geometric behaviour may be indispensable for obtaining a correct structural response and collapse load. Disregard of geometric nonlinearity may result either in stiffening or softening of the structure, depending on the particular problem. In this work the Total Lagrangian approach based on the simplified Von Karman strain expressions described in previous section has been adopted.

For the numerical solution, the general nonlinear algorithm itemised in eqs.(55)–(57) is employed. For the present application the essential steps of the process are detailed below.

At the beginning of the nth load increment the displacements $\mathbf{a}^{n-1}$ and the (local) stresses $\boldsymbol{\sigma}'^{n-1}$ are known, as well as the unbalanced nodal forces $\boldsymbol{\Psi}^{n-1}$ resulting from the previous load increment. The incremental nodal forces are calculated according to:

$$\boldsymbol{\Psi}_o^n = \boldsymbol{\Psi}^{n-1} + \Delta \mathbf{f}^n \tag{1.81}$$

where $\boldsymbol{\Psi}^{n-1}$ are the residuals existing at the end of the previous load increment and $\Delta \mathbf{f}^n$ is the nth load increment. Subsequently, the iterative process is performed with the following steps for a generic iteration, i:

1. *The tangent stiffness matrix* $\mathbf{K}_T$ *is updated or not according to the solution algorithm adopted.*

2. *The incremental displacements* $\Delta \mathbf{a}_i$ *are evaluated using the equilibrium equations,*

$$\Delta \mathbf{a}_i = -\left[\mathbf{K}_T\right]^{-1} \boldsymbol{\Psi}_{i-1} \tag{1.82}$$

where $\boldsymbol{\Psi}_{i-1}$ are the unbalanced nodal forces resulting from the previous iteration. The total displacements vector $\mathbf{a}_i$ is then updated.

$$\mathbf{a}_i = \mathbf{a}_{i-1} + \Delta \mathbf{a}_i \tag{1.83}$$

3. *The incremental local strains* $\Delta \boldsymbol{\varepsilon}'_i$ *and the total* $\boldsymbol{\varepsilon}'_i$ *are evaluated.*

$$\Delta \boldsymbol{\varepsilon}'_i = \bar{\mathbf{B}}' \Delta \mathbf{a}_i \tag{1.84}$$

$$\boldsymbol{\varepsilon}'_i = \mathbf{B}' \mathbf{a}_i \tag{1.85}$$

where $\mathbf{B}'$ and $\bar{\mathbf{B}}'$ are updated strain matrices depending on $\mathbf{a}_i$. Note that $\mathbf{B}'$ and $\bar{\mathbf{B}}'$ are equal to the initial strain matrix $\mathbf{B}'_o$ if nonlinear geometrical behaviour is not considered.

4. *The incremental local stresses* $\Delta\boldsymbol{\sigma}_i'$ *and the total local stresses* $\boldsymbol{\sigma}_i'$ *are calculated,*

$$\Delta\boldsymbol{\sigma}_i' = \mathbf{D}'\Delta\boldsymbol{\varepsilon}_i' \tag{1.86}$$

$$\boldsymbol{\sigma}_i' = \boldsymbol{\sigma}_{i-1}' + \Delta\boldsymbol{\sigma}_i' \tag{1.87}$$

where $\mathbf{D}'$ is the elasticity matrix taken as:

- either the elastic matrix of uncracked concrete or the corresponding non linear constitutive matrix of cracked concrete – for concrete layers.
- the elastic or elasto–plastic matrix – for steel layers.

5. *The stresses are corrected according to the material constitutive equations:*

a) *Concrete layers*
For example,for the *elasto–plastic-brittle model* described in the first part of next chapter we will have the following steps.
   * Using the total local stresses $\boldsymbol{\sigma}_i'$, the maximum principal stress σ_i, acting in the structural plane, is calculated.
   * If $\sigma_i > f_t'$ or, if the concrete is already cracked, the stresses are updated according to the tensile modelling (see next chapter)
   * Using $\boldsymbol{\sigma}_i'$ or the stresses updated in the previous step, the effective stress $\bar{\sigma}$ is calculated (according to the yield function).
   * If $\bar{\sigma}$ is greater than the initial yield stress or if the layer has already yielded, the stresses are corrected according to the elasto–plastic behaviour.

(b) *Steel layers*
   * Using the total local stresses $\boldsymbol{\sigma}_i'$, the stresses in the reinforcement direction σ_s is obtained.
   * If σ_s is greater than the steel yield stress f_y, or if the layer has already yielded, the stresses are treated elasto–plastically.

6. *The equivalent internal nodal forces* $\mathbf{p}_i$ *are evaluated using numerical integration, as,*

$$\mathbf{p}_i = \int_V \mathbf{B}'^T \boldsymbol{\sigma}_i' dV \tag{1.88}$$

where $\boldsymbol{\sigma}_i'$ are the total local stress components corrected according to the constitutive equations.

7. *The out of balance residual forces* Ψ_i *are calculated*

$$\Psi = \mathbf{p}_i - \mathbf{f} \tag{1.89}$$

where f is the current external nodal force vector.

8. *The convergence of the process is checked:*

* If convergence has been achieved proceed to the next load increment.
* If the convergence criterion has not been satisfied restart the iterative cycle from step 1.

The size of the load increments, the solution algorithms and the convergence criterion necesary for efficient numerical solution are now discussed below.

Load increment size

To establish the entire deformational response of structures up to collapse load necessitates the use of an incremental procedure in which a reasonable number of load increments must be used, since the solutions are generally path dependent. Comparative analysis have been performed varying the load increment size. It has been observed that the size of the load increments is not a critical parameter in tracing out the deformational response provided that an appropriate solution algorithm is employed.

In general, the size of the load increments used ranges from 0.1 to 0.2 of the structure cracking load. However, values of increment size about 0.5 times the cracking load have produced reasonable results for some cases [17]. In under–reinforced structures refined load increments should be employed during the first spread of cracking.

To obtain the collapse load within narrow limits the size of load increments must be refined when the structure is about to collapse. Use of a restart facility is particularly useful in this respect [17].

Solution algorithm

A detailed reference to the incremental and iterative modified Newton–Raphson scheme employed in solution has been made in previous section. In general, the tangential stiffness matrix is recalculated for the second iteration of each load increment. However, to improve the solution stability, the stiffness matrix is evaluated at stages within a load increment when the change of material characteristics implies a local increase of stiffness. This recalculation has to be performed more frequently during the first spread of cracked zones and also near the collapse load.

Convergence criterion

A convergence criterion is required in order to terminate the iterative cycle when the solution is considered to be sufficiently accurate. In standard non linear finite element analysis a criterion based on the unbalanced nodal forces was adopted. In the analysis of reinforced structures, however, a force convergence criterion may not be the most suitable as the unbalanced forces often form equilibrium groups [27] which do not have much influence on the overall structural response and the solution is not monotonically convergent. Convergence criteria both in terms of out of balance nodal forces and in terms of incremental nodal displacements are therefore more appropriate. However the sole use a displacement convergence criterion, in which displacements and rotations are separately checked, has been favoured in most of the numerical examples analysed to date.

Together with the convergence criterion, a convergence tolerance must be specified to indicate when the results have converged. Higher solution cost and needless accuracy may result from too tight tolerance and on the other hand inaccurate solutions may result if the tolerance adopted is too coarse. Convergence tolerance varying from 0.1 to 1.0 percent are typically employed in practice. Comparative studies performed on some examples [17] have indicated that a tolerance of 2.5 percent is generally sufficient for practical purposes.

A maximum number of iterations for each increment of load is specified to stop the nonlinear solution if meanwhile the convergence limit has not been achieved. It has been observed that a maximum number of about 15 iterations is generally sufficient to detect the solution divergence or collapse, provided the most appropriate solution algorithm has been utilized. Obviously, this maximum number of iterations also depends on the problem and on the specified tolerance, but a maximum number between 10 an 15 for a tolerance of 0.5 percent has been found adequate [17].

REFERENCES

1. ASCE Committee on concrete and masonry structures, Task Committee on Finite Element Analysis of Reinforced Concrete Structures: A State-of-The-Art Report on Finite Element Analysis of Reinforced Concrete Structures, *ASCE Spec. Pub.*, 1981.
2. W.C. Schnobrich, "Behaviour of reinforced concrete structures predicted by the finite element method", *Computers and Structures*, Vol. **7**, pp. 365–376, 1977.
3. J.H. Argyris, G. Faust, J. Szimmat, E.P, Warnke and K.J. Willam, "Recent developments i the finite element analysis of stressed concrete reactor vessels", *Nuclear Engineering and Design*, Vol. **28**, pp. 42–75, 1974.

4. P.G. Bergan and I. Holand, "Nonlinear finite element analysis of concrete structures", *Computer Methods in Applied Mechanics and engineering*, Vol. **17/18**, pp. 443–467, 1979.
5. K.H. Gerstle, "Material modelling of reinforced concrete", Introductory Report, IABSE Colloqiuum on Advanced Mechanics of Reinforced Concrete, Delft. Volume–band 33, pp. 41–63, 1981.
6. D. Nod and A.C. Scordelis, "Finite element analysis of reinforced concrete beams", *American Concrete Institute Jounal*, Vol. **6**, No. 3, March, 1967.
7. L. Cedolin and S. Deipoli, "Finite element studies of shear–critical R/C beams, *ASCE Journal of th Engineering Mechanics Division*, Vol. **103**, No. EM3, pp. 395–410, Jue 1977.
8. M.N. Fardis and O. Buyukoztuk, "Shear stiffness of concrete by finite elements", *ASCE Journal pf the Structural Division*, Vol. **106**, No. ST6, pp. 1311–1327, June 1980.
9. Z.P. Bazant and L. Cedolin, "Fracture mechanics of reinforced concrete", *ASCE Journal of Eng. Mech. Division*, Vol. **106**, No.EM6, pp. 1287–13106, Decembe, 1980.
10. C.S. Lin, "Nonlinear analysis of reinforced concrete slabs and shells", PhD. Thesis, UC-SESM 73–7, university of California, April 1973.
11. F.R. Hand, D.A. Pecknold and W.C. Schnobrich, "Nonlinear layered analysis of RC Plates and Shels, *ASCE Journal of Structural Division,* Vol. **99**, No. ST7, pp. 1491–1503, July, 1973.
12. G. Mueller, "Numerical problems in nonlinear analysis of reinforcd concrete", report No. UC-SESM 77-5, University of California, Berkeley, September, 1977.
13. H.H.A. Rahman, "Computational models for the nonlinear of reinforced concrete flexural slab systems", Ph. D Thesis, C7Ph/66/82, University of Wales, May, 1982.
14. O.C. Zienkiewicz, and R.L. Taylor, "*The Finite Element Method*", Fourth Edtion Mc.Graw Hill, Vol. I (1989), Vol II (1991).
15. M. Crisfield, "*Finite Element Method and Solution Procedures for Structural Analysis*", Pineridge Press, 1986.
16. J.A. Figueiras and D.R.J. Owen, "Analysis of elasto–plastic and geometrically non linear anisotropic plates and shells" In Finite Element Software for Plates and Shells, E. Hinton and D.R.J. Owen (Eds.), Pineridge Press, 1984.
17. D.R.J. Owen and J.A. Figueiras, "Ultimate load analysis of reinforced concrete plates and shells", In Finite Element Software for Plates and Shells, E. Hinton and D.R.J. Owen (Eds.), Pineridge Press, 1984.
18. Zienkiewcz, O.C., Qu, S., Taylor, R.L. y Nakazawa,S., "The Patch test for mixed formulations", *Int. J. Num. Meth. Eng.*, Vol. **23**, pp. 1873–1883, 1986.

19. Huang, H.C. y Hinton, E., "A new nine node degenerated shell element with enhanced membrane and shear interpolation", *Int. J. Num. Meth. Eng.*, Vol. **22**, pp. 73–92, 1986.
20. H.C. Huang, "*Static and Dynamic Analysis of Plates and Shells*", Springer Verlag, 1989.
21. E. Oñate, O.C. Zienkiewicz, B. Suárez, and R.L. Taylor, "A methodology for deriving shear constrained Reissner-Mindlin plate elements", A publicarse en *Int. Journal Numerical Methods Eng.*, 1991.
22. E. Reissner, "The effect of transverse shear deformation on the bending of elestic plates", *J. Appl. Mech.*, Vol. **12** pp. 69–76, 1945.
23. R.D. Mindlin, "Influence of rotatory inertia and shear in flexural motions of isotropic elastic plates", *J. Appl. Mech.*, Vol. **18**, pp. 31–38, 1951.
24. E.N. Dvorkin and K.J. Bathe, "A continuum mechanics based four node shell element for general non-linear analysis", *Eng. Comp.*, Vol. **1**, pp. 77–88, 1984.
25. K.J. Bathe, '*Finite Element procedures in engineering analysis*", Prentice Hall Inc., 1982.
26. Y.C. Fung, "*Fundations of solid mechanics*", Prentice Hall Inc. 1965.
27. P.G. Bergan and I. Holand, "Nonlinear finite element analysis of concrete structures", *Computer Methods in Applied Mechanics and Engineering*, Vol. **17/18**, pp. 443–467, 1979.
28. K.H. Gerstle, "Material modelling of reinforced concrete", Introductory Report, IABSE Colloqiuum on Advanced Mechanics of Reinforced Concrete, Delft. Volume–band 33, pp. 41–63, 1981.
29. H.A. Mang and H. Floegl, "Tension stiffening concept for reinforced concrete surface structres", IABSE Colloquium on Advanced Mechanics of Reinforced Concrete, final Report, pp. 351–369, Delft, June, 1981.
30. Oñate, E., *Análisis de Estructuras por el método de elementos finitos*, CIMNE, Barcelona, 1992.

LECTURE 2

MATERIAL MODELLING OF CONCRETE AND STEEL FOR ANALYSIS OF REINFORCED/PRESTRESSED CONCRETE SHELLS

SUMMARY

This lecture describes the constitutive behaviour of concrete and steel in a form suitable for numerical computations using the finite element layered shell models described in Lecture 1.

INTRODUCTION

Extensive experimental studies have been undertaken to characterise the response and ultimate strength of plain concrete under multiaxial stress states [1,2]. Considerable scatter of results has been observed and collaborative studies have been undertaken to identify the principal factors influencing this variation [3]. Several approaches, based on experimental data, have been used to represent the constitutive relationship of concrete under multiaxial stress states and these can be categorised into the four following groups: (a) Linear and nonlinear elasticity theories, [4–7] (b) perfect and workhardening plasticity theories [8–10], (c) endochronic theory of plasticity [11] and (d) plastic fracturing theory [12]. Experimental evidendence indicates that the nonlinear deformation in concrete is basically inelastic and therefore the stress-strain behaviour may be separated into recoverable and irrecoverable components. The irrecoverable strain components may either be treated within the classical theory of plasticity or by using a time dependent viscoplastic model.

In this lecture two conceptualy different concrete models are presented in the framework of the layered shell formulations described in previous lecture. The first model is based on elasto–plastic theory to model the compressive behaviour of the concrete whereas a linear orthotropic elasto–brittle model

is used for modelling the cracking behaviour under tensile conditions [18]. This model will be termed hereafter *Elasto–Plastic–Brittle–Model*.

The second model is based on the assumptions that *both* the tensile and compressive behaviour of concrete can be treated under the unified framework of elastoplasticity theory. We will refer to this model as *Plastic–Damage–Model*.

Both concrete models are described in next sections together with a simpler elasto–plastic model for the reinforcing steel bars.

ELASTO–PLASTIC–BRITTLE CONCRETE MODEL

Most of the concepts presented in this section have been taken from the work of Owen and Figueiras [18].

Basic assumptions

The model is based on the following assumptions:

Compressive behaviour

Concrete is assumed to behave as an standard elasto–plastic material under compressive situations. High compression strains induce concrete crushing and this has to be appropriately taken into account in the model.

Tensile behaviour

A linear elastic model is assumed until the maximum tensile stress is reached. The stress evolution after cracking is characterised by the orthotropic versions of eqs.(1.7) of previous lecture.

Both compressive and tensile behaviour models are detailed next.

Compressive behaviour of concrete

The following three conditions have to be considered in establishing the nonlinear stress–strain relations, based on the flow theory of plasticity: (a) The yield criterion, (b) the flow and hardening rules and (c) the crushing condition. The yield criterion for concrete under a triaxial stress state is generally assumed to be dependent on the three stress invariants [13–15]. Nevertheless practical formulations have been developed wich employ either one [16] or two [9,17] stress invariants only. A dependence of the yield function on the mean normal stress I_1 (or σ_{oct}) and the shear stress invariant J_2 (or τ_{oct}) has proved to be adequate for most situations. The plastic volume dilatation observed near failure, under pressure conditions,

can also be modelled by the dependence of the yield function on the first stress invariant.

The yield condition

In the present analysis of thick plates and shells, transverse shear effects are taken into account and therefore a triaxial yield criterion must be employed. This criterion is formulated in terms of the first two stress invariants and only two material parameters are involved in its definiton.

$$f(I_1, J_2) = [\beta(3J_2) + \alpha I_1]^{1/2} = \sigma_o \tag{2.1}$$

where α and β are material parameters and σ_o is the equivalent effective stress taken as the compressive stress from an uniaxial test. In terms of principal stresses the expression for yielding can be written

$$\beta[(\sigma_1^2 + \sigma_2^2 + \sigma_3^2) - (\sigma_1\sigma_2 + \sigma_1\sigma_3 + \sigma_2\sigma_3)] + \alpha(\sigma_1 + \sigma_2 + \sigma_3) = (\sigma_0)^2 \tag{2.2}$$

The Huber-Mises yield condition is recovered by assuming $\alpha = 0$ and $\beta = 1.0$.

The stress state in thick plates and shells is usually not far from a biaxial one, since the stress normal to the middle plate ($\sigma_{z'}$) is neglected. Therefore, it is reasonable to obtain the material parameters by fitting test results. The uniaxial compression and the biaxial test under equal compression stresses ($\sigma_1 = \sigma_2$) are used to define these constants. For practical purposes a relation can be assumed between the equal biaxial yield stress (or strength), f_{cb}, and the uniaxial yield stress (or strength), f_c'.

$$f_{cb} = 1.16(\text{to } 1.20) f_c' \tag{2.3}$$

In such cases, the yield condition is a function of only one material parameter ($\sigma_o = f_c'$) which is the most reliable constant to characterize the concrete behaviour and is easily obtainable from experimental tests. If Kupfer's results [1] are employed, $f_{cb} = 1.16 f_c'$, then use of (2.2) gives

$$\begin{aligned} \alpha &= 0.355\sigma_o \\ \beta &= 1.355 \end{aligned} \tag{2.4}$$

and (2.1) can be written in terms of the stress components* as

$$\begin{aligned} f(0) = \Big\{ 1.355[(\sigma_x^2 + \sigma_y^2 + \sigma_x\sigma_y) + 3(\tau_{xy}^2 + \tau_{xz}^2 + \tau_{yz}^2)] + \\ + 0.355\sigma_o(\sigma_x + \sigma_y)] \Big\}^{\frac{1}{2}} = \sigma_o \end{aligned} \tag{2.5}$$

* Note: From now onwards we will drop the prime superindex $(\cdot)'$ to distinguish local stresses. It will therefore be assumed that all stresses are refered to local axes of each element layer.

This expression is compared in Figure 2.1 whith the experimental results of Kupfer et al [1] in biaxial stress space. In the perfectly plastic model σ_o is taken as the ultimate stress f'_c obtained from an uniaxial compression test. An elastic respose is assumed up to the effective stress value $\sigma_o = f'_c$ after which a perfectly plastic response follows until the crushing surface is reached. In the strain–hardening model the initial yield surface is attained when the effective stress reaches 30 percent of the peak stress f'_c. The subsequent loading surfaces $f(\sigma) = \sigma_o(\chi)$ are functions of the hardening parameter χ defined by the hardening rule expressed in terms of the effective plastic strains as shown in a latter section. When the effective stress, defined by the yield function, reaches the ultimate stress f'_c a perfectly plastic response is assumed until the crushing surface is encountered.

Figure 2.2 illustrates the one dimensional representation of both the perfectly plastic and the strain–hardening model. The tensile behaviour, to be discussed later, is also represented. The two dimensional representation in the principal stress space is shown in Figure 2.3. For the strain–hardening model, once the initial yield surface has been reached, subsequent loading will produce plastic straining which caracterizes the corresponding level of effective stress or loading surface. Unloading follows the initial elastic modulus E_o and an elastic reponse occurs for subsequent loading until the corresponding loading surface is reached. Further loadig causes an elasto–elastic response with increasing plastic deformation and a corresponding expansion of the loading surface according to the hardening rule.

The flow rule

To construct the stress–strain relationship in the plastic range, the normality of the plasticity deformation rate vector to the yield surface is commonly assumed. This associated flow rule is considered for concrete predominantly for practical reasons, since there is very little supportive experimental evidence available [19]. The plastic strain increment is then defined [20,21] as

$$d\varepsilon^p_{ij} = d\lambda \frac{\partial f(\sigma)}{\partial \sigma_{ij}} \tag{2.6}$$

where $d\lambda$ is a proportionality constant which determines the magnitude of the plastic strain increment, and the gradient $\frac{\partial f(\sigma)}{\partial \sigma_{ij}}$, defines its direction to be perpendicular to the yield surface. The current stress function $f(\sigma)$ is the yield condition; or the subsequent loading functions in the strain hardening model.

Formulation of the elasto–plastic constitutive matrix $\mathbf{D}'_{ep}$ follows an identical procedure to that described in the previous lecture.

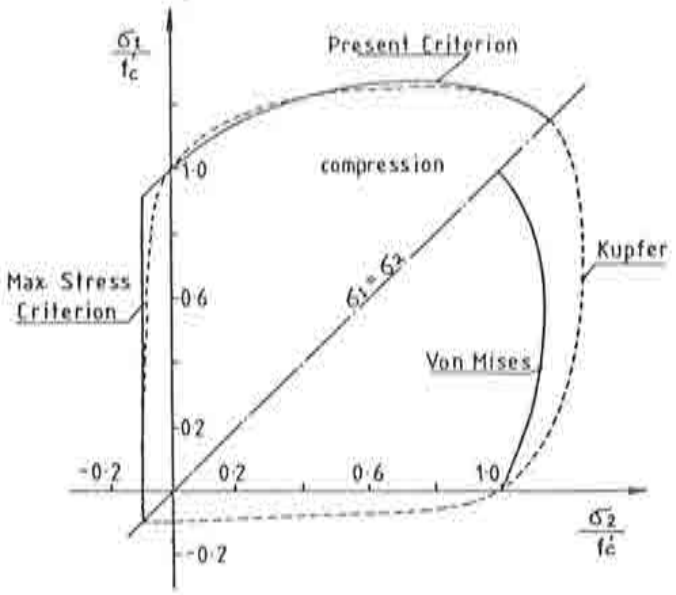

Figure 2.1 Yield condition for elasto–plastic analysis of concrete.

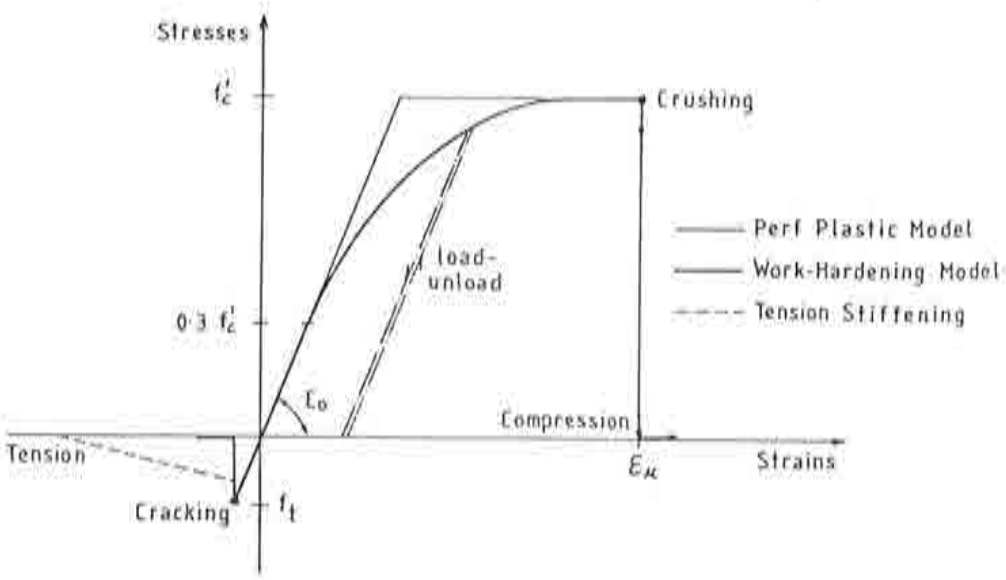

Figure 2.2 One–dimensional representation of the concrete constitutive model.

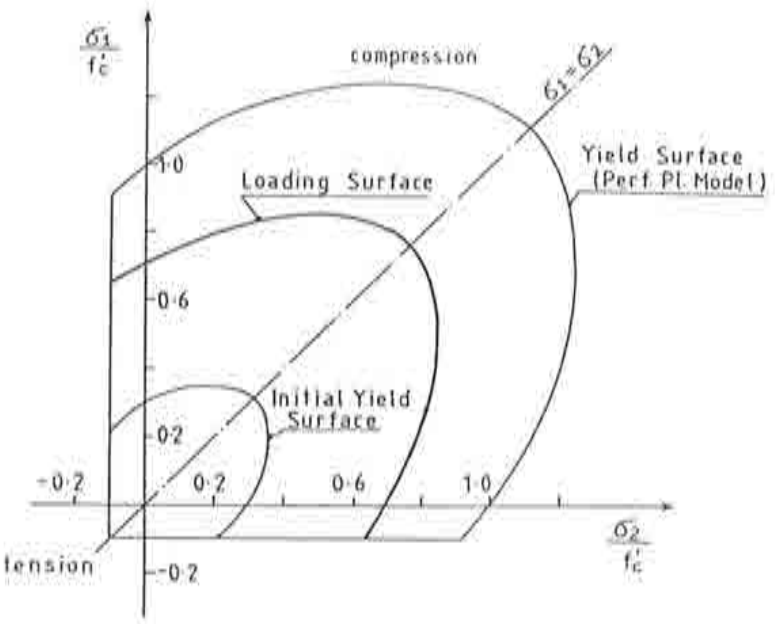

Figure 2.3 Two dimensional stress space representation of the concrete constitutive model.

The yield function derivatives which define the flow vector a take the following explicit expressions for the yield surface given by (2.5)

$$\mathrm{a}^T = \left[\frac{\partial f}{\partial \sigma_x}, \frac{\partial f}{\partial \sigma_y}, \frac{\partial f}{\partial \tau_{xy}}, \frac{\partial f}{\partial \tau_{xz}}, \frac{\partial f}{\partial \tau_{yz}}\right]$$

$$a_1 = \frac{\partial f}{\partial \sigma_x} = \frac{[2(c^2+\beta)\sigma_x + (2c^2-\beta)\sigma_y]}{\mathrm{CONST}} + c \tag{2.7}$$

$$a_2 = \frac{\partial f}{\partial \sigma_y} = \frac{[2(c^2+\beta)\sigma_y + (2c^2-\beta)\sigma_y]}{\mathrm{CONST}} + c$$

$$a_3 = \frac{\partial f}{\partial \tau_{xy}} = \frac{6\beta\tau_{xy}}{\mathrm{CONST}} \tag{2.8}$$

$$a_4 = \frac{\partial f}{\partial \tau_{xz}} = \frac{6\beta\tau_{xz}}{\mathrm{CONST}}$$

$$a_5 = \frac{\partial f}{\partial \tau_{yz}} = \frac{6\beta\tau_{yz}}{\mathrm{CONST}}$$

where $c = \alpha/(2\sigma_o)$ (equal to 0.1775 for Kupfer's results), α and β are material constants previously defined, and

$$\begin{aligned}\text{CONST} = 2[&(c^2+\beta)\sigma_x^2 + (c^2+\beta)\sigma_y^2 + (2c^2-\beta)\sigma_x\sigma_y + \\ &+ 3\beta(\tau_{xy}^2 + \tau_{xz}^2 + \tau_{yz}^2)]^{\frac{1}{2}}\end{aligned} \tag{2.9}$$

The hardening rule

The hardening rule defines the motion of the subsequent yield surface (the loading surfaces) during plastic deformation. It determines the relation between the loading surfaces $f(\sigma, \chi)$ (or effective stress) and the accumulated plastic strain (or effective plastic strain). The concept of effective stress and effective plastic strain makes it possible to extrapolate from a simple uniaxial test to the multiaxial situation. In the present work the relation between effective stress and effective plastic strain is extrapolated from the uniaxial stress–strain relation ship using the conventional "expression"

$$\sigma = E_o\varepsilon - \frac{1}{2}\frac{E_o}{\varepsilon_o}\varepsilon^2 \tag{2.10}$$

where

E_o is the initial elasticity modulus
ε is the total strain
ε_o is the total strain at peak stress f_c'

Substituting the elastic strain component $\varepsilon_e = \sigma/E_o$ in (2.10) we obtain

$$\sigma = -E_o\varepsilon_p + \sqrt{2E_o^2\varepsilon_o\varepsilon_p}; \qquad 0.3f_c' < \sigma \leq f_c' \tag{2.11}$$

where ε_p is the plastic strain component, and ε_o can be taken equal to $2f_c'/E_o$ for normal concrete. Using the current effective plastic strain in expression (2.11), gives the effective stress level $\sigma = \sigma_o$ defining the current loading surface position.

The crushing condition

The crushing type of concrete fracture is a strain controled phenomenon. The lack of available experimental data on concrete ultimate–deformation capacity under multiaxial stress states has resulted in the appropriate strain criterion being developed by simply converting the yield criterion described in terms of stresses directly into strains. Thus

$$\beta(3J_2') + \alpha I_1' = \varepsilon_u^2 \tag{2.12}$$

where I_1' and J_2' are strain invariants [17] and ε_u is an ultimate total strain extrapolated from uniaxial test results. Using the material parameters α and

β determined from Kupfer's results [1], the crushing condition is expressed in terms of the total strain components as

$$\begin{aligned} &1.355[(\varepsilon_x^2 + \varepsilon_y^2 - \varepsilon_x\varepsilon_y) + 0.75(\gamma_{xy}^2 + \gamma_{xz}^2 + \gamma_{yz}^2)] \\ &+ 0.355\varepsilon_u(\varepsilon_x + \varepsilon_y) = \varepsilon_u^2 \end{aligned} \tag{2.13}$$

when ε_u reaches the value specified as the ultimate strain, the material is assumed to lose all its characteristics of strength and rigidity.

Elasto–brittle tensile behaviour of concrete

The reponse of concrete under tensile stresses is assumed to be linear elastic until the fracture surface is reached and its behaviour is characterised by the isotropic versions of relations (1.7) of the previous lecture. The tensile type of fracture, or cracking, is governed by a maximum tensile stress criterion (tension cut–off). Cracks are assumed to form in planes perpendicular to the direction of maximum principal tensile stress as soon as this stress reaches the specified concrete tensile strength f_t'. In order to avoid further complexities, cracks are assumed to form only in planes perpendicular to the structural plane (x', y' plane). After cracking has occurred, the elasticity modulus and Poisson's ratio are reduced to zero in the direction perpendicular to the cracked plane, and a reduced shear modulus is employed. Taking 1 and 2 as the two principal directions in the plane of the structure, the stress–strain relationship for concrete cracking in the 1 direction, is

$$\begin{bmatrix} \sigma_1 \\ \sigma_2 \\ \tau_{12} \\ \tau_{13} \\ \tau_{23} \end{bmatrix} = \begin{bmatrix} 0 & 0 & 0 & 0 & 0 \\ 0 & E & 0 & 0 & 0 \\ 0 & 0 & G_{12}^c & 0 & 0 \\ 0 & 0 & 0 & G_{13}^c & 0 \\ 0 & 0 & 0 & 0 & \frac{5G}{6} \end{bmatrix} \begin{bmatrix} \varepsilon_1 \\ \varepsilon_2 \\ \gamma_{12} \\ \gamma_{13} \\ \gamma_{23} \end{bmatrix} \tag{2.14}$$

When the tensile stress in the 2 direction reaches the value f_t' a second cracked plane perpendicular to the first one is assumed to form, and the stress–strain relationship becomes:

$$\begin{bmatrix} \sigma_1 \\ \sigma_2 \\ \tau_{12} \\ \tau_{13} \\ \tau_{23} \end{bmatrix} = \begin{bmatrix} 0 & 0 & 0 & 0 & 0 \\ 0 & 0 & 0 & 0 & 0 \\ 0 & 0 & G_{12}^c/2 & 0 & 0 \\ 0 & 0 & 0 & G_{13}^c & 0 \\ 0 & 0 & 0 & 0 & G_{23}^c \end{bmatrix} \begin{bmatrix} \varepsilon_1 \\ \varepsilon_2 \\ \gamma_{12} \\ \gamma_{13} \\ \gamma_{23} \end{bmatrix} \tag{2.15}$$

The cracked concrete is anisotropic and these relations must be transformed to the reference axes $x'y'$.

In the analysis and design of reinforced concrete plates and shells we are not directly interested in the tensile strength of the concrete, which is relatively small and unreliable, but in the influence of the cracked concrete zones on the structural behaviour. Therefore a simplified averaging process more convenient for finite element formulation is used. A smeared representation for cracked concrete is assumed, which implies that cracks are not discrete but distributed across a region of the finite element.

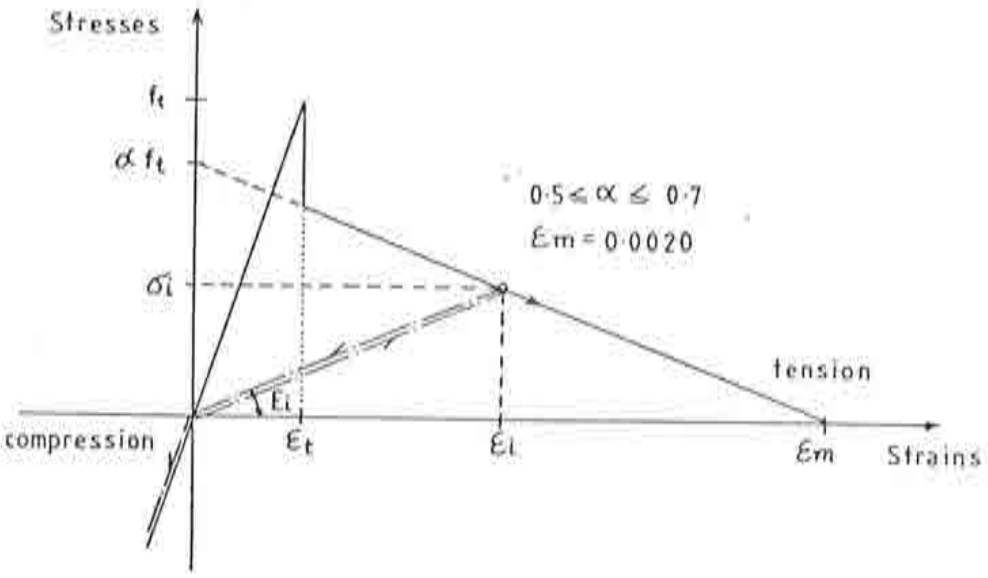

Figure 2.4 Loading and unloading behaviour of cracked concrete illustrating tension sttiffening behaviour.

Tension stiffening

Due to bond effects, cracked concrete carries between cracks, a certain amount of tensile force normal to the cracked plane. The concrete adheres to the reinforcing bars and contributes to the overall stiffness of the structure [22]. Several approaches based on experimental results have been employed to simulate this tension stiffening behaviour [8,23–25]. A gradual relase of the concrete stress component normal to the cracked plane (Figure 2.4) is adopted in this work. The process of loading and unloading of cracked concrete is also illustrated in Figure 2.4. Unloading and reloading of cracked concrete is assumed to follow the linear behaviour shown with a fictitious elasticity modulus E_i given by

$$E_i = \alpha f_t' \frac{\left(\frac{1-\varepsilon_i}{\varepsilon_m}\right)}{\varepsilon_i}; \qquad \varepsilon_t \leq \varepsilon_i \leq \varepsilon_m \tag{2.16}$$

where α, ε_m are tension stiffening parameters (Figure 2.4) and ε_i is the maximum value reached by the tensile strain at the point considered. If the crack closes, i.e. if the strain component normal to the crack plane becomes negative, the concrete acquires the uncracked behaviour in the corresponding direction, but the crack direction and the maximum tensile strain continue to be stored. The value ε_i can be readily modified to simulate bond deterioration during reloading. The normal stress σ_1 (and or σ_2) is obtained by the following expression (Figure 2.4)

$$\sigma_1 = \alpha f_t' \left(\frac{1 - \varepsilon_1}{\varepsilon_m} \right), \qquad \varepsilon_t \leq \varepsilon_1 \leq \varepsilon_m \tag{2.17}$$

or by,

$$\sigma_1 = \frac{\sigma_i \varepsilon_1}{\varepsilon_i}, \qquad \text{if} \qquad \varepsilon_1 < \varepsilon_i \tag{2.18}$$

where ε_1 is the current tensile strain in material direction 1.

A layered approach is used to discretize the structure through the thickness and for each layer different material propierties can be specified. A modified tension stiffening diagram can be employed for those which are relatively distant from reinforcing bars. Particularly, the tension stiffening effect can be negleted ($\alpha = 0$ for $0 < \varepsilon_m < \varepsilon_t$) in layers where the steel cannot supply tensile stresses due to the particular reinforcing arrangement. The value of f_t' should be taken as the modulus of rupture of the concrete. This modulus can be related to the uniaxial compression strength [26] by

$$f_r = 0.62 (f_c')^{1/2} \tag{2.19}$$

where f_r and f_c' are expressed in MPa. However experimental tests have shown large variations in the above coefficient. The tension stiffening constant α in Figure 2.4 is taken equal to 0.5, 0,6 or 0.7 depending on the relative percentage of steel in the section. However the change in structural behaviour with this variation is generally small and a constant value of $\alpha = 0.6$ could be used. For the tension stiffening constant, ε_m, a fixed value of 0.002 is employed.

Cracked shear modulus

Experimental results indicate that a considerable amount of shear stress can be transferred across the rough surfaces of cracked concrete [27–29]. Also, the dowel action of steel bars contribute to the shear stiffness across cracks [27]. These tests have shown that the primary variable in the shear transfer mechanism is the crack width, although aggregate size, reinforcement ratio and bar size also have an influence. A common procedure to account for aggregate interlock and dowel action in a smeared cracking model is to

attribute an appropriate value to cracked shear modulus G^c [30,31]. We present here an approach similar to that used in reference [30] is adopted, where the cracked shear modulus is assumed to be a function of the current tensile strain. For concrete cracked in the 1 directon

$$\begin{aligned} G^c_{12} &= 0.25 * G\left(\frac{1-\varepsilon_1}{0.04}\right); \qquad G^c_{12} = 0 \quad \text{if} \quad \varepsilon_1 \geq 0.004 \\ G^c_{13} &= G^c_{12} \\ G^c_{23} &= \frac{5G}{6} \end{aligned} \tag{2.20}$$

where G is the uncracked concrete shear modulus and ε_1 is the tensile strain in the 1 direction. For concrete cracked in both directions,

$$\begin{aligned} G^c_{13} &= 0.25 * G\left(\frac{1-\varepsilon_1}{0.004}\right); \qquad G^c_{13} = 0 \quad \text{if} \quad \varepsilon_1 \geq 0.004 \\ G^c_{23} &= 0.25 * G\left(\frac{1-\varepsilon_2}{0.004}\right); \qquad G^c_{23} = 0 \quad \text{if} \quad \varepsilon_2 \geq 0.004 \\ G^c_{12} &= 0.5 * G^c_{13}; \quad \text{or } G^c_{12} = 0.5 * G^c_{23} \qquad \text{if} \quad G^c_{23} = G^c_{13} \end{aligned} \tag{2.21}$$

If the crack closes the uncracked shear modulus G is again assumed in the corresponding direction

A PLASTIC DAMAGE MODEL FOR NON LINEAR ANALYSIS OF CONCRETE

Introduction

Classical models for non–linear analysis of concrete assume elasto–plastic (or viscoplastic) constitutive equations for compression behaviour, whereas a conceptually more simple elasto–brittle model is used for defining onset and progression of cracks at points in tension. Different versions of this model which has been detailed in previous section have been successfully used by different authors for non–linear analysis of plain and reinforced concrete structures [2–31].

The elasto–plastic–brittle model, in spite of its popularity, presents various controversial features such as the need for defining uncoupled behaviour along each principal stress (or strain) direction: the use of a shear retention factor to ensure some shear resistence along the crack; the lack of equilibrium at the cracking point when more than one crack is formed [33]; the difficulties in defining stress paths following the opening and closing of cracks under cycling loading conditions and the difficulty for dealing with the combined effect of cracking an plasticity at the damaged point.

It is well known that microcracking in concrete takes place at low load levels due to physical debonding between aggregate and mortar particles, or to simple microcracking in the mortar area. Cracking progresses following a non-homogeneous path which combines the two mentioned mechanisms with growth and linking between microckacks along different directions. Experiments carried out on mortar specimens shown that the distribution of microcracking is fairly discontinuos with arbitrary orientations [32]. This fact is supported by many experiments which shown that *cracking can be considered, at microscopic level, as a non-directional phenomenon* and that the propagation of microcraks at aggregate level follows an erratic path which depends on the size of the aggregate particles. Thus, the *dominant cracking directions can be interpreted at macroscopic level as the locus of trajectories of the damage points* (Figure 2.5).

The above concepts support *the idea that the nonlinear behavior of concrete can be modelled using concepts of classical plasticity theory* only provided an adequate yied functions is defined for taking into account the different response of concrete under tension and compression states. Cracking can, therefore, be interpreted as a *local damage effect*, defined by the evolution of known material parameters and by a single yield function which controls the onset and evolution of damage.

One of the advantages of such a model is the independence of the analysis with respect to crack directions which can be simply identified *a posteriori* from the converged values of the nonlineal solution. This allows to overcome the problems associated to most elastic-plastic-brittle smeared cracking models such as the need for an uncoupled constitutive equation along each cracking direction, the use of an arbitrary defined shear retention factor, the lack of equilibrium in the damage points when more than one crack is formed [33], the difficulty of defining stress paths at the crack under complex loading/unloading conditions and the difficulty of combining cracking and plasticity phenomena at the damage points.

In this work an elastoplastic model developed by the author's group for nonlinear analysis of concrete based on the concepts of *plastic damage* mentioned above is presented [34-35]. The model takes into account all the important aspects which should be considered in the nonlinear analysis of concrete, such as the different response under tension and compression, the effect of stiffness degradation and the problem of objectivity of the results with respect to the finite element mesh.

The layout of this section is as follows. First, details of the yield function and the evolution laws of all material parameters are given. Secondly, the effects of elastic and plastic stiffness degradations are briefly described. Then, the *problem of mesh objectivity* and the *a posteriori* determination of cracking is presented. Examples of applications of this model are given in Lecture 4.

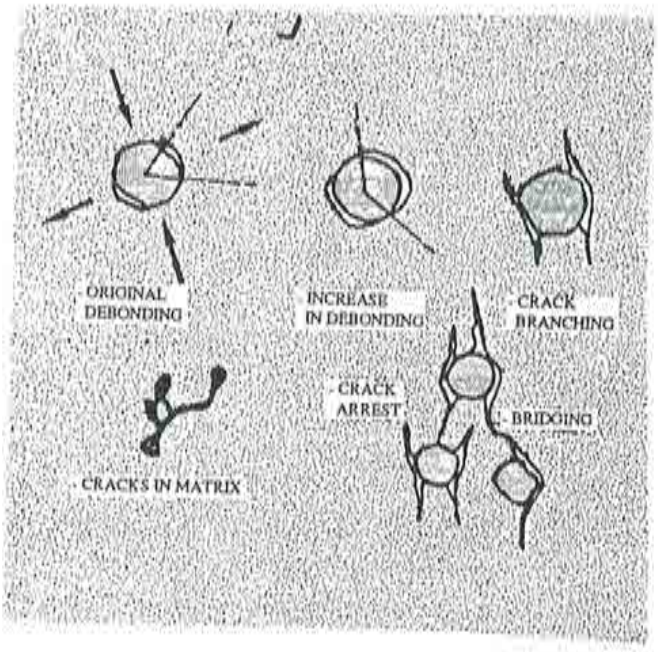

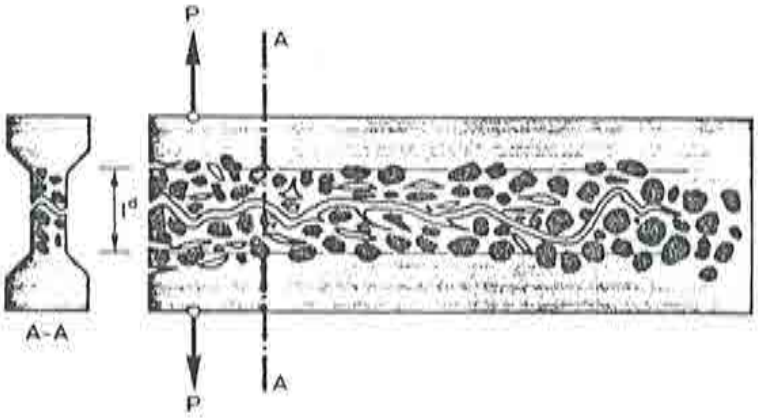

Figure 2.5 Mechanics of damage and propagation of macroscopic crack in concrete.

Basic concepts of the "Plastic Damage Model"

The plastic damage model proposed can be considered as a general form of classical plasticity in which the standard hardening variable is replaced by a normalized plastic damage variable κ^p, such that $0 \leq \kappa^p \leq 1$. This variable is similar to the former in the sense that it never decreases and it only increases if plastic deformation takes place which is associated to the existence of microcraking. The limit value of $\kappa^p = 1$ denotes total damage at a point with complete loss of cohesion. This can be interpreted as the formation of a macroscopic crack.

If stiffness degradation effects are negleted (and this will be separately treated in a latter section) the basic equations of the model are:

(a) *The yield function* defined as:

$$\mathcal{F}(\boldsymbol{\sigma}, \phi, c) = f(\boldsymbol{\sigma}, \phi) - c = 0 \tag{2.22}$$

where c is a cohesion or some constant multiple thereof, and ϕ is an internal friction angle, $f(\boldsymbol{\sigma}, \phi)$ is a function of the stress components that is first degree homogeneous in the stresses $\boldsymbol{\sigma}$, given a physical meaning of scaled stress to the cohesion. The particular form of $\mathcal{F}$ used in this work are presented in next section.

(b) *The elasto-plastic strain descomposition* as:

$$d\boldsymbol{\varepsilon} = \mathbf{D}_s^{-1} d\boldsymbol{\sigma} + \boldsymbol{\varepsilon}^p = d\boldsymbol{\varepsilon}^e + d\boldsymbol{\varepsilon}^p \tag{2.23}$$

where $\mathbf{D}_s$ is the elastic constitutive matrix.

(c) *The flow rule* is defined for the general case of non-associated plasticity as:

$$d\boldsymbol{\varepsilon}^p = \lambda \frac{\partial \mathcal{G}(\boldsymbol{\sigma}, \psi, c)}{\partial \boldsymbol{\sigma}} = \lambda \mathrm{g} \tag{2.24}$$

where λ is the plastic loading factor, ψ is a dilatancy angle and g is a plastic flow vector, normal to the plastic potential surface $\mathcal{G}(\boldsymbol{\sigma}, \psi, c)$. From eqs.(2.22)-(2.24) the standard elastoplastic incremental constitutive equation can be obtained as:

$$d\boldsymbol{\sigma} = \mathbf{D}^{ep} \cdot d\boldsymbol{\varepsilon} \tag{2.25}$$

with the elastoplastic constitutive matrix given by:

$$\mathbf{D}^{ep} = \mathbf{D}_s - \frac{\left[\mathbf{D}_s \cdot \left\{\frac{\partial \mathcal{G}}{\partial \boldsymbol{\sigma}}\right\}\right] \otimes \left[\mathbf{D}_s \cdot \left\{\frac{\partial \mathcal{F}}{\partial \boldsymbol{\sigma}}\right\}\right]}{A + \left[\left\{\frac{\partial \mathcal{F}}{\partial \boldsymbol{\sigma}}\right\} \cdot \mathbf{D}_s \cdot \left\{\frac{\partial \mathcal{G}}{\partial \boldsymbol{\sigma}}\right\}\right]} \tag{2.26}$$

where A is the hardenening parameter. Note from eq.(2.26) that $\mathbf{D}^{ep}$ is only symmetric for $\mathcal{G} = \mathcal{F}$ (associated plasticity). In this case (2.26) coincides with (1.63b)

(d) *The evolution laws* for internal variables κ^p and c of the form:

$$d\kappa = \lambda \left[\mathrm{h}_k(\boldsymbol{\sigma}, \kappa^p, c) \cdot \frac{\partial \mathcal{G}(\boldsymbol{\sigma}, \psi, c)}{\partial \boldsymbol{\sigma}}\right] = \mathrm{h}_K(\boldsymbol{\sigma}, \kappa^p, c) \cdot \boldsymbol{\varepsilon}^p \tag{2.27}$$

$$dc = \lambda \left[h_c(\boldsymbol{\sigma}, \kappa^p, c) \mathrm{h}_K(\boldsymbol{\sigma}, \kappa^p, c) \cdot \frac{\partial \mathcal{G}(\boldsymbol{\sigma}, c)}{\partial \boldsymbol{\sigma}}\right] = h_c(\boldsymbol{\sigma}, \kappa^p, c) \cdot \kappa^{*p} \tag{2.28}$$

The forms of functions $\mathbf{h}_K$ and h_c will be given in next sections. The cohesion c is a scaled uniaxial stress, so that its initial value c_o coincides with the initial yield stres f_{c_o} obtained from a uniaxial compression test. This value can be interpreted as a discontinuity stress, i.e. the stress for which the volumetric strain reaches a minimum. Therefore, $c = c_o = f_{c_o}$ for $\kappa^p = 0$, and $c = c_o = 0$ for $\kappa^p = 1$. Note, however, that c is not determined by an explicit fuction of κ^p, as is the case in simple plasticity models with isotropic hardening, but is itself an *internal variable*, depending on the load process, whose evolution is expressed by eq.(2.28)

DEFINITION OF THE YIELD SURFACE

Recent work has shown that the behaviour of concrete under triaxial compression states can be adequately modelled by yield criteria of the type of eq.(2.22) with $\mathcal{F}$ being a function with straight meridians, that is first degree homogeneous in the stress components.

In this work two different yield functions that satisfy the above requirement have been developed. The first one, is based on a simple modification of the well known Mohr–Coulomb yield surface as shown in Figure 2.6 [36–38]. The new yield surface is monitored by a reduction parameter α_R which allows to shift the $R-\phi$ curve (R being the ratio between the maximum tension and compression stresses) towards a region in which the related values of R and ϕ are compatible with those of concrete ($\phi \simeq 30°$ for $R \simeq 10$). Numerical results obtained with this simple yield function were good and they can be seen in [36–38].

A more detailed study of the experimental work reported for biaxial and triaxial behaviour of concrete allowed to define a new function of the form [34,35] (Figure 2.6)

$$\mathcal{F} = \mathcal{F}(\boldsymbol{\sigma}, \phi, c) = \frac{1}{(1-\alpha)}[\sqrt{3J_2} + \alpha I_1 + \beta < \sigma^{max} > -\gamma < -\sigma^{max} >] - c = 0 \tag{2.29}$$

where I_1 is the first invariant of stress, α, β and γ are dimensionless parameters that can be expressed as functions of the friction angle ϕ, σ^{max} is the maximum principal stress and $< \pm x >= \frac{1}{2}[x \pm |x|]$ is a ramp function. Note that when $\sigma^{max} = 0$ (biaxial compression) $\mathcal{F}$ is just the Drucker–Prager criterion, with the exception of parameter α. This can be obtained comparing the initial equibiaxial compression stress f_{b_o} with initial uniaxial compression stress f_{c_o}, yielding [34,35]:

$$\alpha = \frac{\left(\frac{f_{b_o}}{f_{c_o}} - 1\right)}{\left(\frac{2f_{b_o}}{f_{c_o}} - 1\right)} \tag{2.30}$$

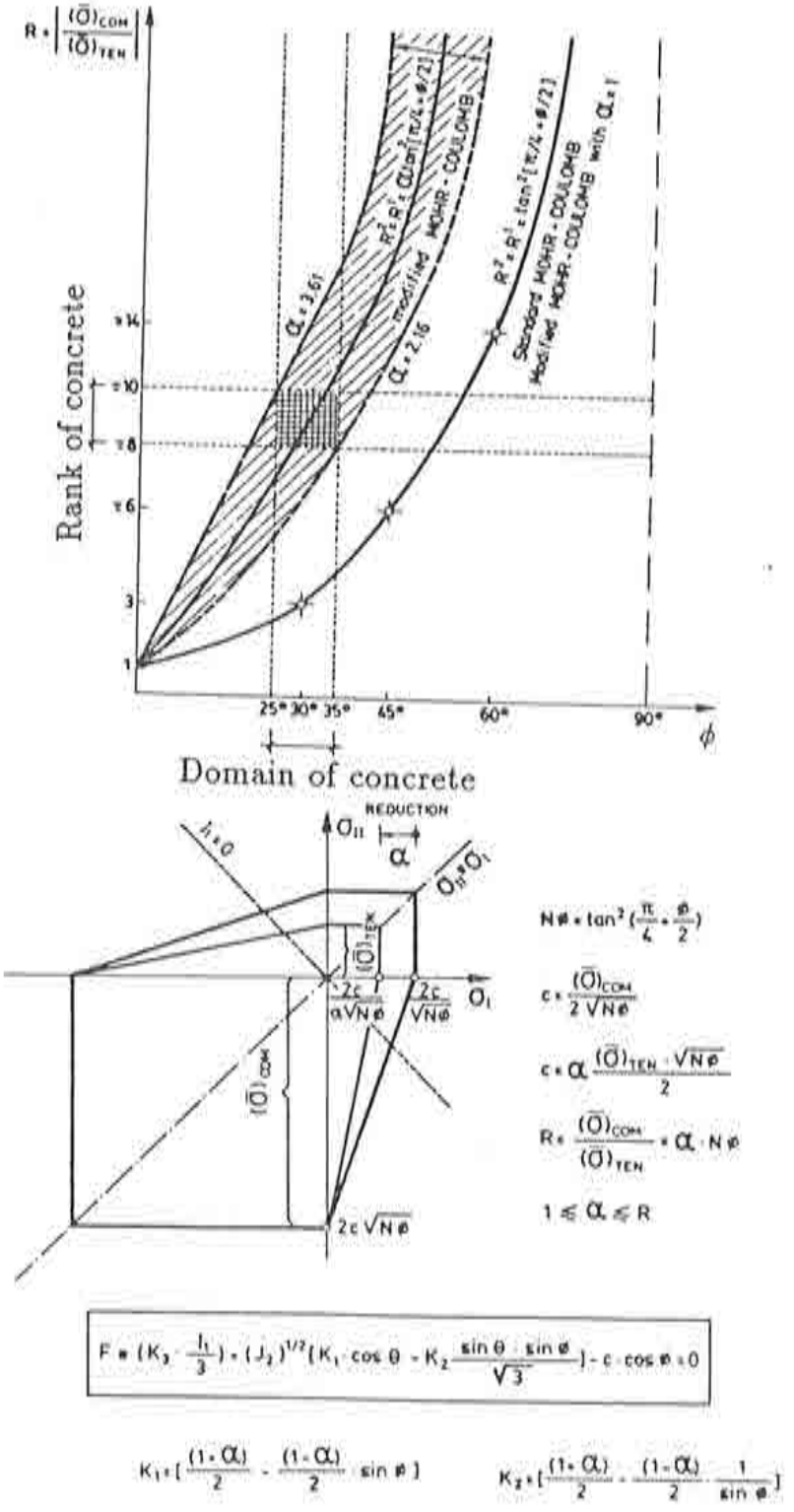

Figure 2.6 $R - \phi$ ratios for Mohr–Coulomb and modified Mohr–Coulomb surface.

Experimental values give $1.10 \leq f_{b_o}/f_{c_o} \leq 1.16$ which yields $0.08 \leq \alpha \leq 0.1212$.

Once α is known, β can be determined from the value of $R = f_{c_o}/f_{T_o}$, where f_{T_o} is the initial uniaxial tensile yield, as [34,35]:

$$\beta = (1-\alpha)R - (1+\alpha) \tag{2.31}$$

and for $R \simeq 10$ and $\alpha \simeq 0.10$ gives $\beta \simeq 7.50$

The parameter γ appears only in triaxial compression with $\sigma^{max} < 0$. Considering the equations of the straight tension (TM) and compression (CM) meridians of the yield surface it can be obtained [34,35]

$$\gamma = \frac{3(1-r_{oct}^{max})}{2r_{oct}^{max}-1} \tag{2.32}$$

where

$$r^{max}{}_{oct} = (\sqrt{J_2})_{TM}/(\sqrt{J_2})_{CM} \qquad \text{at a given} \quad I_1 \tag{2.33}$$

Experimental tests show thar r_{oct}^{max} has a constant mean values of $\simeq 0.65$ [34,35] which yields a value of $\lambda \simeq 3.5$

Definition of the plastic damage variable κ^p

Let us consider stress–plastic strain diagrams for uniaxial tension and compression tests (see Figure 2.7) for each test we define

$$\begin{aligned} \kappa^p &= \frac{1}{g_T^p}\int_{t=0}^{t} \sigma_T d\varepsilon_T^p, \qquad \text{for uniaxial tension, and} \\ \kappa^p &= \frac{1}{g_T^p}\int_{t=0}^{t} \sigma_C d\varepsilon_C^p, \qquad \text{for uniaxial compression} \end{aligned} \tag{2.34}$$

where g_T^p and g_C^p are the specific plastic works, defined by the areas under each of the curves $\sigma_T - \varepsilon_T^p$ and $\sigma_C - \varepsilon_C^p$ (Figure 2.8) obtained from the tension and compression uniaxial tests, respectively. The eqs.(2.34) allow the transformation of uniaxial diagrams: $\sigma = f(\varepsilon^p)$ in other: $\sigma = f(\kappa^p)$ such that (Figure 2.8)

$$\begin{aligned} &\text{tension test:} && f_T(0) = f_{T_o} \quad \text{and} \quad f_T(1) = 0 \\ &\text{compression test:} && f_C(0) = f_{C_o} \quad \text{and} \quad f_C(1) = 0 \end{aligned}$$

Starting from these concepts, the evolution law for κ^p can be generalized

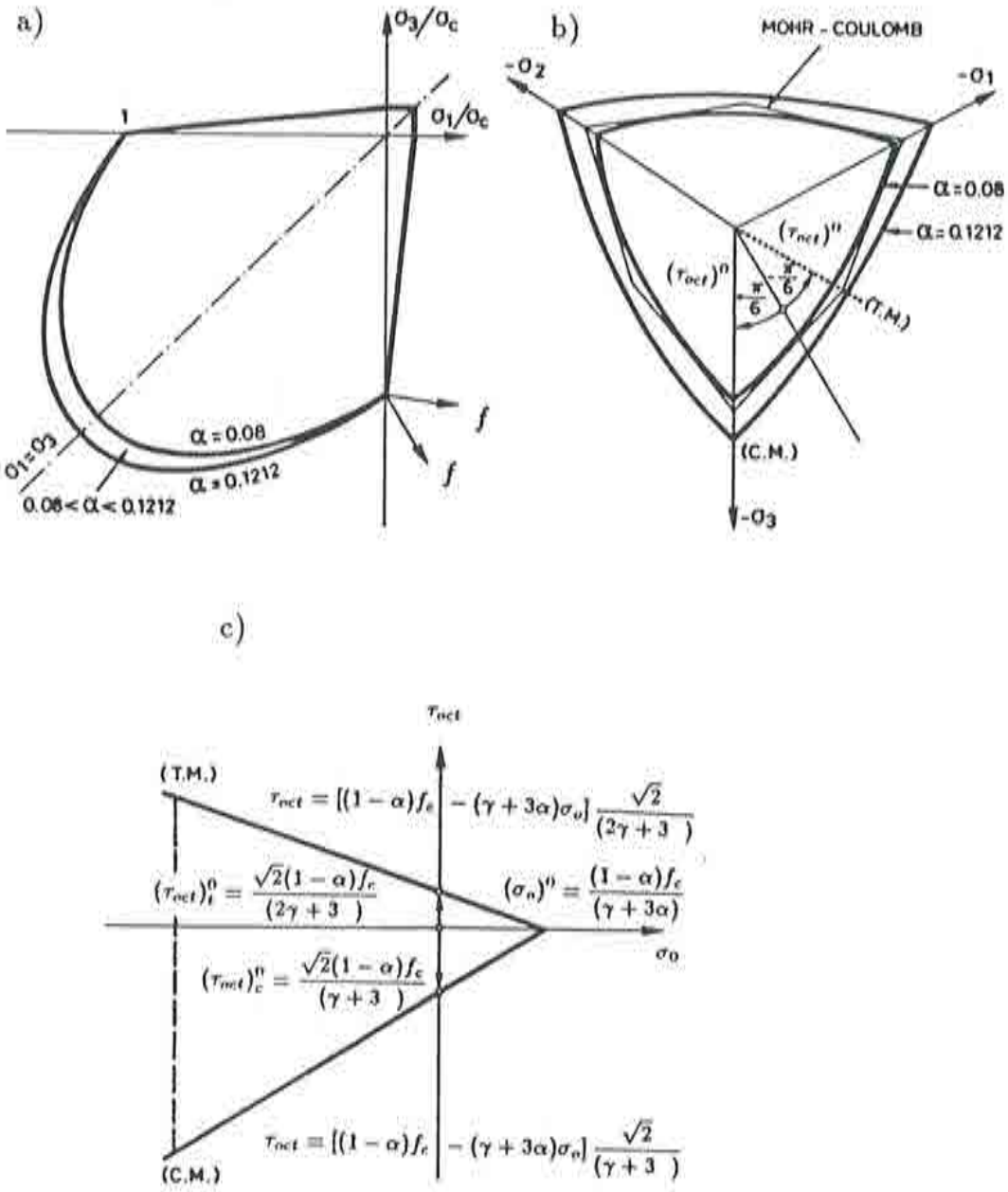

Figure 2.7 Proposed yield surface: (a) ($\sigma_{11} - \sigma_{33}$; $\sigma_{22} = 0$) plane; (b) octahedral plane; (c) meridian plane.

for a multiaxial stress state (written in terms of principal stress and plastic strain), as [34,35]

$$d\kappa^p = \mathrm{h}_K(\boldsymbol{\sigma}, \kappa^p, c)d\boldsymbol{\varepsilon}^p = \sum_{i=1}^{3}(h_{c_i o}d\varepsilon_i^p) \tag{2.35}$$

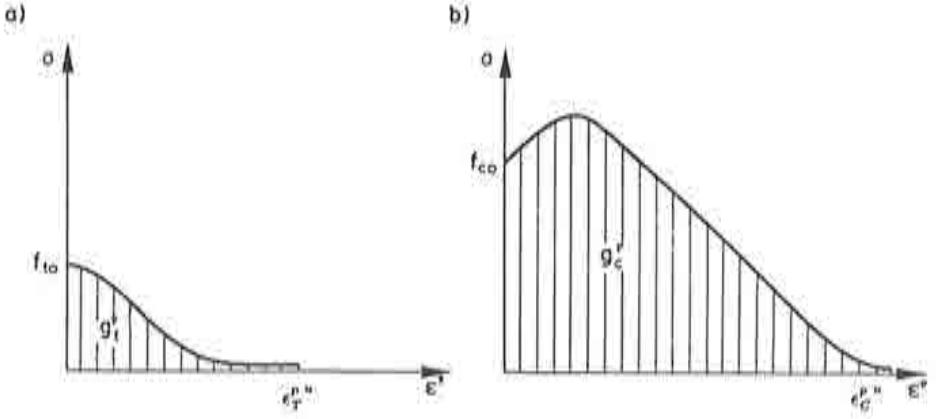

Figure 2.8 Uniaxial curves ($\sigma - \varepsilon^p$). (a) Tension; (b) compression.

with:

$$h_{\kappa_i} = [(h_{\kappa_i})_T + (h_{\kappa_i})_C] = \frac{1}{g_T^{p*}} < \sigma_i > + \frac{1}{g_C^{p*}} < -\sigma_i >$$
$$g_T^{p*} = g_T^p \frac{\sum_{i=1}^3 < \sigma_i >}{\sigma_T}; \quad g_C^{p*} = g_C^p \frac{\sum_{i=1}^3 < -\sigma_i >}{\sigma_C} \tag{2.36}$$

where subscrits T and C denote values obtained from uniaxial tension and compression tests, respectively. In eq.(2.36) g_T^{p*} and g_C^{p*} are normalized values of the uniaxial specific plastic work for tension and compression processes, accordingly to the yield function chose and also to the uniaxial tension and compression stresses σ_T and σ_T. For further details see [34,35].

Evolution law for the internal variable of cohesion c

The evolution of the cohesion c must satisfy $c \to 0$ for $\kappa^p \to 1$. In this model the evolution law for the cohesion is given by eq.(2.28) with the evolution function $h_c(\boldsymbol{\sigma}, \kappa^p, c)$ defined by [6,7,12, 15, 16]:

$$h_c((\boldsymbol{\sigma}, \kappa^p, c) = \left[\frac{r(\boldsymbol{\sigma})}{c_T(\kappa^p)} \frac{dc_T(\kappa^p)}{d\kappa^p} + \frac{1 - r(\boldsymbol{\sigma})}{c_C(\kappa^p)} \frac{dc_C(\kappa^p)}{d\kappa^p}\right] \tag{2.37}$$

where c is the actual value of the cohesion, $c_T(\kappa^p)$ and $c_C(\kappa^p)$ are the cohesion functions obtained from tension and compression uniaxial tests, respectively (see Figure 2.9), and $r(\boldsymbol{\sigma})$ is a function defining the stress stated, being $0 \leq r(\boldsymbol{\sigma}) \leq 1$ with $r(\boldsymbol{\sigma}) = 1$ if $\sigma_i \geq 0$ over all $i = 1,2,3$ and $r(\boldsymbol{\sigma}) = 0$ if $\sigma_1 \leq 0$ over all $i = 1,2,3$.

We have taken

$$r(\boldsymbol{\sigma}) = \frac{\sum_{i=1}^3 < \sigma_i >}{\sum_{i=1}^3 |\sigma_i|} \tag{2.38}$$

For further details the reader is referred to [6,7,15,16].

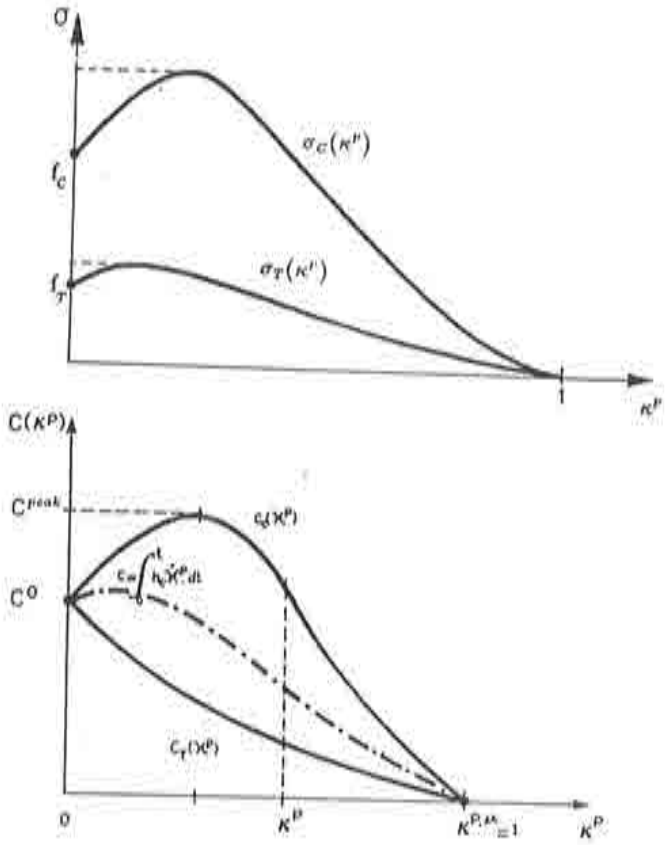

Figure 2.9 Uniaxial curves for tension and compression tests. (a) Uniaxial curves ($\sigma - \kappa$), (b) uniaxial curves ($c - \kappa$).

EVOLUTION LAW FOR THE INTERNAL FRICTION ANGLE ϕ

It has been shown [6,15,17] that the loss of cohesion in concrete due to increase plastic damage affects the value of angle of internal friction, which ranges from $\phi \simeq 0$ for initial cohesion c_0 until $\phi = \phi^{max}$ for the ultimate value of cohesion $c = c_u = 0$. In this work the following evolution law for ϕ has been chosen

$$\sin\phi = \begin{cases} 2\frac{\sqrt{\kappa^p \kappa^L}}{\kappa^p + \kappa^L} \sin\phi^{max}; & \forall \kappa^p \leq \kappa^L \\ \sin\phi^{max}; & \forall \kappa^p > \kappa^L \end{cases} \tag{2.39}$$

where κ^L denotes the limit damage for which the value of ϕ remains constant (see Figure 2.10).

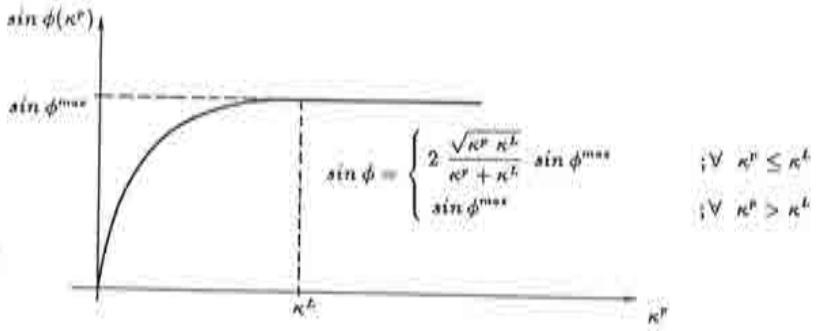

Figure 2.10 Evolution law for the internal friction angle.

PLASTIC POTENTIAL FUNCTION AND DILATANCY ANGLE ψ

Granular materials like concrete exhibit dilatancy phenomenon. This can be modelled introducing an adequate plastic potential function G to mach the numerical values obtained for the inelastic volume change with experimental data. In this work we have chosen for G the modified Mohr-Coulomb yield function of Figure 2.6 with the angle of dilatancy ψ substituting the internal friction angle ϕ. The evolution law for ψ has been obtained via a simple modification of the general expression used by De Borst and Vermeer [39] as

$$\psi(\kappa^p) = \arcsin\left[\frac{\sin\phi(\kappa^p) - \sin\phi_{cv}}{1 - \sin\phi(\kappa^p)\sin\phi_{cv}}\right] \tag{2.40}$$

where ϕ_{cv} can be taken as a constant value. For concrete $\phi_{cv} \simeq 13°$.

The eq.(2.40) gives for the initial stages of the process a negative dilatancy, which increase as plastic damage increases, takes a zero value for $\phi = \phi_{cv}$ and reaches a maximum for $\phi = \phi^{max}$. For concrete a negative value of ψ has not physical meaning and, therefore, it must be taken $\phi = 0$ for $\phi \le \phi_{cv}$ (see Figure 2.11).

Generalization of the model to include stiffness degradation

Experimental results show that near and beyond peak strength comented granular materials exhibit an increacing degradation of sttiffness due to microcracking (Figure 2.12). The consideration of the phenomenon of stiffness degradation makes it necessary some modification in the basic concepts of the theory of plasticity used in previous sections and, in particular, that of associated plasticity.

Taking into account the stiffness degradation effects implies modifying the elastic secant constitutive matrix $\mathbf{D}_s$ in terms of two sets of internal variables: the elastic degradation variables and the plastic degradation variables whose evolutions will be assumed to be governed by rate equations

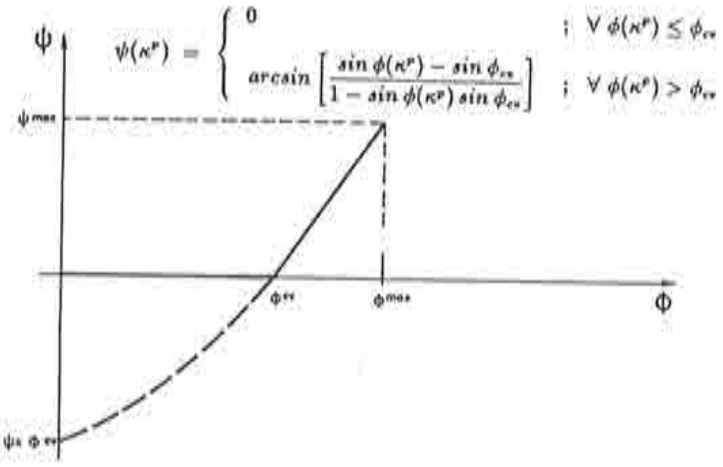

Figure 2.11 Evolutions law for the dilatancy angle [17].

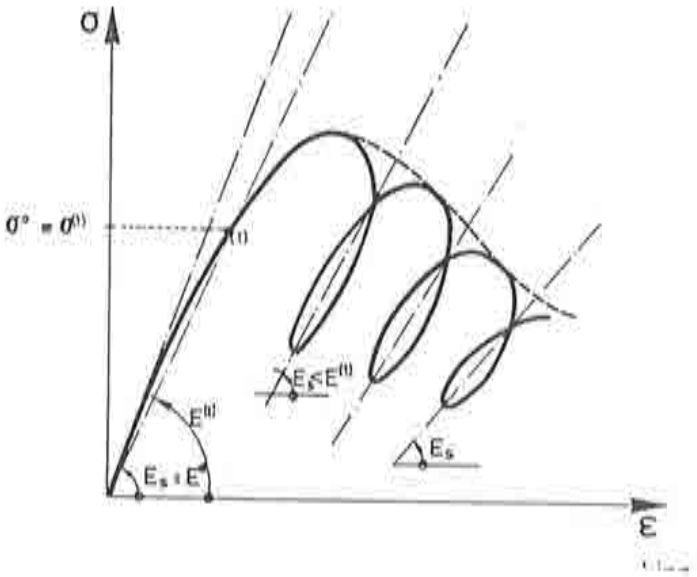

Figure 2.12 Degradation of stiffness module due to microcraking.

of the form: $\dot{d}_i^e = \phi_i < \mathbf{k}_i \cdot \dot{\boldsymbol{\varepsilon}} >$ and $\dot{d}_j^p = \mathbf{I}_j \cdot \dot{\boldsymbol{\varepsilon}}^p$ [34,35] repectively; where $\mathbf{k}_i$ and $\mathbf{I}_j$ are vectors in the stresses space denoting the directions of elastic and plastic degradation, respectively; and ϕ_i is a positive scalar factor (for further details the reader is referred to [34,35].

The simplest assumption for elastic degradation based on a simple isotropic degradation can be variable: d^e, such that the secant constitutive matrix is modified by:

$$\mathbf{D}_s(d^e) = (1 - d^e)\mathbf{D}^o \tag{2.41}$$

where $\mathbf{D}^o$ is the initial stiffness. Parameter d^e can be interpreted as the ratio between the area of degradated material and the total area, and it can be expressed [34,35] as

$$d^e = 1 - e^{-\phi w^e} \tag{2.42}$$

where $2w^e = \boldsymbol{\varepsilon}^e \cdot \mathbf{D}^o \cdot \boldsymbol{\varepsilon}^e$ is the square of the undamaged energy norm of the strain, $\boldsymbol{\varepsilon}^e$ is the elastic strain and ϕ is a constant given for this particular case by [34,35]:

$$\phi = \frac{2}{E^o(\varepsilon^1)^2} \ln \frac{E'}{E^o} \tag{2.43}$$

E^o is initial Young modulus; E' and ε^1 are the secant Young modulus and the elastic deformation at the limit stress point of elastic degradation, respectively. For further details the reader is referred to [34,35].

For the plastic degradation a simple one-parameter model can also be used [34,35]. This is based on the assumption that plastic degradation takes place only in the softening branch and that the stiffness is then is then proportional to the cohesion. The secant constitutive matrix is thus given by:

$$\mathbf{D}_s(d^p, \mathbf{d}^e) = (1 - d^p)\mathbf{D}_s(\mathbf{d}^e) \tag{2.44}$$

with the plastic degradation parameter d^p given by

$$d^p = 1 - \frac{c}{c^{peak}} \tag{2.45}$$

where c is the actual value of cohesion and c^{peak} is the maximum cohesion value reached [34,35].

Problem of objectivity response

It has been made abundantly clear over the past decade that the strain-softening branch of the stress-strain curves cannot represent a local physical property of the material. The argument have been advanced both on physical grounds and on the basis of the mesh-sensitivity of numerical solutions obtained by means of the finite-element method. The mesh-sensitivity can be largely eliminated if one defines $g_T^p = G_T/l$ and $g_C^p = G_C/l$, where l is a characteristic length related to mesh size, and G_T and G_C are quantities with the dimensions of energy/area that are assumed to be material properties.

In problem involving tensile cracking, G_T may be identified with the specific fracture energy G_f, defined as the energy required for form a unit area of crack. It has generally been assumed that G_f is a true property,

and methods have been developed for determining it. For the characteristic length l, various approaches have been proposed [40].

Not so much attention has been paid to the corresponding compressive problem. Compressive failure may occur through several mechanisms–crushing, shearing and transverse cracking–and consequently G_c, if indeed it is a material property, cannot be readily identified with any particular physical energy. Moreover, it must be kept in mind that it is only the descending portion of the stress-strain curve that is mesh–sensitive.

Determination of cracks by postprocessing the numerical results

The amount and directions of cracking at a point in the plastic–damage model is obtained *a posteriori*, once convergence of the non–linear solution has been reached, as follows:

(a) Cracking initiates at a point when the effective plastic strain, $\bar{\varepsilon}^p$, is greater than zero. The direction of cracking is assumed to be orthogonal to that of the maximum principal strain at the point (see Figure 2.13).

(b) The increment of plastic strains along the directions of the crack, $\Delta \mathbf{e}^{cr}$, can be obtained as $\Delta \mathbf{e}^{cr} = \mathbf{T} \cdot \Delta \boldsymbol{\varepsilon}^p$, where $\Delta \boldsymbol{\varepsilon}^p$ is the vector of plastic strain increment expressed in global Cartesian axes and $\mathbf{T}$ is a transformation matrix given by:

$$\mathbf{T} = \begin{bmatrix} \cos^2\theta & \sin^2\theta & \frac{\sin^2\theta}{2} \\ \sin^2\theta & \cos^2\theta & -\frac{\sin^2\theta}{2} \\ -\sin 2\theta & \sin 2\theta & \cos 2\theta \end{bmatrix} \tag{2.46}$$

where θ is the angle which the direction of the maximum principal strain forms with the global x axis (See Figure 2.13).
Vector $\Delta \mathbf{e}^{cr}$ is used to accumulate the plastic strain dissipated along the crack local axes.

(c) The energy dissipated in the structure due to cracking in a load increment is obtained as:

$$\Delta W^p = \int_V \boldsymbol{\sigma}^T \cdot \Delta \boldsymbol{\varepsilon} \cdot dV \tag{2.47}$$

where V is the volume of the structure.

(d) The model also allows to obtain the shear retention factor a crack as $\beta = \tau/\tau^e$ where τ is the actual shear stress parallel to the direction of the crack and τ^e is the value of τ obtained from a linear elastic analysis.

Therefore, the elasto–plastic model proposed here allows the computations of all the necesary information for fully defining the state of

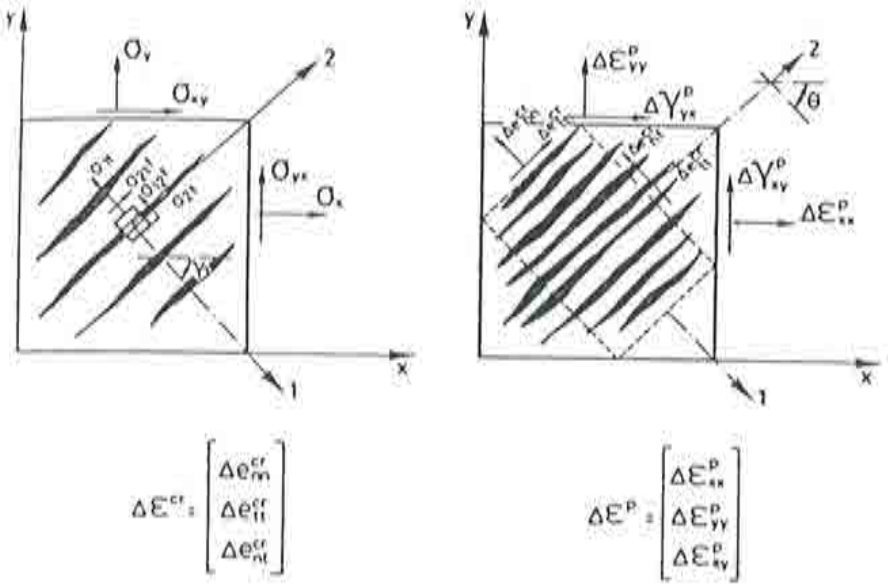

Figure 2.13 Direction of cracking at a damaged point.

cracking in the structure. However, the fact that all this information is obtained *a posteriori* can be considered a clear advantge with respect to other discrete or smeared cracking models, which involve detailed transformations during the non–linear numerical solution stage.

BEHAVIOUR OF REINFORCING STEEL IN TENSION AND COMPRESSION

The reinforcing bars are considered as steel layers of equivalent thickness in the present model. Each steel layer has an uniaxial behaviour resisting only the axial force in the bar direction. A bilinear or a trilinear idelization can be adopted in order to model the elasto–plastic stress-strain relationship. The basic relationships for uniaxial elasto –plastic behaviour and the corresponding numerical formulation can be found in reference [20].

REFERENCES

1. H. Kupfer, K.H. Hilsdorf and H. Rush, "Behaviour of concrete under biaxial stresses", Proceedings, American Concrete Institute, Vol. **66**, No. 8, pp. 656–666, August 1969.
2. L.L. Mills and R. M. Zimmerman, "Compressive strength under multiaxial loading conditions", *ACI Journal Proc.*, Vol. **67**, M–10, pp. 802–2087, Oct. 1970.
3. K.H. Gerstle et al. "Behaviour of concrete under multiaxial stress states", *ASCE Journal of Eng. Mech. Div.*, Vol. **106**. No. EM6, pp. 1383–1403, December 1980.

4. H.B. Kupfer and K.K. Gerstle, "Behaviour of concrete under biaxial stresses", *ASCE Journal of the Eng. Mech. Div.*, Vol. **99**, No. EM4, pp. 853–866, August 1973.
5. T.C.Y. Liu, A.H. Nilson and F.O. Slate, "Biaxial stress–strain relations for concrete", *ASCE Journal of the Structural Division*, Vol. **98**, No. ST5, pp. 1025–1034, May 1972.
6. L. Cedolin, Y.R.J. Crutzen and S. Deipoli, "Triaxial stress–strain relationship for concrete", *ASCE J. of the Eng. Mech. Div.*, Vol. **103**, No. EM3, pp. 423–439, June 1977.
7. K.H. Gerstle, "Simple formulation of biaxial concrete behaviour", *ACI Journal*, Vol. **78**, pp. 62–68, Feb. 1981.
8. C.S. Lin and A.C. Scordelis, "Nonlinear analysis of BC shells of general form", *ASCE Journal of the Structural Division*, Vol. **101**, No ST3, pp. 523–538, March 1975.
9. A.C.T. Chen and W.F. Chen, "Constitutive relations for concrete", *ASCE Journal of the Eng. Mech. Div.*Vol. **101**, No. EM4, pp. 465–481, August 1973.
10. O. Buyukozturk, "Nonlinear analysis of reinforced concrete structures", *Computer and Structures*, Vol. **7**, pp. 149–156, 1977.
11. Z.P. Bazant and P..D. Bhat, "Endochronic theory inelasticity and failure of concrete", *ASCE Journal of the Eng. Mech. Div.*, Vol. **102**, No. EM4, pp. 701–722, August, 1976.
12. Z.P. Bazant and S.S. Kim, "Plastic–Fracturing theory for concrete", *ASCE Journal of The Eng. Mech. Div.*, Vol. **105**, No. EM3, pp. 407–428., June 1979.
13. N.S. Ottosen, "A failure criterion for concrete", *ASCE Journal of Eng. MEch. Div.*, Vol. **103**, No. EM4, pp. 527–535, 1977.
14. J. Wastiels, "Behaviour of concrete under multiaxial stresses a leview", *Cement and Concrete Research*, Vol. **9**, pp. 35–44, 1979.
15. J. Wastiels, "Failure criteria for concrete subject to multiaxial stresses", Lecture held at Univ. of Illinois at Chicago Circle, Dept. of Materials Eng., 1981.
16. C.S. Lin, "Nonlinear analysis of reinforced concrete slabs and shells", PhD. Thesis, UC-SESM 73–7, university of California, April 1973.
17. W.F. Chen. "*Plasticity in Reinforced Concrete*", McGraw–Hill Book Company, 1982.
18. D.R.J. Owen and J.A. Figueiras, "Ultimate load analysis of reiforced concrete plates and shells", In *Finite Element Software for Plates and Shells*, E. Hinton and D.R.J. Owen (Eds.), Pineridge Press, 1984.
19. E. Andenaes, K. Gerstle and H.Y. Ko, "Response of mortar and concrete to biaxial compression", *ASCE Journal of Eng. Mech. Div.*, Vol. **103**, No. EM4, pp. 515–526, 1977.
20. D.R.J. Owen and E. Hinton, "*Finite Element in Plasticity*"Theory and

Practice, Pineridge Press, Swansea, U.K., 1980.
21. O.C. Zienkiewicz and R.L. Taylor, "*The Finite Element Method*", Fourth Edition, Vol. **I**, 1989, Vol. **II**, 1991.
22. Y. Goto, " Cracks formed in concrete around deformed tension bars", *ACI Journal*, pp. 244–251, 1971.
23. H.H.A. Rahman, "Computatioal models for the nonlinear of reinforced concrete flexural slab systems", Ph. D Thesis, C7Ph/66/82, University of Wales, May, 1982.
24. R.I. Gilbert and R.F. Warner, " Tension stiffnening in reinforced concrete slabs", *ASCe Journal of the Structural Division*, Vol. **104**, No. ST12, pp. 1885–1900, 1978.
25 R.J. Cope, P.V. Rao, L.A. Clark and P. Norris, "Modelling of reinforced concrete behaviour for finite element analysis of bridge slabs", Numerical Meth. for Nonlinear Problems, Vol. **1**, Pineridge Press, Proceedings of the International Conference held at Univ. College of Swansea, pp. 457–470, 2–5 September, 1980.
26. A. Arnesen, S.L. Sorensen and P.G. Bergan, "Nonlinear analysis of Requirements for Reinforced Concrete", *ACI Standard* 318–77, Building Code, American Concrete Institute, Detroit, 1977.
27. R.C. Fenwick and T. paulay, "Mechanics of shear resistence of concrete beams", *ASCE Journal of the Structural Division*, Vol. **94**, No. ST10, pp. 2325–2350, October 1968.
28. J.A. Hofbeck, I.O. Ibrahim and A.H. Mattock, " Shear transfer in reinforced concrete", *ACI Journal*, pp. 119–128, 1969.
29. Y.D. Hamadi and P.E. Regan, "Bahaviour in shear of beams with flexural cracks", *Magazine of Concrete Research*, Vol. **32**, No. 111, pp. 67–78, 1980.
30 L. Cedolin and S. Deipoli, "Finite element studies of shear–critical R/C beams, *ASCE Journal of the Engineering Mechanics Division*, Vol. **103**, No. EM3, pp. 395–410, Jue 1977.
31. F.R. Hand, D.A. Pecknold and W.C. Schnobrich, "Nonlinear layered analysis of RC Plates and Shels, *ASCE Journal of Structural Division*, Vol. **99**, No. ST7, pp. 1491–1503, July, 1973.
32. Z. Bazant, "Mechanics of distributed cracking, *Appl. Mech. Rev.*, Vol. **39**, pp. 675–705, 1986.
33. E. Oñate, J. Oliver and G. Bugeda, "Finite element analysis of nonlinear response of concrete dams subject to internal loads"Europe–US Symposium on Finite Element Methods for Nonlinear Problems, (Edited by Bergan, Bathe and Wunderlich) Springer-Verlag, 1986.
34. S, Oller, "Un Modelo de daño continuo para materiales friccionales, Tesis Doctoral, Dept. De Estructuras, Univ. Politécnica de Catalunya, Barcelona, España, 1988.
35. J. Lubliner, S. Oller, J. Oliver and E. Oñate, "A plastic damage model

for nonlinear analysis of concrete", *Int. J. Solids Struct.*, Vol. **25**, 3, pp. 299–326, 1989.

36. E. Oñate, S. Oller And J. Lubliner, "A constitutive model of concrete based on the incremental theory of plasticity", *Engng. Comput.*, Vol. **5**, 4, 1988.
37. E. Oñate, S. Oller, J. Oliver and J. Lubliner, "A fully elastoplastic constititutive model nonlinear analysis of concrete, Proc. Second Int. Conf. Advances Methods in Numerical Methods in Engineering, Theory and Applications–NUMETA (Edited by G. Pande and J. Middleton). Martinus Nijhoff, Swansea, 1987.
38. E. Oñate, S. Oller and J. Lubliner, "A constitutive model cracking of concrete based on the incremental theory of plasticity", in Proc. Int Conf. Computational Plasticity (Edited by D.R.J. Owen, E. Hinton and E. Oñate), Part 2, pp 1311-1327, Pineridge Press, Barcelona, 1987.
39. R. De Borst and P. Verneer, "Non associated plasticity for soils, concrete and rock", *Heron* 29, Delft, Netherlands, 1984.
40. J. Oliver, "A consisten characteristic length for smeared cracking models", *Commun, Appl. Num. Meth. in Engng.*

Lecture 3

STIFFENED SHELLS. MODELLING OF ECCENTRIC BEAM STIFFENERS

SUMMARY

This lecture describes the basic finite element formulations for the analysis of stiffened shells via the use of eccentric beams.

INTRODUCTION

Beam stiffened shells are very common in practice. Typical examples of application are found in slab–beam bridges, edge beams in shell roofs and beam stiffened ship hulls (Figure 3.1).

The finite element analysis of these structures precises an adequate modelling of both the beam and the shell structures. For the shell any of the flat or degenerate shell elements formulations presented in Lecture 1 can be used. On the other hand the analysis of the beam can be based on standard straight two node beam elements, more elaborated curved beam elements or even more sophisticated beam elements developed from a degeneration of 3D solid elements. Also for each of these element types the hypothesis of orthogonality of the transverse normal sections after deformation can or can not be assumed yielding the so called Euler–Bernoulli or Timoshenko beam theories, respectively.

In this chapter we will concentrate on the study of beam elements based on Timoshenko beam theory. Both curved and straight elements will be considered. Also the study is focused on the analysis of reinforced concrete beams for use as eccentric stiffners in concrete shells, and also in slab beam bridges. Therefore, the non linear material behaviour will be treated using a layered approach, similar to that studied in lecture 1 for shells. Also non linear geometrical effects will be negleted in the analysis.

The content of the lecture is the following. Firstly the basic theory of curved Timoshenko concrete beams is presented. Then, the modelling of eccentric beam stiffness is considered. Finally examples of application to the analysis of some concrete structures are presented.

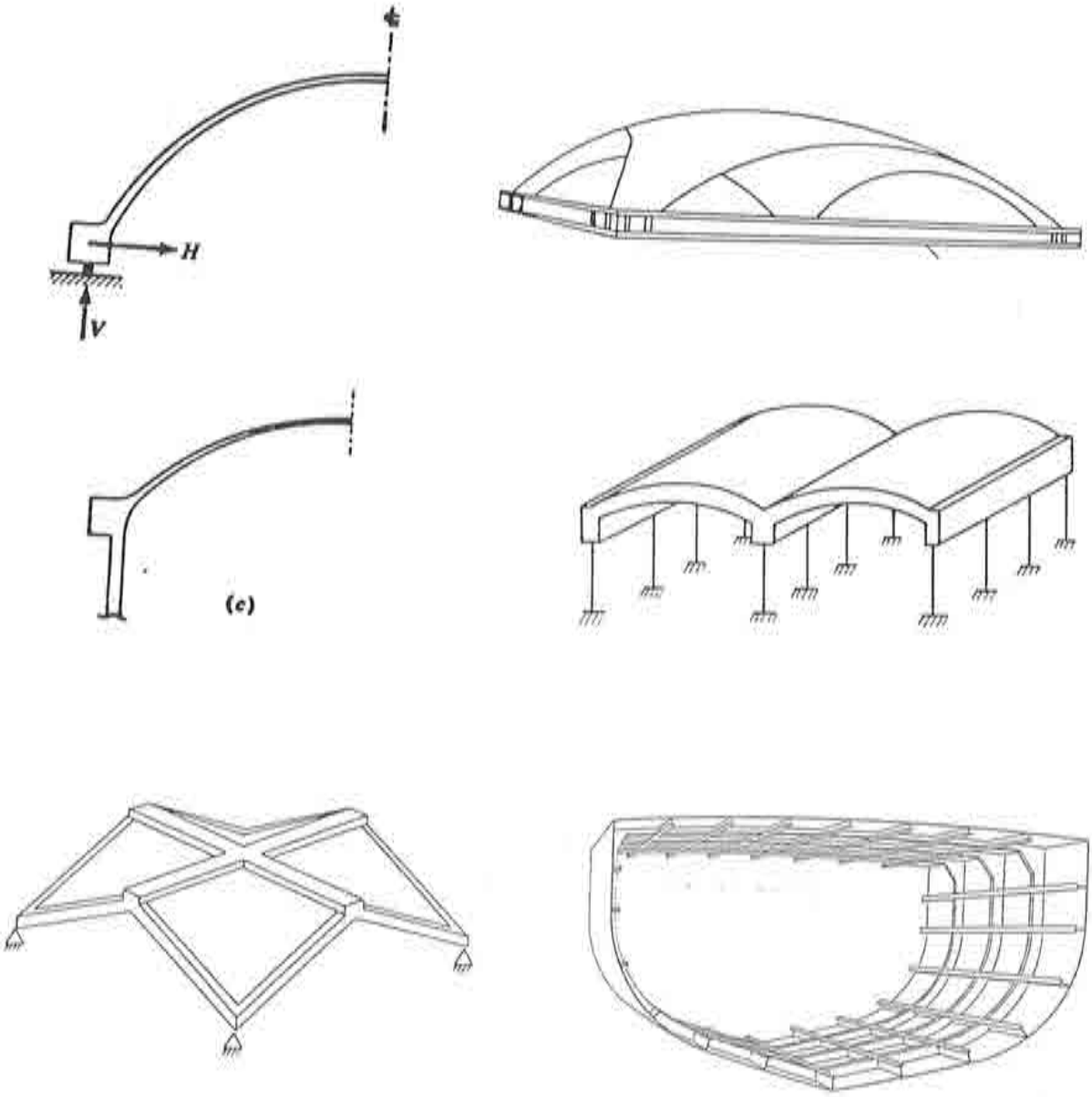

Figure 3.1 Some beam stiffened structures.

CURVED TIMOSHENKO BEAM ELEMENTS

Basic theory

Let's consider a curved beam defined in a global coordinate system xyz by the center line S and the different transverse sections of area $A(S)$ (Figure 3.2). A local coordinate system $\bar{x}\bar{y}\bar{z}$ is defined at the centroid of each section G so that $\bar{x}$ is normal to the transverse section and tangent to the center line in G and $\bar{y}$ and $\bar{z}$ coincide with the two principal directions of the transverse

section. For simplicity we will assume that the shear center coincides with G.

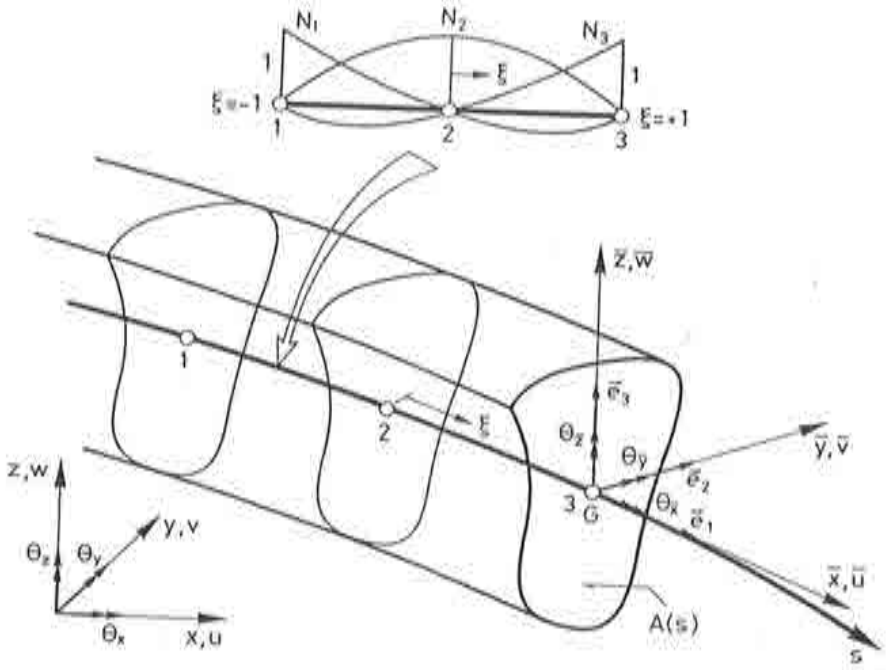

Figure 3.2 Geometric description of a curved beam element.

The kinematic description is based on Timoshenko beam theory, i.e. the transverse sections remain plane, but not necessarily normal to the center line after deformation. This assumption is analogous to that of Reissner-Mindlin for shells used in Lecture 1.

With this assumption the displacement field can be written as

$$\begin{aligned} \bar{u} &= \bar{u}_G + \bar{z}\theta_{\bar{y}} - \bar{y}\theta_{\bar{z}} \\ \bar{v} &= \bar{v}_G - \bar{z}\theta_{\bar{x}} \\ \bar{w} &= \bar{w}_G + \bar{y}\theta_{\bar{y}} \end{aligned} \tag{3.1}$$

where $(\cdot)_G$ denotes displacements of the centroid, $\theta_{\bar{x}}$ is the torsional rotation and $\theta_{\bar{y}}, \theta_{\bar{z}}$ are the two rotations about $\bar{y}$ and $\bar{z}$ axes, respectively (see Figure 3.2).

The local and displacement vectors of a point are related by

$$\mathbf{u}' = \mathbf{L}\mathbf{u} \tag{3.2}$$

with
$$\begin{aligned} \mathbf{u}' &= [\bar{u}_G, \bar{v}_G, \bar{w}_G, \bar{\theta}_{\bar{x}}, \bar{\theta}_{\bar{y}}, \bar{\theta}_{\bar{z}}]^T \\ \mathbf{u} &= [u_G, v_G, w_G, \theta_x, \theta_y, \theta_z]^T \end{aligned} \tag{3.3}$$

$$\mathbf{L} = \begin{bmatrix} \mathbf{T} & \mathbf{0} \\ \mathbf{0} & \mathbf{T} \end{bmatrix} \quad ; \quad \mathbf{T} = [\mathbf{e}_1, \mathbf{e}_2, \mathbf{e}_3]$$

where $\mathbf{e}_1, \mathbf{e}_2$ and $\mathbf{e}_3$ are the cartesian components of the unit vectors in local directions $\bar{x}, \bar{y}$ and $\bar{z}$ respectively.

The three non–zero local strains are

$$\begin{aligned} \varepsilon_{\bar{x}} &= \frac{\partial \bar{u}}{\partial \bar{x}} = \frac{\partial \bar{u}_G}{\partial \bar{x}} + \bar{z}\frac{\partial \theta_{\bar{y}}}{\partial \bar{x}} - \bar{y}\frac{\partial \theta_{\bar{z}}}{\partial \bar{x}} \\ \gamma_{\bar{x}\bar{y}} &= \frac{\partial \bar{u}}{\partial \bar{y}} + \frac{\partial \bar{v}}{\partial \bar{x}} = \frac{\partial \bar{v}_G}{\partial \bar{x}} - \theta_{\bar{z}} - \bar{z}\frac{\partial \theta_{\bar{x}}}{\partial \bar{x}} \\ \gamma_{\bar{x}\bar{z}} &= \frac{\partial \bar{u}}{\partial \bar{z}} + \frac{\partial \bar{w}}{\partial \bar{x}} = \frac{\partial \bar{w}_G}{\partial \bar{x}} + \theta_{\bar{y}} + \bar{y}\frac{\partial \theta_{\bar{x}}}{\partial \bar{x}} \end{aligned} \tag{3.4}$$

The stress–strain constitutive law is for linear–elasticity

$$\boldsymbol{\sigma}' = \begin{Bmatrix} \sigma_{\bar{x}} \\ \tau_{\bar{x}\bar{y}} \\ \tau_{\bar{x}\bar{z}} \end{Bmatrix} = \begin{bmatrix} E & 0 & 0 \\ 0 & G & 0 \\ 0 & 0 & G \end{bmatrix} \begin{Bmatrix} \varepsilon_{\bar{x}} \\ \gamma_{\bar{x}\bar{y}} \\ \gamma_{\bar{x}\bar{z}} \end{Bmatrix} = \mathbf{D}'\boldsymbol{\varepsilon}' \tag{3.5}$$

If a layer approach is used as shown in Figure 3.3 (3.5) will be written for each individual layer. Also, if material non–linearities of the type explained in Lecture 2 are considered eq.(3.5) will be expressed in the standard incremental form as

$$d\boldsymbol{\sigma}' = \mathbf{D}'_{NL} d\boldsymbol{\varepsilon}'$$

where $\mathbf{D}'_{NL}$ is the non–linear tangent constitutive matrix obtained using any of the two non–linear material models for concrete explained in Lecture 2.

The virtual work principle is written as

$$\int\int\int_V [\delta\varepsilon_{\bar{x}}\sigma_{\bar{x}} + \delta\gamma_{\bar{x}\bar{y}}\tau_{\bar{x}\bar{y}} + \delta\gamma_{\bar{x}\bar{z}}\tau_{\bar{x}\bar{z}}]dV = \int_l \delta\mathbf{u}^T \mathbf{t} ds + \sum_i \delta\mathbf{u}_i^T \mathbf{p}_i \tag{3.6}$$

where

$$\begin{aligned} \mathbf{t} &= [t_x, t_y, t_z, m_x, m_y, m_z]^T \\ \mathbf{p}_i &= [P_{x_i}, P_{y_i}, P_{z_i}, M_{x_i}, M_{y_i}, M_{z_i}]^T \end{aligned} \tag{3.7}$$

are the distributed and point load vectors in global axes, respectively.

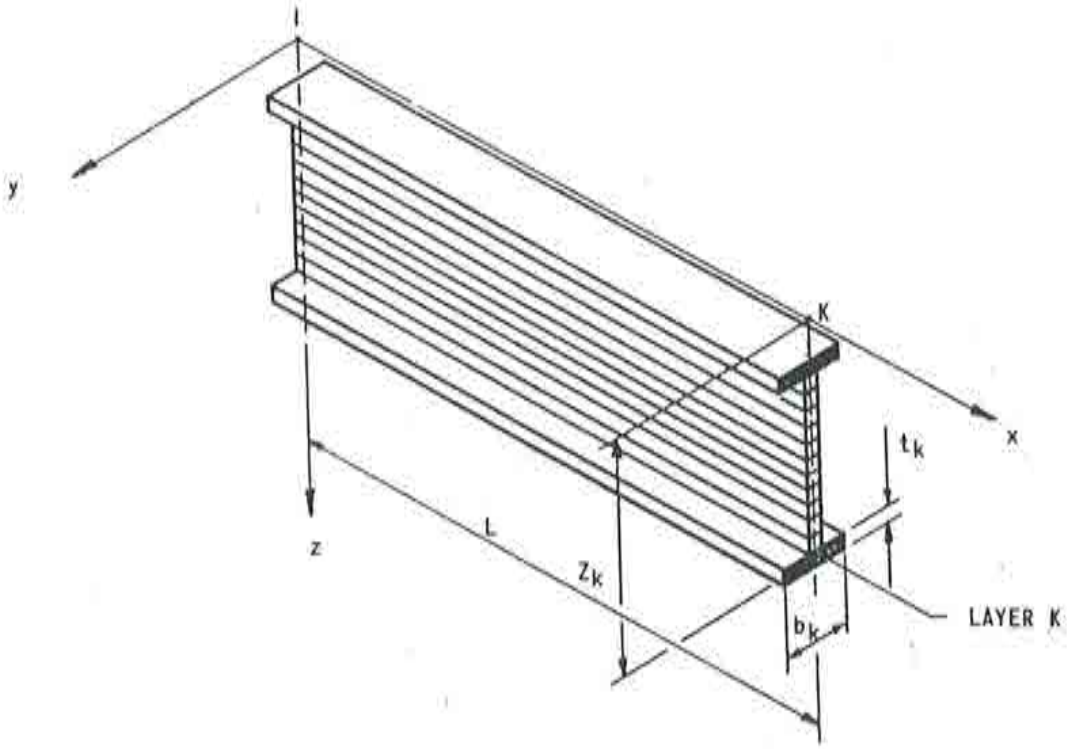

Figure 3.3 Layer discretization of a beam.

If the beam curvature is small we can take $\frac{\partial}{\partial \bar{x}} \equiv \frac{\partial}{\partial s}$ and eq.(3.6) can be written after some algebra

$$\begin{aligned}\int_l \Big[&\delta\left(\frac{\partial \bar{u}_G}{\partial s}\right) N + \delta\left(\frac{\partial \theta_{\bar{y}}}{\partial s}\right) M_{\bar{y}} - \delta\left(\frac{\partial \theta_{\bar{z}}}{\partial s}\right) M_{\bar{z}} + \\ &+ \delta\left(\frac{\partial \theta_{\bar{x}}}{\partial s}\right) T + \delta\left(\frac{\partial \bar{v}_G}{\partial s} - \theta_{\bar{z}}\right) Q_{\bar{y}} + \\ &+ \delta\left(\frac{\partial \bar{w}_G}{\partial s} + \theta_{\bar{y}}\right) Q_{\bar{z}} \Big] ds = \int_l \delta \hat{\varepsilon}'^T \hat{\sigma}' ds\end{aligned} \tag{3.8}$$

where

$$\hat{\varepsilon}' = \left[\frac{\partial \bar{u}_G}{\partial s}, \frac{\partial \theta_{\bar{y}}}{\partial s}, -\frac{\partial \theta_{\bar{z}}}{\partial s}, \frac{\partial \theta_{\bar{x}}}{\partial s}, \left(\frac{\partial \bar{v}_G}{\partial s} - \theta_{\bar{z}}\right), \left(\frac{\partial \bar{w}_G}{\partial s} + \theta_{\bar{y}}\right)\right]^T \tag{3.9}$$

is the local generalized strain vector in which $\frac{\partial \bar{w}_G}{\partial s}$ is the axial elongation, $\frac{\partial \theta_{\bar{y}}}{\partial s}$ and $\frac{\partial \theta_{\bar{z}}}{\partial s}$ are the beam curvatures, $\frac{\partial \theta_{\bar{x}}}{\partial s}$ the gradient of torsional rotation and $\frac{\partial \bar{v}_G}{\partial s} - \theta_{\bar{z}}$ and $\frac{\partial \bar{w}_G}{\partial s} + \theta_{\bar{y}}$ the shear deformations.

Also in (3.8)

$$\hat{\sigma}' = [N, M_{\bar{y}}, M_{\bar{z}}, T, Q_{\bar{y}}, Q_{\bar{z}}]^T \tag{3.10}$$

is the vector of local resultant stresses given by

$$[N, M_{\bar{y}}, M_{\bar{z}}, T, Q_{\bar{y}}, Q_{\bar{z}}]^T = \int\int_A [\sigma_{\bar{x}}, \bar{z}\sigma_{\bar{x}}, \bar{y}\sigma_{\bar{x}}, (\bar{y}\tau_{\bar{x}\bar{z}} - \bar{z}\tau_{\bar{x}\bar{y}}), \tau_{\bar{x}\bar{y}}, \tau_{\bar{x}\bar{z}}]^T dA \tag{3.11}$$

For the sign convection see Figure 3.4.

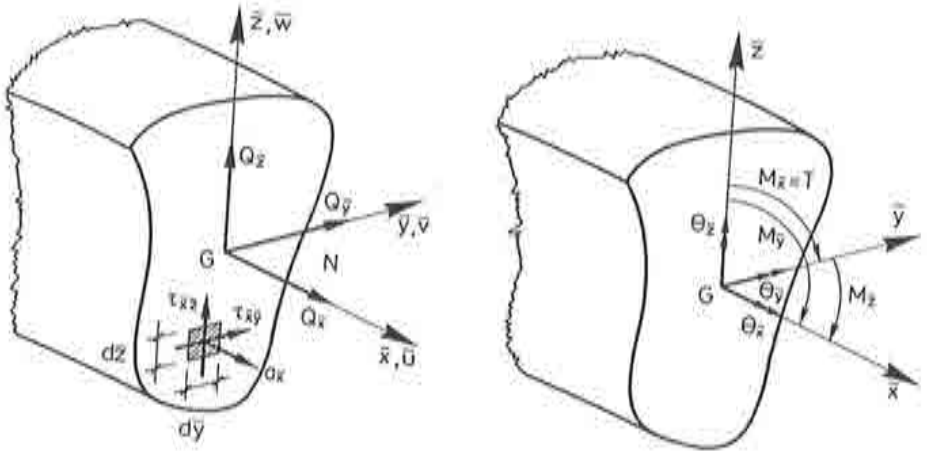

Figure 3.4 Sign convention for resultant stresses.

From (3.5) and (3.11), the relationship between resultant stresses and generalized strains can be written as

$$\hat{\boldsymbol{\sigma}}' = \hat{\mathbf{D}}'\hat{\boldsymbol{\varepsilon}}' \tag{3.12}$$

where

$$\hat{\mathbf{D}}' = \int\int_A \begin{bmatrix} E & & & & & \\ & \bar{z}^2E & & & \mathbf{0} & \\ & & \bar{y}^2E & & & \\ & & & (\bar{y}^2+\bar{z}^2)G & & \\ & \mathbf{0} & & & G & \\ & & & & & G \end{bmatrix} dA \tag{3.13}$$

In a layer formulation the integral in eq.(3.13) must be computed taking into account the material properties of each concrete or steel layer. For homogeneous material eq.(3.13) reduces to the well known expression

$$\hat{\mathbf{D}}' = \begin{bmatrix} EA & & & & \mathbf{0} & \\ & EI_{\bar{y}} & & & & \\ & & EI_{\bar{z}} & & & \\ & & & GJ & & \\ & \mathbf{0} & & & \alpha_{\bar{y}}GA & \\ & & & & & \alpha_{\bar{z}}GA \end{bmatrix} \tag{3.14}$$

where $I_{\bar{y}}$ and $I_{\bar{z}}$ are the principal moments inertia of the section, J is the torsional inertia ($J = I_{\bar{y}} + I_{\bar{z}}$) and $\alpha_{\bar{y}}$ and $\alpha_{\bar{z}}$ are the warping coefficients (for rectangular sections $\alpha_{\bar{y}} = \alpha_{\bar{z}} = 5/6$)

For non linear material analysis eq.(3.13) is written in an incremental form and the computation of $\hat{\mathbf{D}}'_{NL}$ involves now integration of the tangent material operator across the different layers.

Formulation of Timoshenko beam element

We consider a discretization of the beam in one dimensional curved C_o finite element, as the three node element shown in Figure 3.1. The center line coordinates are interpolated in the standard isoparametric form as

$$\mathbf{x} = [x_G, y_G, z_G]^T = \sum_{i=1}^{n} \mathbf{N}_i \mathbf{x}_i \tag{3.15}$$

where $\mathbf{N}_i = N_i(\xi)\mathbf{I}_3$ and $N_i(\xi)$ is the 1D shape function of node i [1] and n the number of nodes of the element.

The tangent vector $\mathbf{e}_1$ is given by

$$\mathbf{e}_1 = \frac{1}{|\frac{\partial \mathbf{x}}{\partial s}|}\frac{\partial \mathbf{x}}{\partial s} = \frac{1}{|\sum_{i=1}^{n} \frac{\partial N_i}{\partial s}\mathbf{x}_i|}\sum_{i=1}^{n}\frac{\partial N_i}{\partial s}\mathbf{x}_i \tag{3.16}$$

Vectors $\mathbf{e}_2$ and $\mathbf{e}_3$ are obtained from the principal inertia directions of the section defined at each nodal section: Once $\mathbf{e}_1, \mathbf{e}_2$ and $\mathbf{e}_3$ are computed the transformation matrix $\mathbf{L}$ of eq.(3.3) can be obtained for each node.

The local displacements $\mathbf{u}'$ are interpolated as

$$\mathbf{u}' = \sum_{i=1}^{n} N_i \mathbf{I}_6 \mathbf{a}_i'^{(e)} \quad ; \quad \mathbf{a}_i'^{(e)} = [\bar{u}_i, \bar{v}_i, \bar{w}_i, \theta_{\bar{x}_i}, \theta_{\bar{y}_i}, \theta_{\bar{z}_i}]^T \tag{3.17}$$

From (3.9) and (3.17) we deduce

$$\hat{\varepsilon}' = \sum_{i=1}^{n} \mathbf{B}'_i \mathbf{a}_i'^{(e)} = \sum_{i=1}^{n} \mathbf{B}'_i \mathbf{L}_i \mathbf{a}_i^{(e)} = \sum_{i=1}^{n} \mathbf{B}_i \mathbf{a}_i^{(e)} \tag{3.18}$$

where

$$\mathbf{B}_i = \mathbf{B}'_i \mathbf{L}_i \tag{3.19}$$

and

$$\mathbf{B}_i' = \begin{bmatrix} \frac{\partial N_i}{\partial s} & 0 & 0 & 0 & 0 & 0 \\ 0 & 0 & 0 & 0 & \frac{\partial N_i}{\partial s} & 0 \\ 0 & 0 & 0 & 0 & 0 & -\frac{\partial N_i}{\partial s} \\ 0 & 0 & 0 & \frac{\partial N_i}{\partial s} & 0 & 0 \\ 0 & \frac{\partial N_i}{\partial s} & 0 & 0 & 0 & -N_i \\ 0 & 0 & \frac{\partial N_i}{\partial s} & 0 & N_i & 0 \end{bmatrix} \tag{3.20}$$

is the local generalized strain matrix of node i.

The element stiffness matrix and the equivalent nodal load vector can be obtained in the standard manner as

$$\mathbf{K}_{ij}^{(e)} = \int_{l(e)} \mathbf{B}_i^T \hat{\mathbf{D}}' \mathbf{B}_j ds \tag{3.21}$$

$$\mathbf{f}_i^{(e)} = \int_{l(e)} \mathbf{N}_i^T \mathbf{t} ds + \mathbf{p}_i \tag{3.22}$$

The integrals along the element lenght are computed using numerical integration as

$$\begin{aligned} \mathbf{K}_{ij}^{(e)} &= \sum_{p=1}^{n_p} [\mathbf{B}_i^T \hat{\mathbf{D}}' \mathbf{B}_j J^{(e)}]_p W_p \\ \mathbf{f}_i^{(e)} &= \mathbf{p}_i + \sum_{p=1}^{n_p} [\mathbf{N}_i^T \mathbf{t} J^{(e)}]_p W_p \end{aligned} \tag{3.23}$$

where n_p and W_p are respectively the sampling point and weight of the 1D Gaussian quadrature and $J^{(e)} = \frac{ds}{d\xi}$ is obtained from the isoparametric geometrial definition of the centroidal axis as

$$J^{(e)} = \frac{(dx^2 + dy^2 + dz^2)^{1/2}}{d\xi} = \left[\left(\sum_{i=1}^{n} \frac{dN_i}{d\xi} x_{p_i} \right)^2 + \left(\sum_{i=1}^{n} \frac{dN_i}{d\xi} y_{p_i} \right)^2 + \left(\sum_{i=1}^{n} \frac{dN_i}{d\xi} z_{p_i} \right)^2 \right]^{\frac{1}{2}}$$

The derivatives in (3.20) are computed using $J^{(e)}$ as

$$\frac{\partial N_i}{\partial s} = \frac{\partial N_i}{\partial \xi} \frac{\partial \xi}{\partial s} = \frac{l}{J^{(e)}} \frac{\partial N_i}{\partial \xi} \tag{3.24}$$

Timoshenko beam elements suffer from shear locking behaviour when used for slender beam situations. The simplest approach to avoid locking in this case is to use *reduced integration* for the shear terms in the stiffness

matrix. In fact, it has been proved that a *uniform reduced integration* for all terms of $\mathbf{K}^{(e)}$ provides excellent results [2]. This simply requires to use one, two and three point quadratures for the linear, quadratic and cubic beam elements, respectively.

Of particular practical interest is the simple two node linear (straight) beam element with a single integration point for which the stiffness matrix can be explicitely computed as

$$\mathbf{K}_{ij}^{(e)} = \bar{\mathbf{B}}_i^T \bar{\hat{\mathbf{D}}}' \bar{\mathbf{B}}_j l^{(e)} \tag{3.25}$$

where $(\bar{\cdot})$ denotes values at the element mid–point. The form of $\bar{\mathbf{B}}_i$ can be directly obtained form (3.14) and (3.20) by making $N_i = \frac{1}{2}$ and $\frac{\partial N_i}{\partial \bar{s}} = \frac{(-1)^i}{l^{(e)}}$. Also as the element is straight $\mathbf{L}_i = \mathbf{L}_j = \mathbf{L}$.

FORMULATION OF ECCENTRIC BEAM STIFFENER ELEMENTS

Figure 3.5 shows a typical case of a shell element stiffed by an eccentric beam element. The shell element formulation could be based on any of the flat or degenerated layered shell elements presented in Lecture 1 and will not be repeated here. We will also assume for simplicity that the stiffner is based on the Timoshenko beam theory studied in previous section.

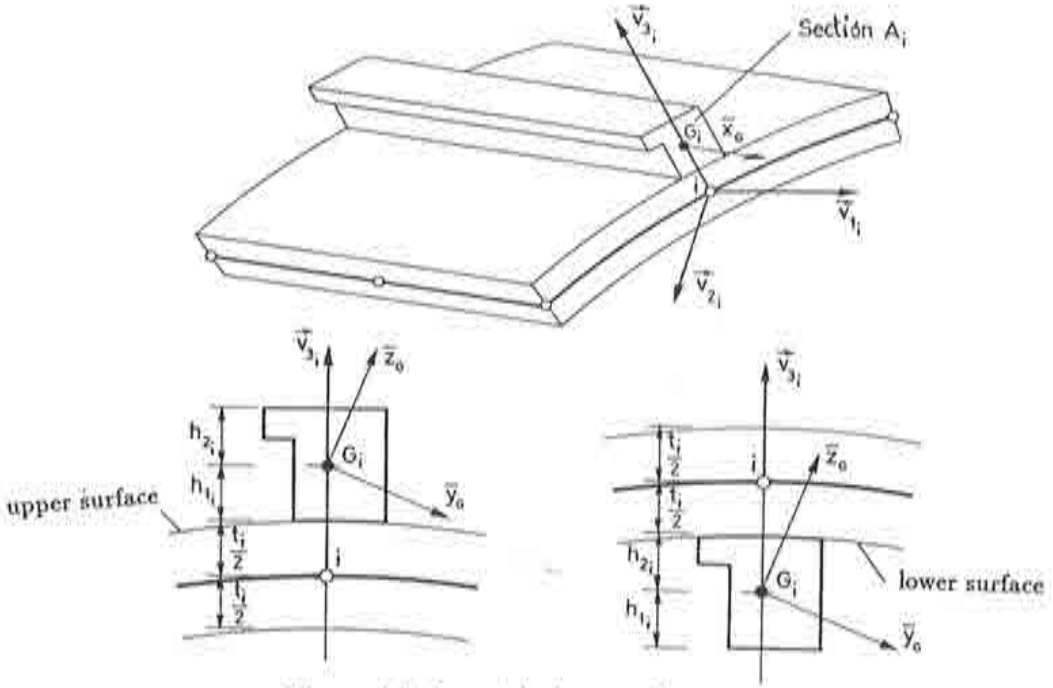

Figure 3.5 Eccentric beams element.

A further assumption will be that the beam stiffener is rigidly connected to one of the two shell surfaces along a nodal line. Therefore displacement compatibility conditions along that line require that the order of the beam and shell elements be the same. Also if both elements are rigidly connected the beam transverse section A_i has the same global rotations as the ith shell node to which it is connected. Finally we will assume that the normal nodal axe of the shell element $\vec{v}_{3_i}$ crosses the centroid of the beam section. Note, however, that it is not necessary that the directions of the nodal vectors in the shell coincide with the local axes of the beam section.

With these assumptions we can express the global displacements of the beam centroid G_i in terms of the displacements of the shell ith node as

$$\vec{u}_{G_i} = \vec{u}_i + \vec{\theta}_i \times \alpha_i \vec{v}_{3_i} \quad ; \quad \vec{\theta}_{G_i} = \vec{\theta}_i \tag{3.26}$$

or

$$\mathbf{u}_{G_i} = \mathbf{u}_i + \mathbf{A}_i \boldsymbol{\theta}_i \quad ; \quad \boldsymbol{\theta}_{G_i} = \boldsymbol{\theta}_i \tag{3.27}$$

with

$$\begin{aligned} \mathbf{u}_{G_i} &= [u_{G_i}, v_{G_i}, w_{G_i}]^T \\ \mathbf{u}_i = [u_i, v_i, w_i]^T \quad ; \quad \mathbf{A}_i &= \alpha_i \begin{bmatrix} 0 & v_{3_i}^z & -v_{3_i}^y \\ -v_{3_i}^z & 0 & v_{3_i}^x \\ v_{3_i}^y & -v_{3_i}^x & 0 \end{bmatrix} \\ \boldsymbol{\theta}_{G_i} = \boldsymbol{\theta}_i &= [\theta_{x_i}, \theta_{y_i}, \theta_{z_i}]^T \end{aligned} \tag{3.28}$$

and

$$\alpha_i = \begin{cases} \left(\dfrac{t_i}{2} + h_{1_e}\right) & \text{if the beam stiffner lays on the} \\ & \textit{upper} \text{ surface of the shell} \\ -\left(\dfrac{t_i}{2} + h_{2_e}\right) & \text{if the beam stiffner lays on the} \\ & \textit{lower} \text{ surface of the shell} \end{cases}$$

where t_i is the thickness of ith shell node and h_{1_i} and h_{2_i} are the distances of the beam centroid to the upper and lower shell surfaces, as shown in Figure 3.5. From 3.17 we deduce that the global displacements vector of the beam centroid G_i can be expressed in terms of the global displacements of node i in the shell element as

$$\mathbf{a}_i^B = \begin{Bmatrix} \mathbf{u}_{G_i} \\ \boldsymbol{\theta}_{G_i} \end{Bmatrix} = \begin{bmatrix} \mathbf{I} & \mathbf{A}_i \\ \mathbf{0} & \mathbf{I} \end{bmatrix} \begin{Bmatrix} \mathbf{u}_i \\ \boldsymbol{\theta}_i \end{Bmatrix} = \hat{\mathbf{A}}_i \mathbf{a}_i^S \tag{3.29}$$

where super–indexes B y S denote beam and shell displacements, respectively.

Eq.(3.29) allows to express the local generalized strains in the beam stiffner in terms of the nodal displacements of the shell element as

$$\hat{\boldsymbol{\epsilon}}' = \sum_{i=1}^{n} \mathbf{B}_i \mathbf{a}_i^B = \sum_{i=1}^{n} \mathbf{B}_i \hat{\mathbf{A}}_i \mathbf{a}_i^S = \sum_{i=1}^{n} \hat{\mathbf{B}}_i \mathbf{a}_i^S \tag{3.30}$$

The stiffness matrix of the eccentric beam stiffner in global axes is computed by eq.(3.21) substituting simply matrix $\mathbf{B}_i$ of (3.19) by $\hat{\mathbf{B}}_i = \mathbf{B}_i \hat{\mathbf{A}}_i$.

The final step is the assembly of the beam and shell stiffness equations. This may require in some cases to transform the stiffness equations on the shell element so that the nodal rotations at the connecting nodes are also expressed in global axes. This poses no additional difficulty even for coplanar nodes since the beam stiffner introduces the necessary rotational stiffness to avoid singularity of the global stiffness matrix [2].

In some cases the beam stiffner may have an arbitrary orientation with respect the shell mid–surface as shown in Figure 3.6. The only difference with the formulation described above is that now the relative position of each centroidal node in the beam with respect to the connecting ith shell node has to be precisely defined. Then the distance h_{G_i} between these two points and the unit vector $\vec{e}_{G_i}$ linking the two points must be computed. These two values replace now in (3.28) the distance α_i and the normal nodal vector $\vec{v}_{3_i}$, respectively. The rest of the formulation is identical to that presented above.

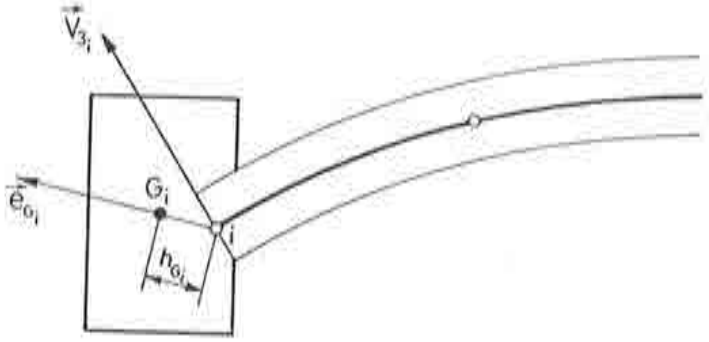

Figure 3.6 Beam stiffner arbitrary oriented with respect the shell mid surface.

Analysis of slab–beam bridges

Slab–beam bridges are a particular case of applications of the eccentric beam stiffener formulation described. For simplicity we will consider the bridge shown in Figure 3.7, formed by an assembly of a rectangular slab and straight beams of rectangular cross section. However, the case of inertia varying beams poses no greater difficulty.

In the more general case the slab will behave as a flat shell element and the beam element will require the 3D formulation as described earlier in this

lecture. Again, for simplicity we will assume the same basic C_o finite element formulation for both type of elements (Reissner–Mindlin shell elements for the slab and Timoshenko beam elements for the beam).

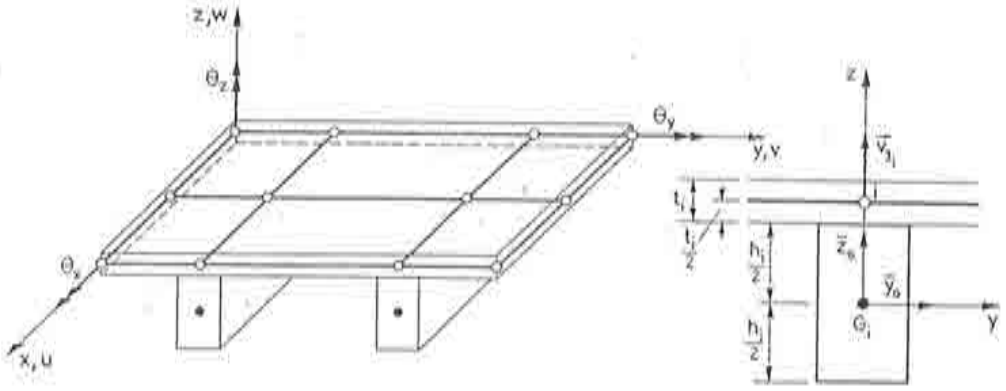

Figure 3.7 Slab–beam bridge.

Following the arguments given in previous section the displacement field of the beam nodal centroids can be written in terms of the slab nodal displacements as

$$\begin{aligned} u_{G_i} &= u_i + \frac{1}{2}(t_i + h_i)\theta_{y_i} \;,\; v_{G_i} = v_i - \frac{1}{2}(t_i + h_i)\theta_{x_i} \\ w_{G_i} &= w_i \;,\; \theta_{x_{G_i}} = \theta_{x_i} \;,\; \theta_{y_{G_i}} = \theta_{y_i} \;,\; \theta_{z_{G_i}} = \theta_{z_i} \end{aligned} \tag{3.31}$$

Therefore, matrix $\mathbf{A}_i$ of (3.28) can now simply be written as

$$\mathbf{A}_i = \begin{bmatrix} 0 & \frac{1}{2}(t_i + h_i) & 0 \\ -\frac{1}{2}(t_i + h_i) & 0 & 0 \\ 0 & 0 & 0 \end{bmatrix} \tag{3.32}$$

The beam stiffness matrix is transformed for direct assembly with that of the slab as

$$\hat{\mathbf{K}}^b_{ij} = \hat{\mathbf{A}}^T_i \mathbf{K}^b_{ij} \hat{\mathbf{A}}_i \tag{3.33}$$

where $\mathbf{K}^b_{ij}$ is the standard beam stiffness matrix given by eq.(3.21) and $\hat{\mathbf{A}}_i$ is deduced from (3.29).

A simpler alternative to analyse slab beam bridges is to neglect the beam eccentricity effect. In this case the slab is modeled with simpler plate

elements and the beams with standard 1D beam elements including torsional effects. In the next section we present an example where the different options to analyse a slab–beam bridge are compared.

Example of linear analysis of a slab–beam bridge

Figure 3.8 shows the geometry of a slab beam bridge simply supported in four points of each end section analyzed under unformly distributed loading of $q = 10KN/m^2$. A quarter of the structure has been analyzed due to symmetry as shown in Figure 3.8. For the slab and beams $E = 10^7 KN/m^2$ and $\nu = 0.3$. The analysis has been carried out with three different elements.

a) 4 node quadrilateral flat shell elements [5] for modelling both the slab and beams (Figure 3.8a).
b) 4 node quadrilateral flat shell elements [5] for the slab and 2 node 3D Timoshenko beam element (Figure 3.8b).
a) 4 node quadrilateral plate elements [5] for the slab and simple 1D Timoshenko beams including torsional effects (Figure 3.8c).

Figure 3.9 shows the results for the normal stresses at the central section obtained with each of the three formulations. It can be noted that errors in the values computed with the simpler (c) formulation do not exceed 20% of those obtained with the more precise (a) and (b) assumptions.

NON LINEAR ANALYSIS OF SHELLS WITH ECCENTRIC BEAM STIFFNESS

The non linear analysis of concrete beam–shell assemblies follows precisely the lines explained in Lecture 1 for the shell case.Material non linearities in the beam and shell elements are modelled using a layered approach together with an adequate constitutive model for concrete and reinforcing steel as described in Lecture 2. The layered model allows to monitor onset and evolution of damage (i.e. cracking in concrete or plasticity in steel) at each individual layer in both the shell and beam stiffeners.

Geometric non linear effects can also be properly taken into account following the lines described in Lecture 1. Details of the adequate geometrically non linear formulations for the beam stiffeners can be found in [3,4].

Some examples of the non linear behaviour of beam–shell assemblies are given in Lecture 4.

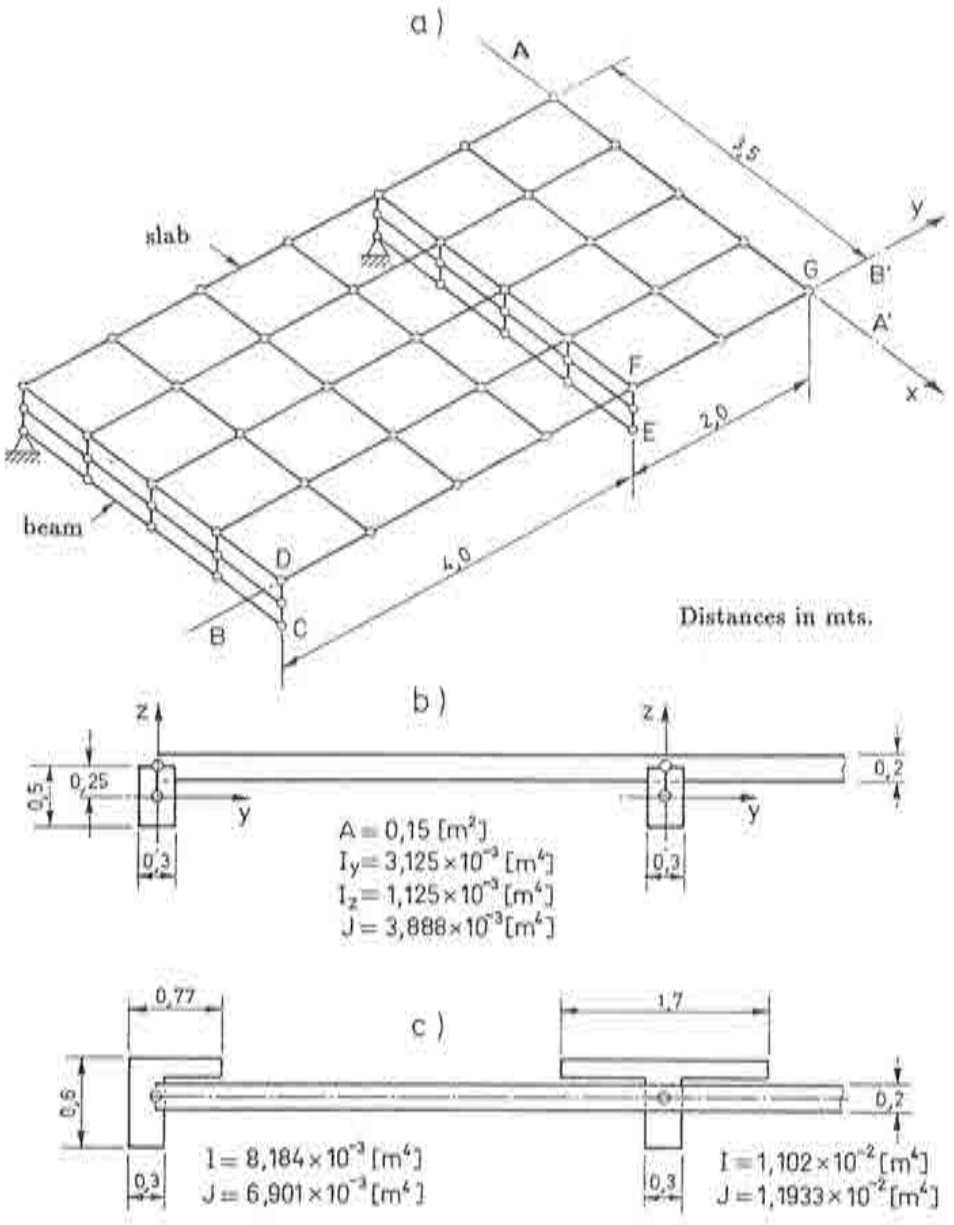

Figure 3.8 Slab–beam bridge under uniformly distributed loading. (a) Discretization of slab and beams in flat shell elements (b) Discretization in flat elements (slab) and 2 node 3D Timoshenko beams, (c) Discretization in plate elements (slab) and 2 node 1D Timoshenko beams. 1/4 of the structure analized for symmetry.

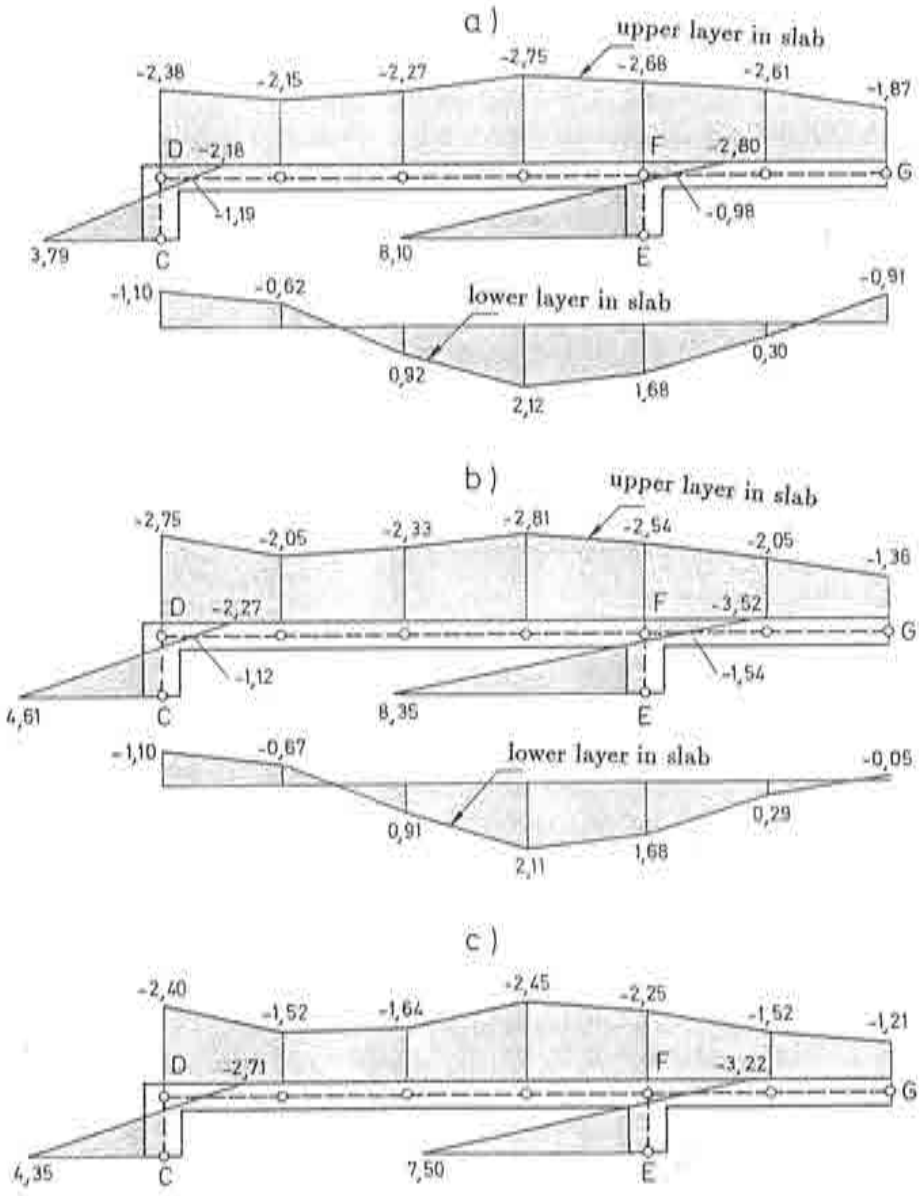

Figure 3.9 Slab–beam bridge under uniformly distributed loading. Normal stresses in central section for the formulations (a), (b) and (c) as described in Figure 3.8.

REFERENCES

1. O.C. Zienkiewicz, and R.L. Taylor, "*The Finite Element Method*", Fourth Edtion Mc.Graw Hill, Vol. I (1989), Vol II (1991).
2. M. Crisfield, "*Finite Element Method and Solution Procedures for Structural Analysis*", Pineridge Press, 1986.

3. K.J. Bathe. '*Finite Element procedures in engineering analysis*", Prentice hall Inc. 1982.
4. M. Crisfield, "*Finite element methods for non linear structural analysis*", J Wiley, 1991.
5. E.N. Dvorkin and K.J. Bathe, "A continuum mechanics based four node shell element for general non-linear analysis", *Eng. Comp.*, Vol. **1**, pp. 77–88, 1984.

Lecture 4

SOME EXAMPLES OF FINITE ELEMENT NON LINEAR ANALYSIS OF CONCRETE SHELLS

SUMMARY

This lecture presents some practical applications of the finite element formulations for non linear analysis of reinforced concrete shells studied in previous lectures. Examples presented range from the analysis of plain and pre–stressed concrete beams to more sophisticated shell type structures, including the non linear behaviour of a composite steel–concrete girder bridge and a cryogenic concrete liquid gas tank under severe thermal actions.

EXAMPLE 1. BENDING TEST OF A SIMPLY SUPPORTED NOTCHED BEAM UNDER CENTRAL POINT LOAD (FRACTURE MODE I)

Figure 4.1 shows the geometry and material properties of the beam and the finite element mesh of isoparametric 8 node Serendipity elements, used [1]. The non linear behaviour of concrete has been modelled with the plastic–damage model described in Lecture 2.

Experimental results for the load–displacement curve for this example are shown in Figure 4.2 [2] together with the numerical results obtained in the analysis.

Figure 4.1 shows an amplification of the notched zone for the final state (point C in the load–displacement curve of Figure 4.2). Note the strain localization in a band of elements modelling the progression of the crack towards the upper part of the beam.

Figure 4.3 shows the distribution of cracks for the maximum and final loads (points B and C in Figure 4.2). The length of each crack line represents the amount of plastic deformation in the corresponding ortogonal direction thus providing an indicator of the opening of the crack. The damaged elements zone has been amplified in Figure 4.4 showing the typical fracture mode I as expected.

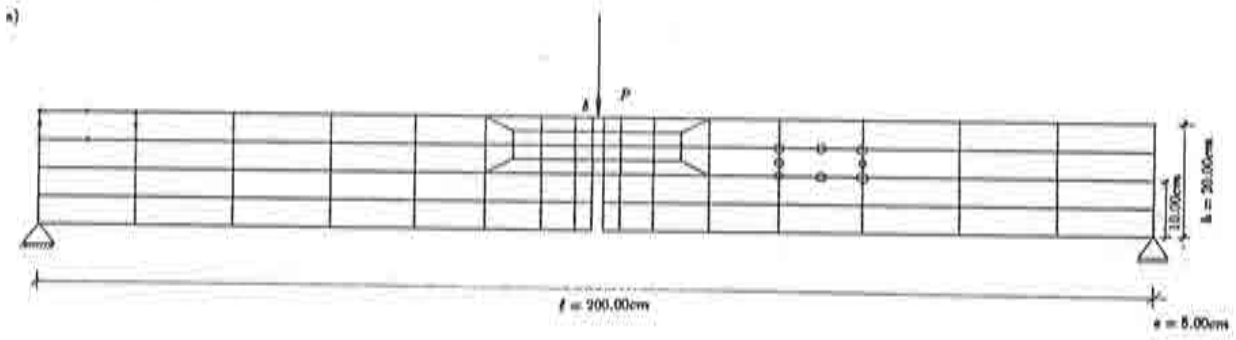

$E_0 = 305810.40\ kg/cm^2$.
$\nu_0 = 0.20$
$\phi_0 = cte. = 32^0$
$\psi_0 = cte. = 32^0$

$\sigma_c^{max} = 339.45\ kg/cm^2$
$\sigma_c^{resh} = 360.00\ kg/cm^2$
$\sigma_t^{max} = 36.00\ kg/cm^2$
$G_f = 0.126\ kg/cm$
$G_c = 12.000\ kg/cm$

Associated plasticity (no stiffness degradation)

Figure 4.1 Simple supported notched beam under point load. Geometry, mesh and material properties.

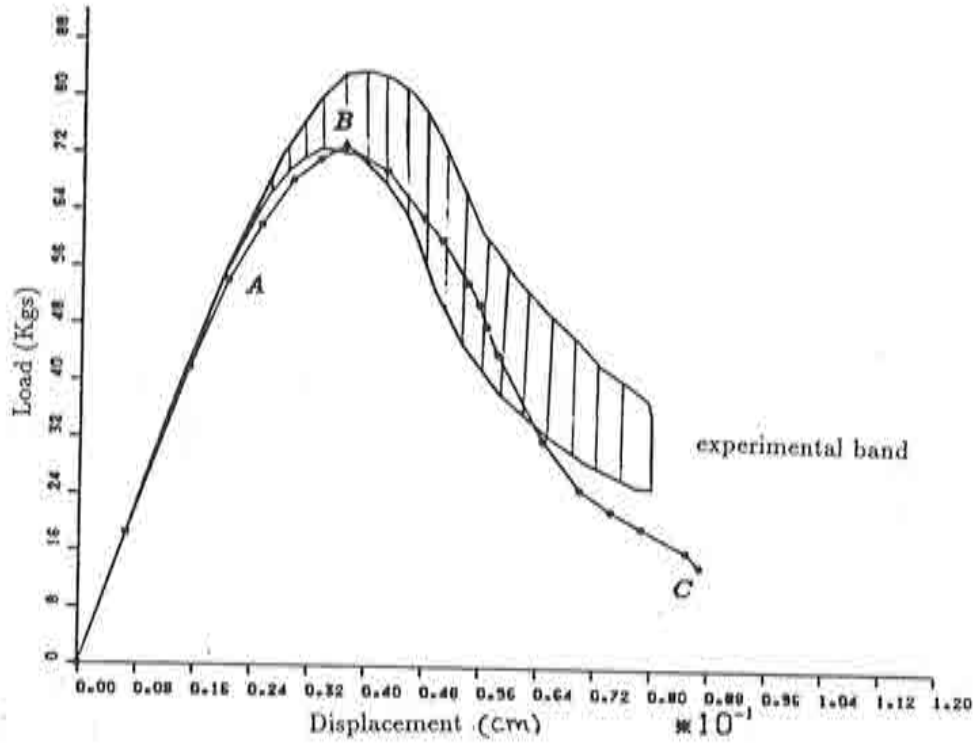

Figure 4.2 Simple supported notched beam. Load–displacement curve. Point A: onset of cracking; Point B: maximum load; Point C: Final state.

Finally in Figure 4.5 the distribution of principal stresses for load points A,B, and C of Figure 4.2 is also shown. Note the relaxation of tensible stresses as cracking develops and the intensity of compressive stresses in the upper part ot the beam for the final state which requires adequate modelling of non linear compressive behaviour of concrete in these zones. For further information see [5].

EXAMPLE 2 ANALYSIS OF A NOTCHED BEAM (MIXED FRACTURE MODE)

This example is a reproduction of the experimental test performed by Arrea and Ingraffes [3]. The geometry of the notched beam, material data and loading conditions used to induce a mixed fracture mode (modes I and II) are shown in Figure 4.6. As it can be seen the steel beams, used to transmit the loads to the concrete beam, have also been considered in the analysis (assuming a linear behaviour) in order to take in account its rigidity. The numerical analysis was performed using eight–noded two dimensional finite elements, and the mesh used is shown in Figure 4.6. The *crack mounth sliding displacenent* (CMSD) at the notch tip (see Figure 4.6) was controlled using a spherical path technique [4]. Again the plastic–damage model for concrete described in Lecture 2 has been used.

Numerical results for the load–CMSD showing the points of onsetting of cracking (point A), instability (point B) and ultimate state analized (point C) have been plotted in Figure 4.7. Good agreement with experimental results [3] also plotted in the same figure, is obtained.

In Figure 4.8 the cracking pattern at the peak (point B of Figure 4.7) and ultimate load (point C of Figure 4.7) are shown.It is interesting to note that cracking localizes in a narrow curved band after the peak load, for which all cracks are distributed almost vertically and form an angle of approximately 60° with the horizontal axis (see Figure 4.8a). Excellent agreement between the localized cracking band obtained numerically and experimentaly is achieved, as it can be seen in Figure 4.8d.

The principal stress distributions at the onset of cracking (point A of Figure 4.7) and the ultimate state (point C of Figure 4.7) are shown in Figure 4.9. It is worth noting the stress relaxation in the zone where cracking localizes (see Figure 4.9b). This localization can also be clearly seen in Figure 4.10, where the deformed shape of the beam (amplified 300 times) at the end of the test is shown. Further details can be found in [6].

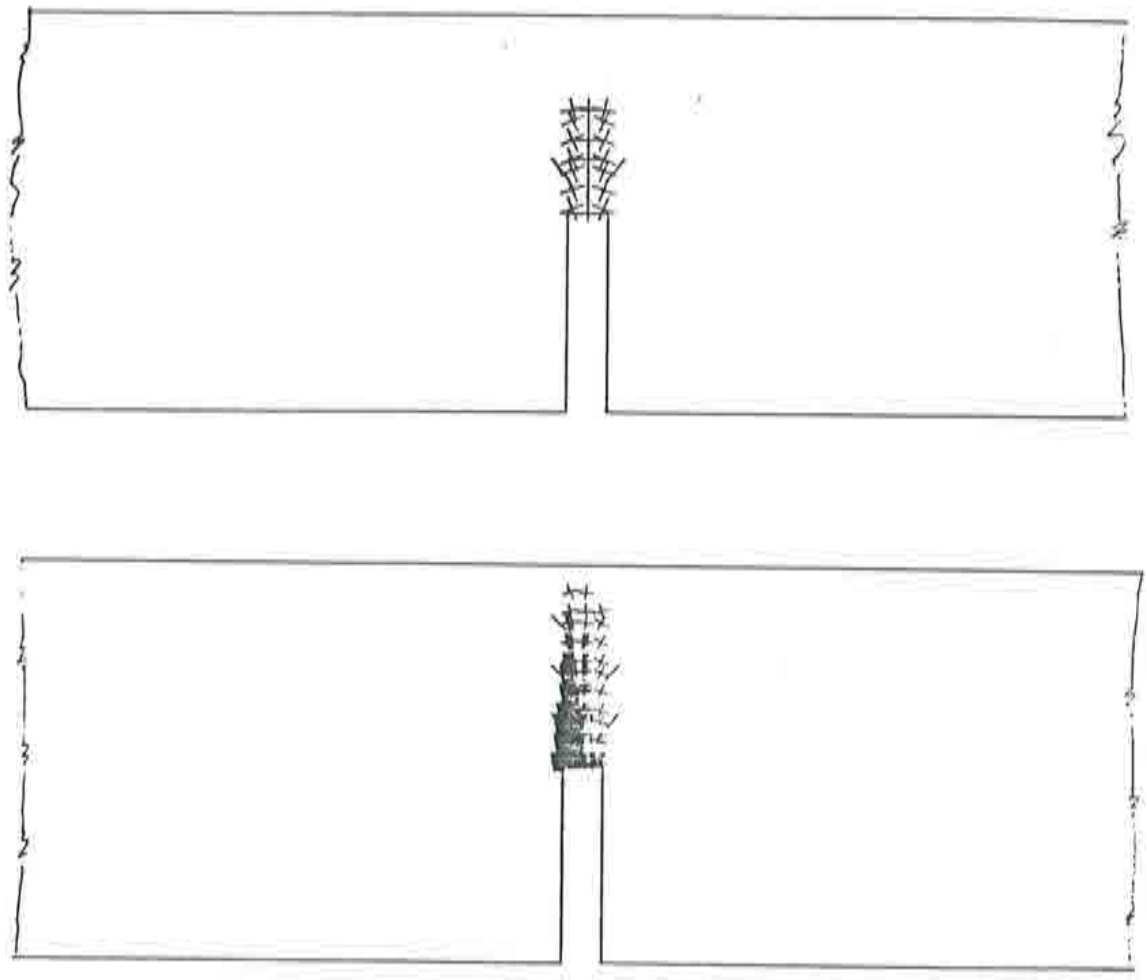

Figure 4.3 Simply supported notched beam. Cracking patters for points B and C of Figure 4.2.

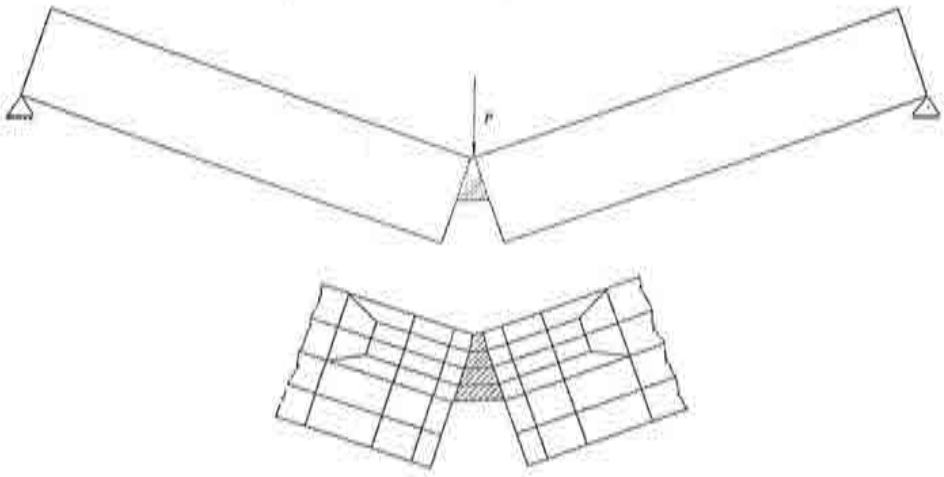

Figure 4.4 Straim localization in the notched region.

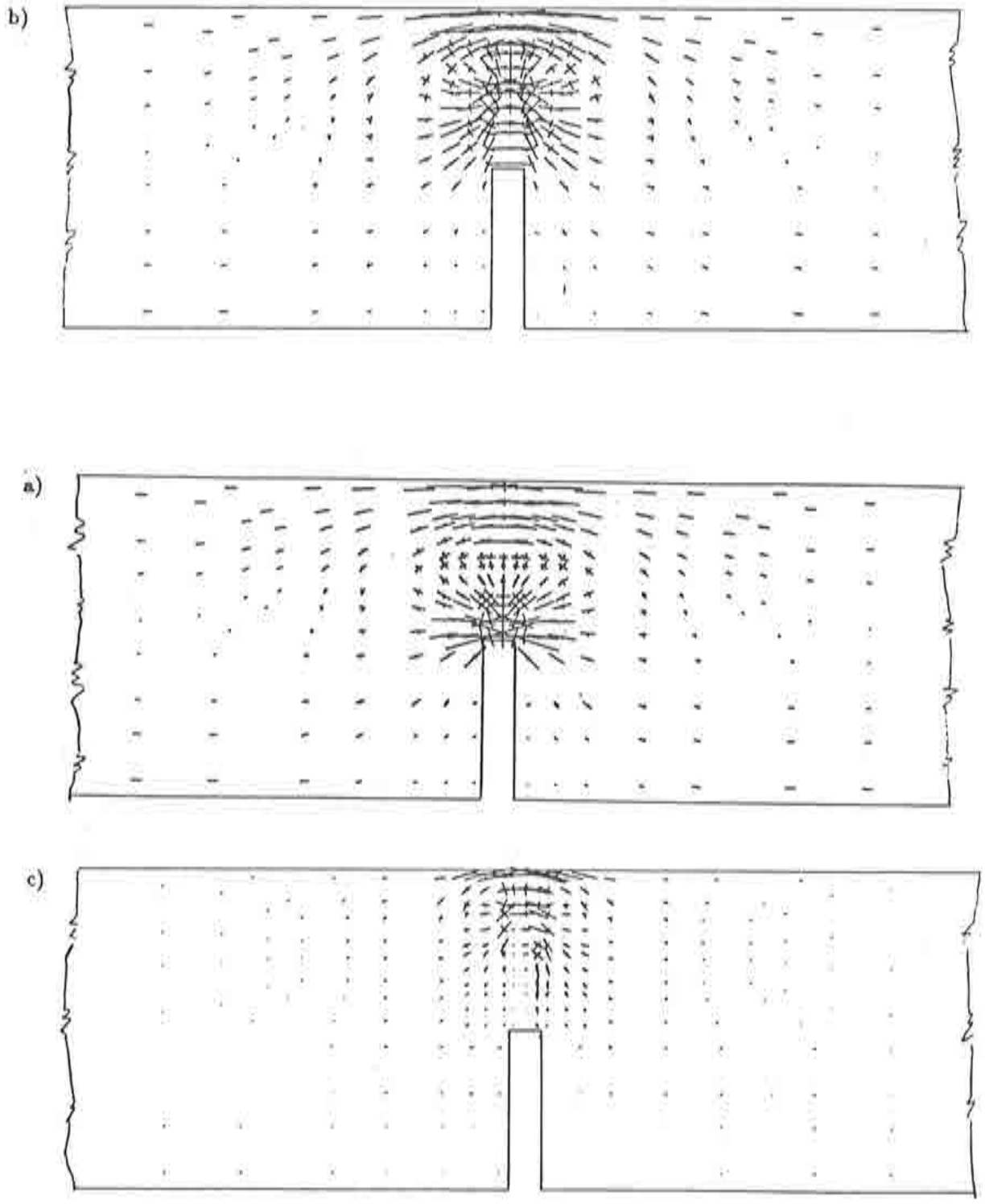

Figure 4.5 Simply supported notched beam. Principal stress distribution for points A, B and C of Figure 4.2.

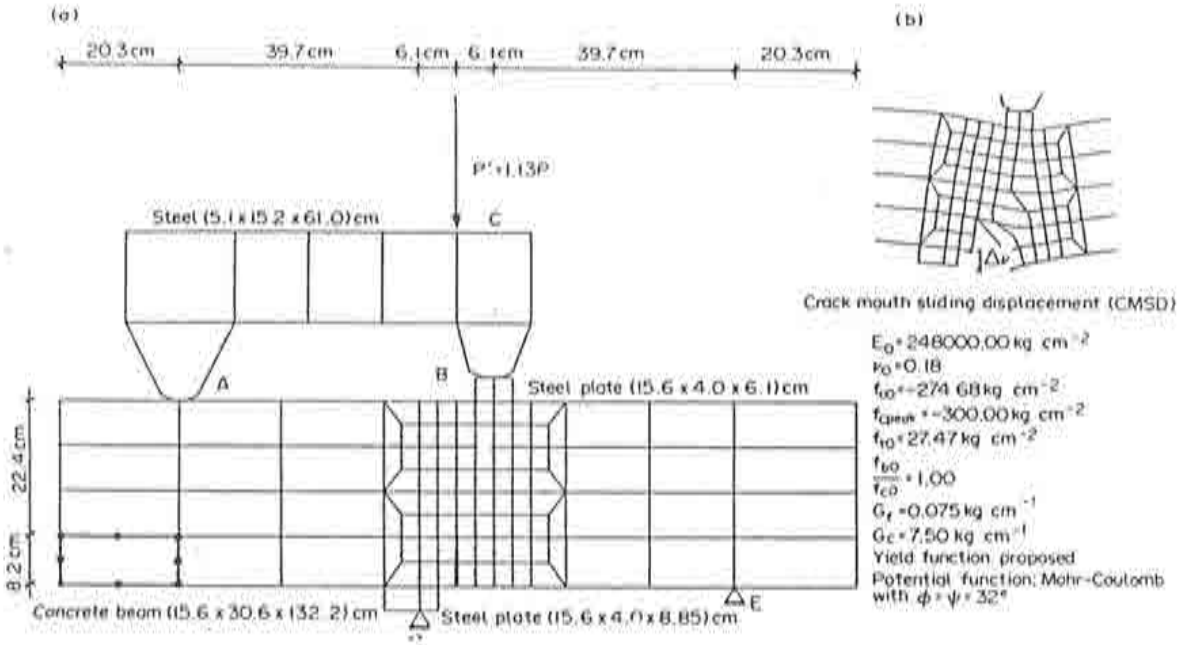

Figure 4.6 Notched beam (mixed fracture mode). Material parameters and finite element mesh.

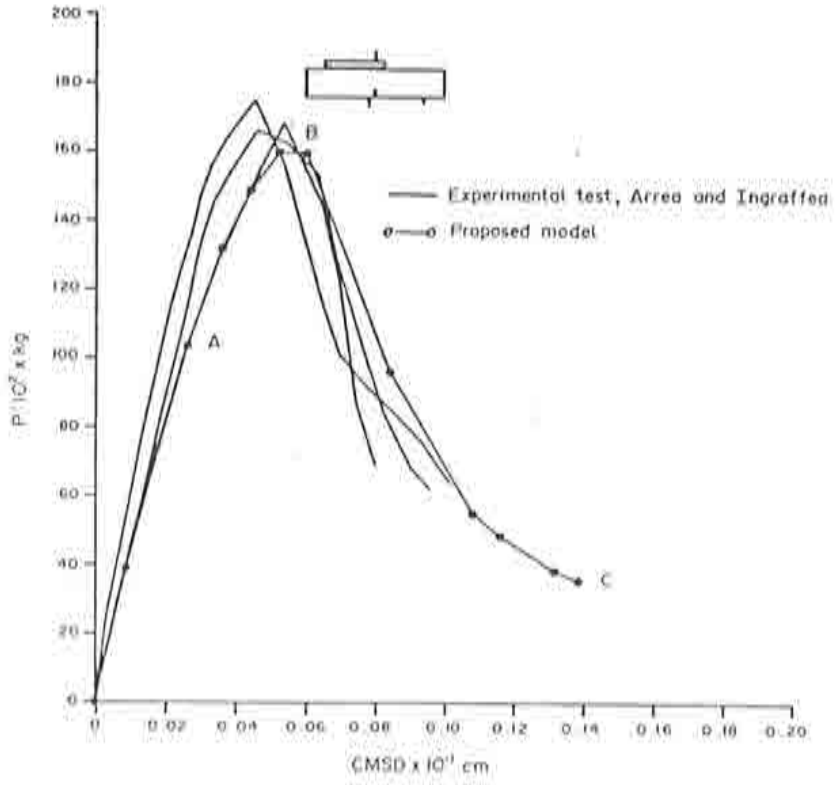

Figure 4.7 Notched beam (mixed mode). Load–displacemenet curves. Comparison with experimental test.

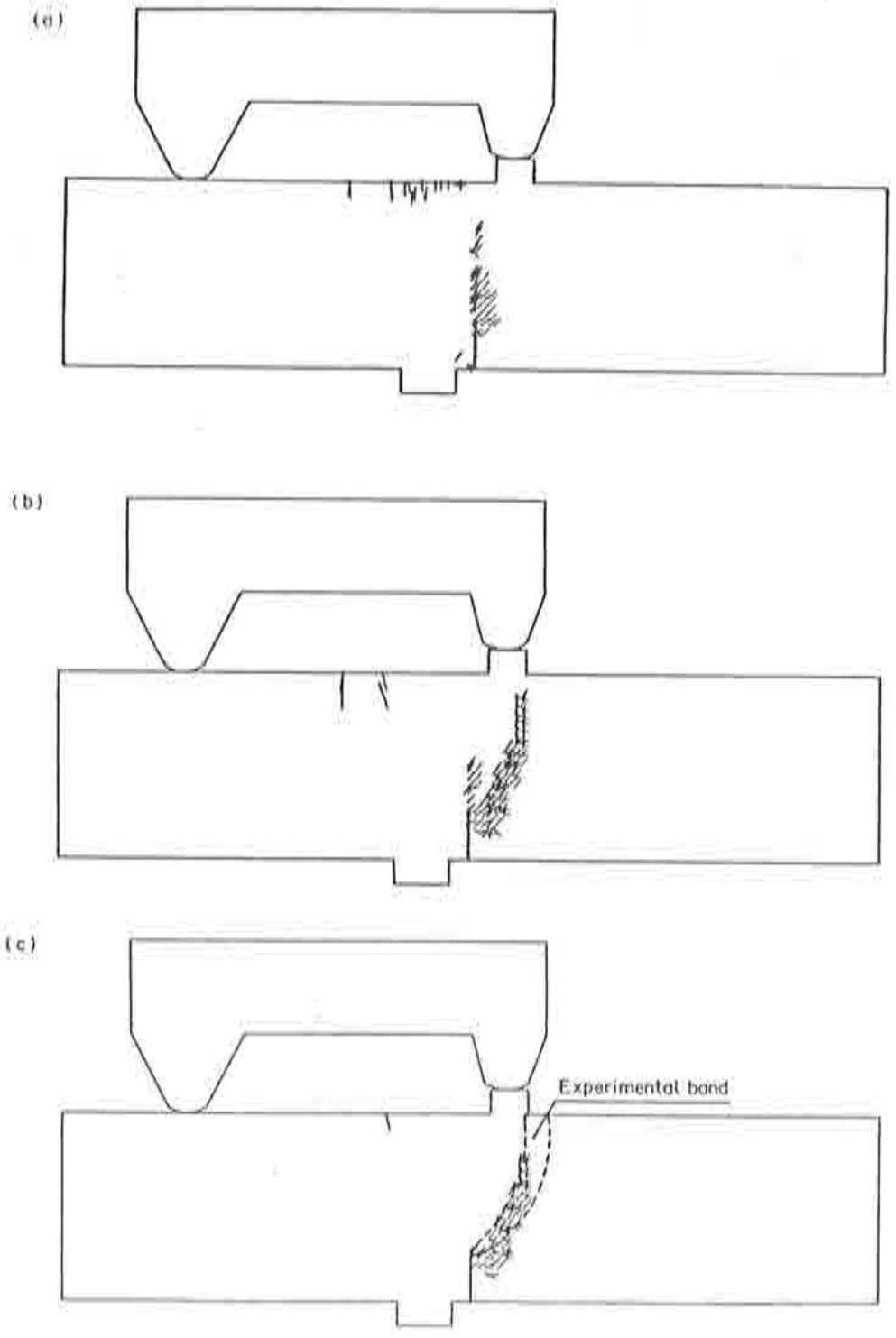

Figure 4.8 Notched beam (mixed mode). Distribution and localization of cracking
a) at the peak of stress (B) – All cracks;
b) at the ultimate state (C) – Cracks greater that 3% of the maximum crack:
c) at the ultimate state (C) – Cracks greater that 5% of the maximum crack.

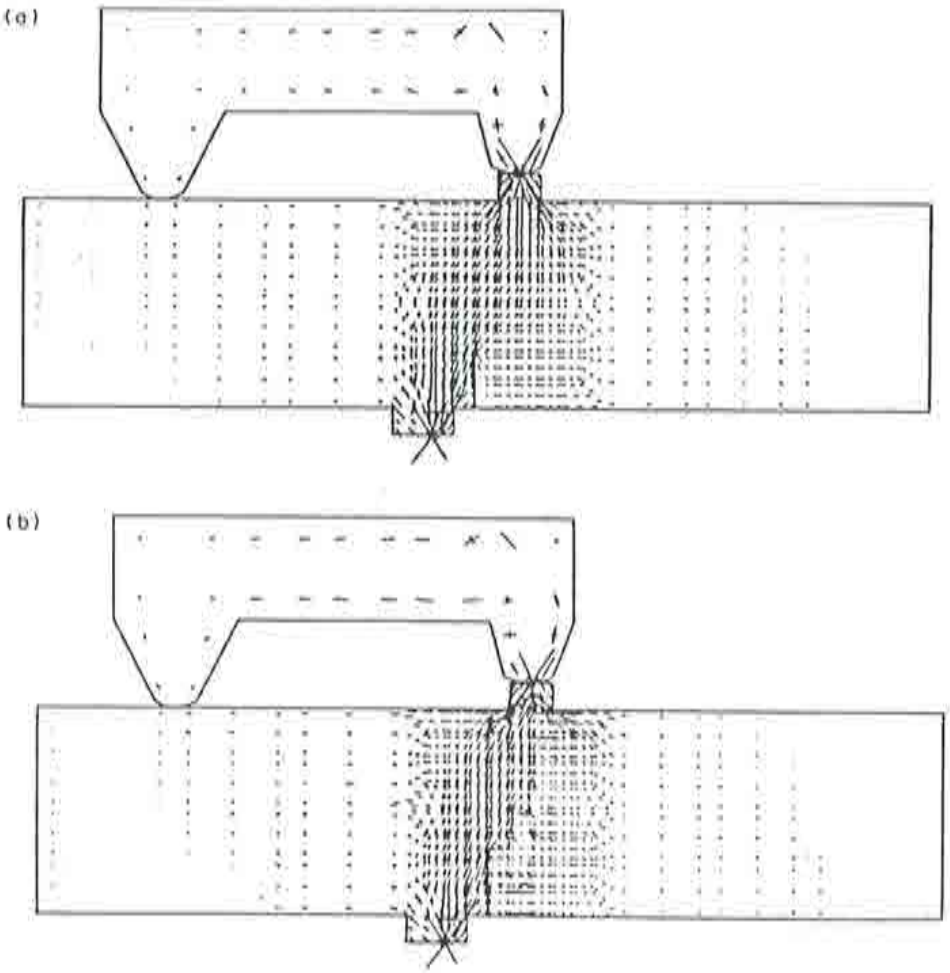

Figure 4.9 Notched beam mixed mode. Stress state: (a) at the elastic state (A); (b) at the ultimate state (C).

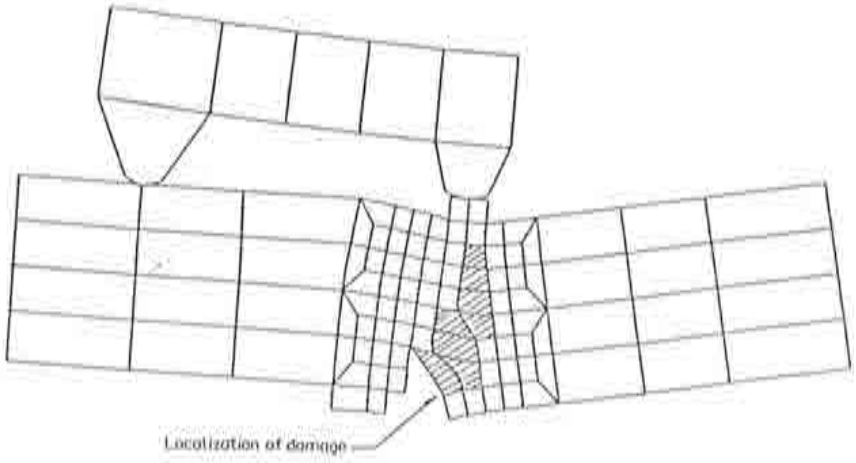

Figure 4.10 Notched beam mixed mode. Strain locatization for the final state (deformation are amplified 300 times).

EXAMPLE 3. PRESTRESSED CANTILEVER BEAM

The beam shown in Figure 4.11 has been analized under the following loading conditions [7]: (a) prestressing in a direction parallel to the neutral axis, and (b) subsequent transversal loading as shown in Figure 4.11. This corresponds to an experimental test numerically studied by Rots *et al.* in [2].

The material parameters and finite element mesh used are also shown in Figure 4.11a. Four node cuadrilateral elements have been employed in the narrow band shown, whereas eight node cuadrilateral elements are used in the rest of the beam. 2×2 Gaussian quadrature has been used for all elements. The plastic damage model for concrete described in Lecture 2 has been used.

The load–displacement curve obtained is plotted in Figure 4.11b. Comparison of the results obtained with those presented in [2] is good. It can be seen that the applied load does not reach a zero value. This is due to the vertical component of the prestressing load, which oposes the opening of the two beam edges. The dissipated energy is shown in Figure 4.11c where it can be seen that the solution estabilizes to the correct value. In Figure 4.11d the stress changes in the point under more severe damage are presented. Finally Figure 4.12 clearly shows the localization of deformation and the evolution of cracks and stresses in the damaged zone. Again it is worth noting that the cracked elements simulate the effect of a single crack ocurring in practice. Further details of this analysis can be found in [7].

EXAMPLE 4. SIMPLY SUPPORTED MIXED BEAM-SLAB BRIDGE

We consider here the analysis of a simply supported mixed steel beams-reinforced concrete slab bridge using the elasto-plastic-brittle model presented en Lecture 2. The geometry of the bridge is shown in Figure 4.13. Details of the cross section discretization in layers are shown in Figure 4.14.

Some typical results of the analysis displaying the load-strain and load-deflection curves for two loading cases corresponding to two and four point loads acting on the midspan section are shown in Figures 4.15–4.16. Very good agreement of the measured midspan deflections with the numerical results obtained are also shown in Figure 4.16. For more information on this example see [8].

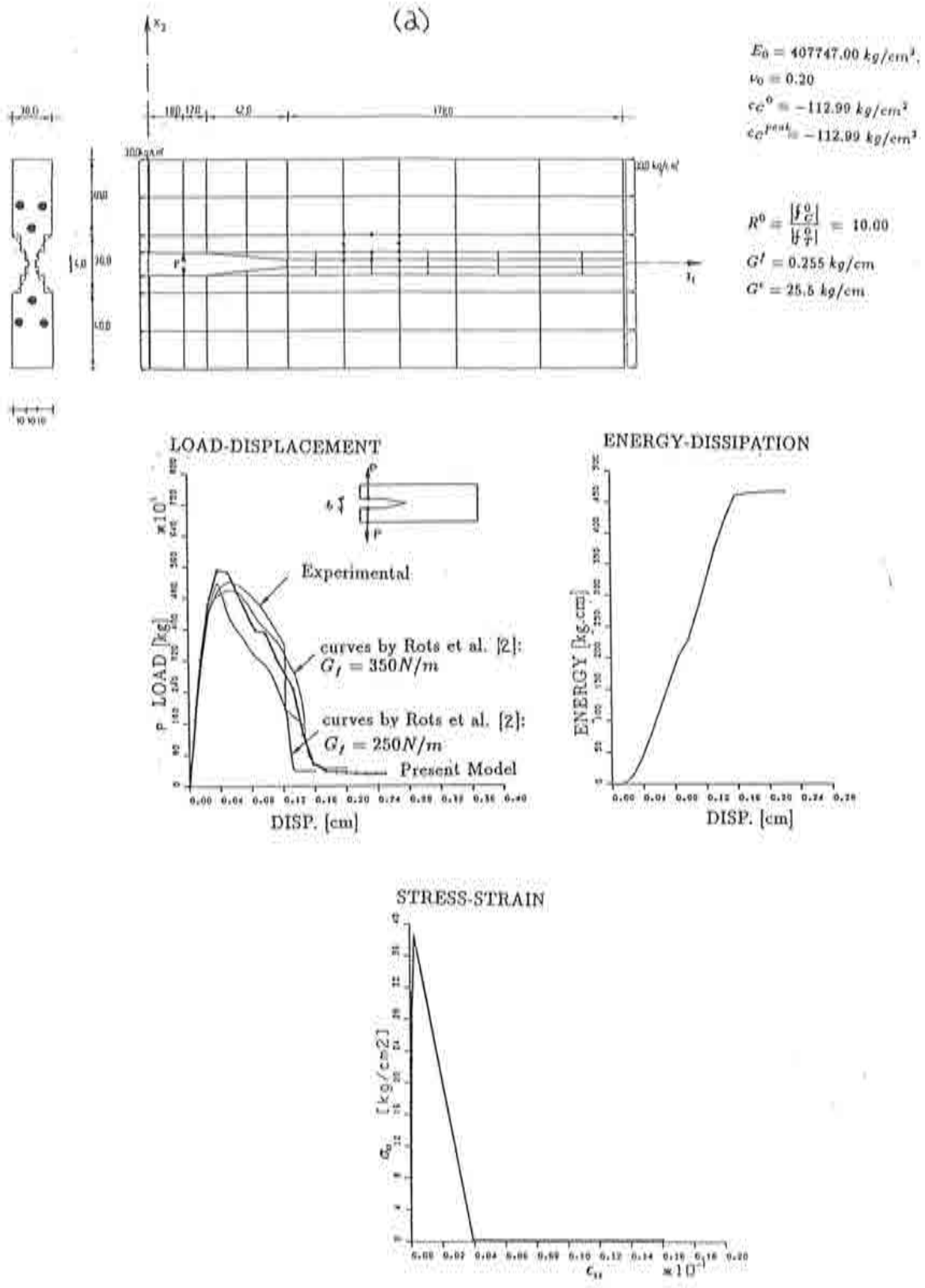

Figure 4.11 Prestressed beam (a) Material parameters and finite element mesh (b) Load–displacement curve, (c) Energy disipation curve, (d) Stress–strain curve in the more damaged integration point.

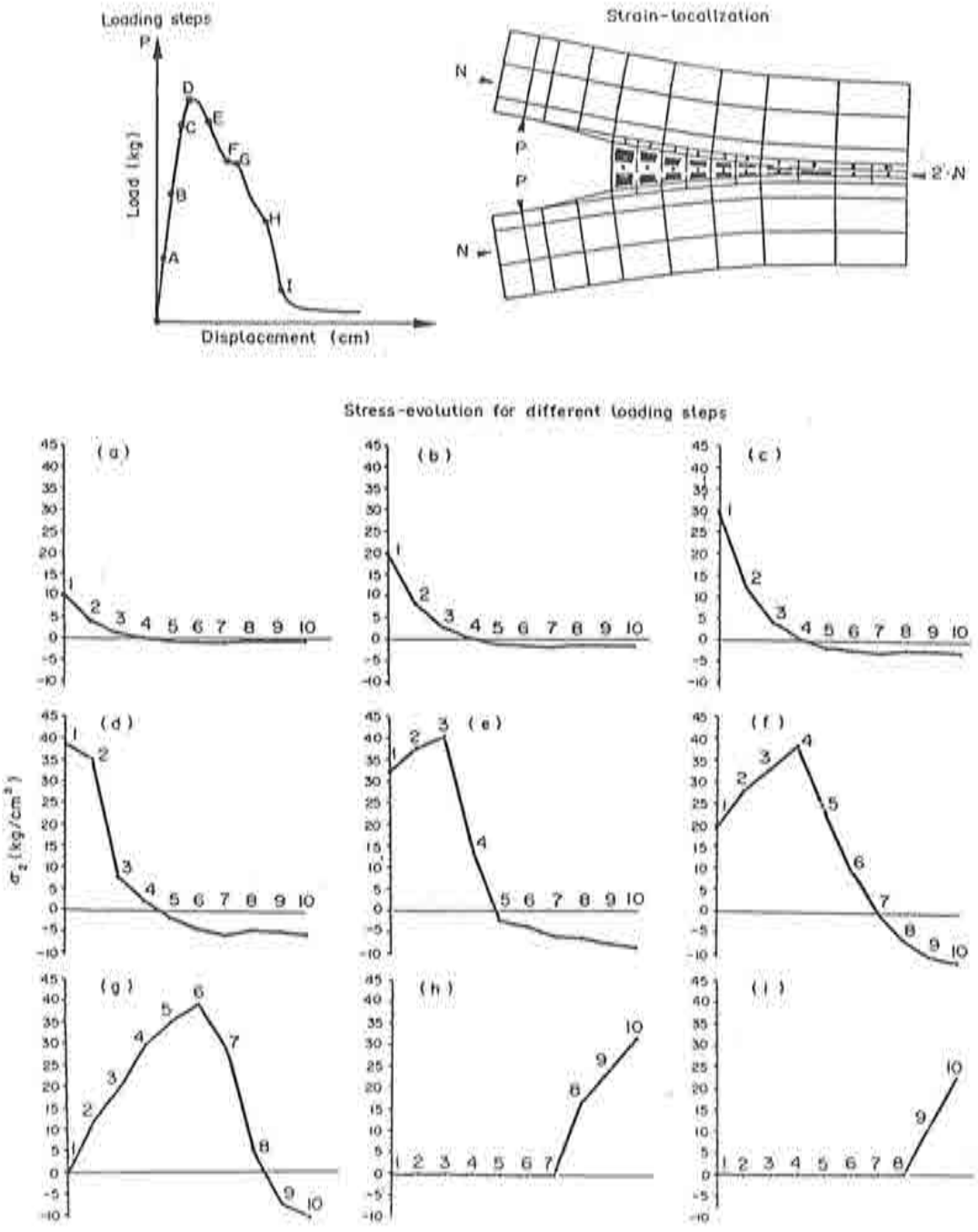

Figure 4.12 Prestressed beam, localization of cracking, and stress evolution along the damaged zone.

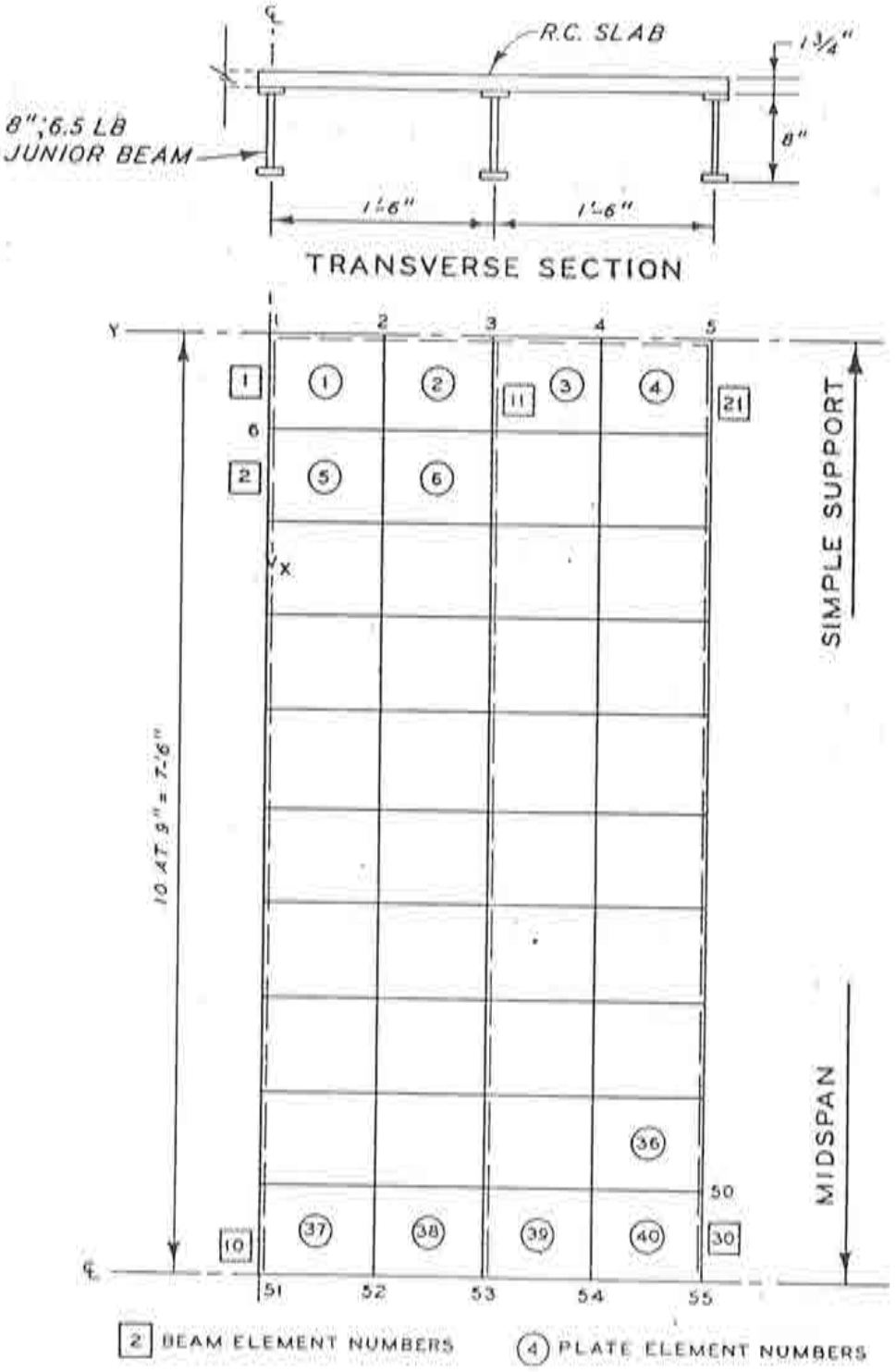

Figure 4.13 Discretization of simply supported mixed steel-concrete bridge.

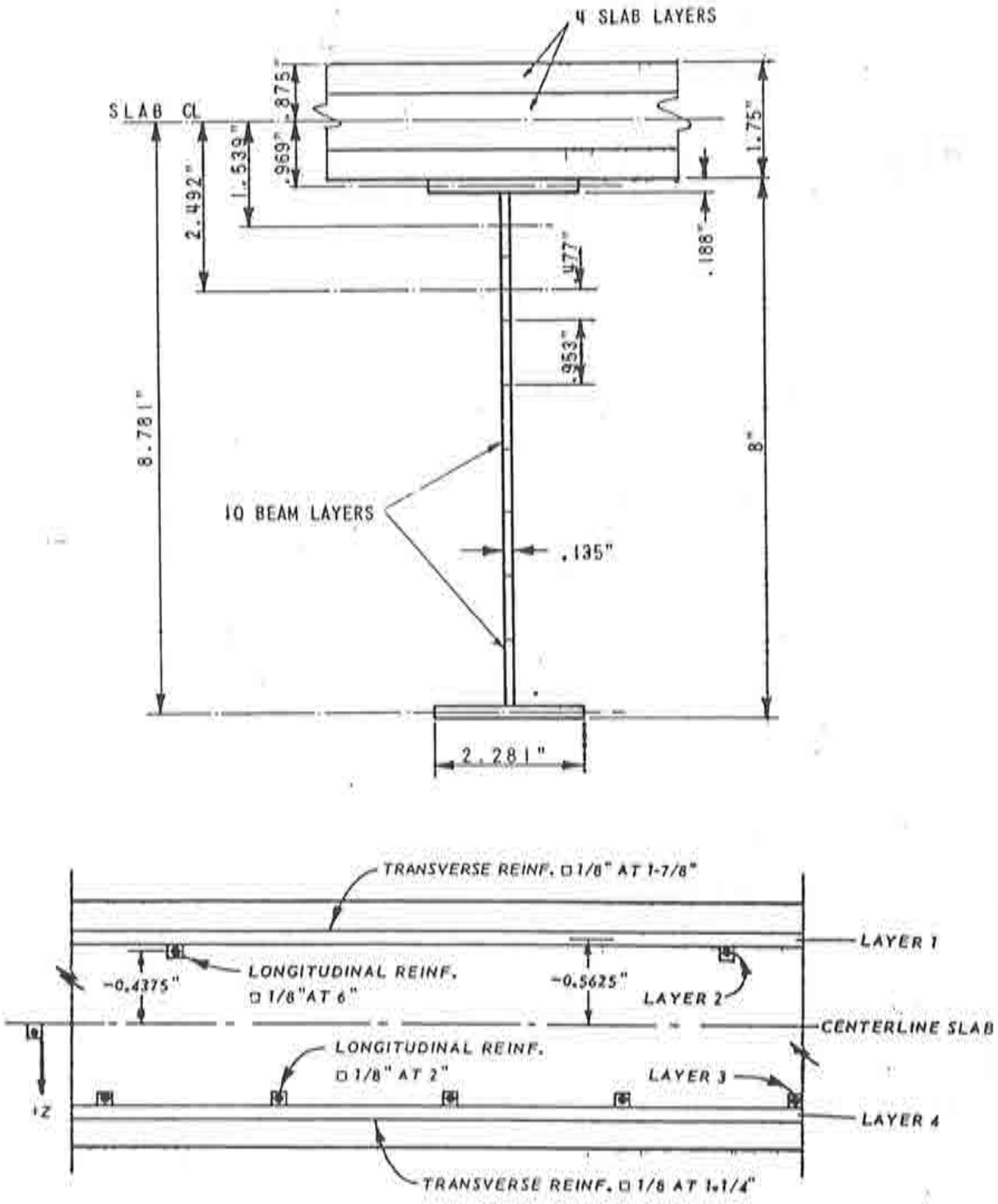

Figure 4.14 Simply supported mixed steel-concrete bridge. Layer discretization and reinforcement distribution in slab for two central load case.

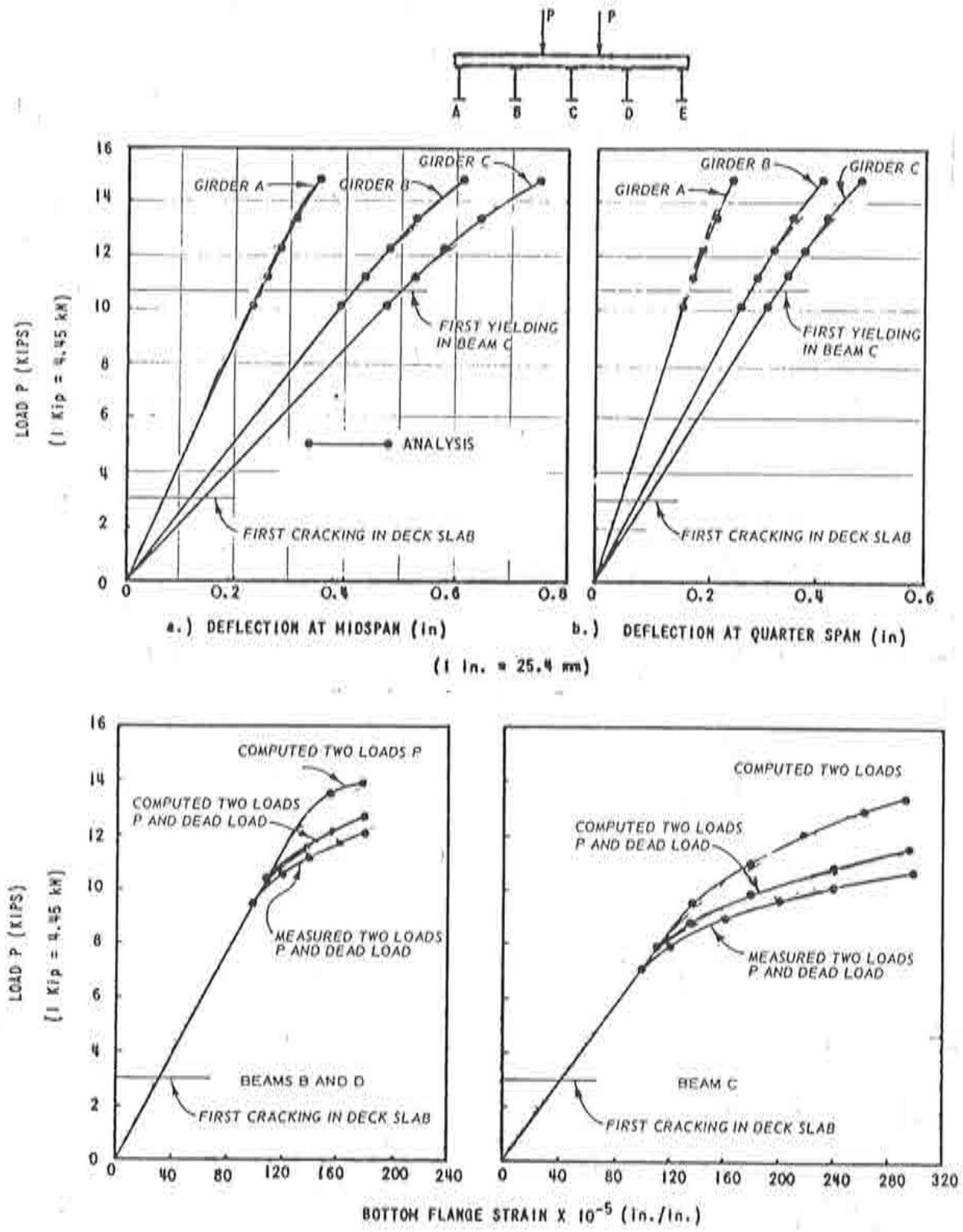

Figure 4.15 Simply supported mixed steel-concrete bridge. Load-deflection and load-strain curves.

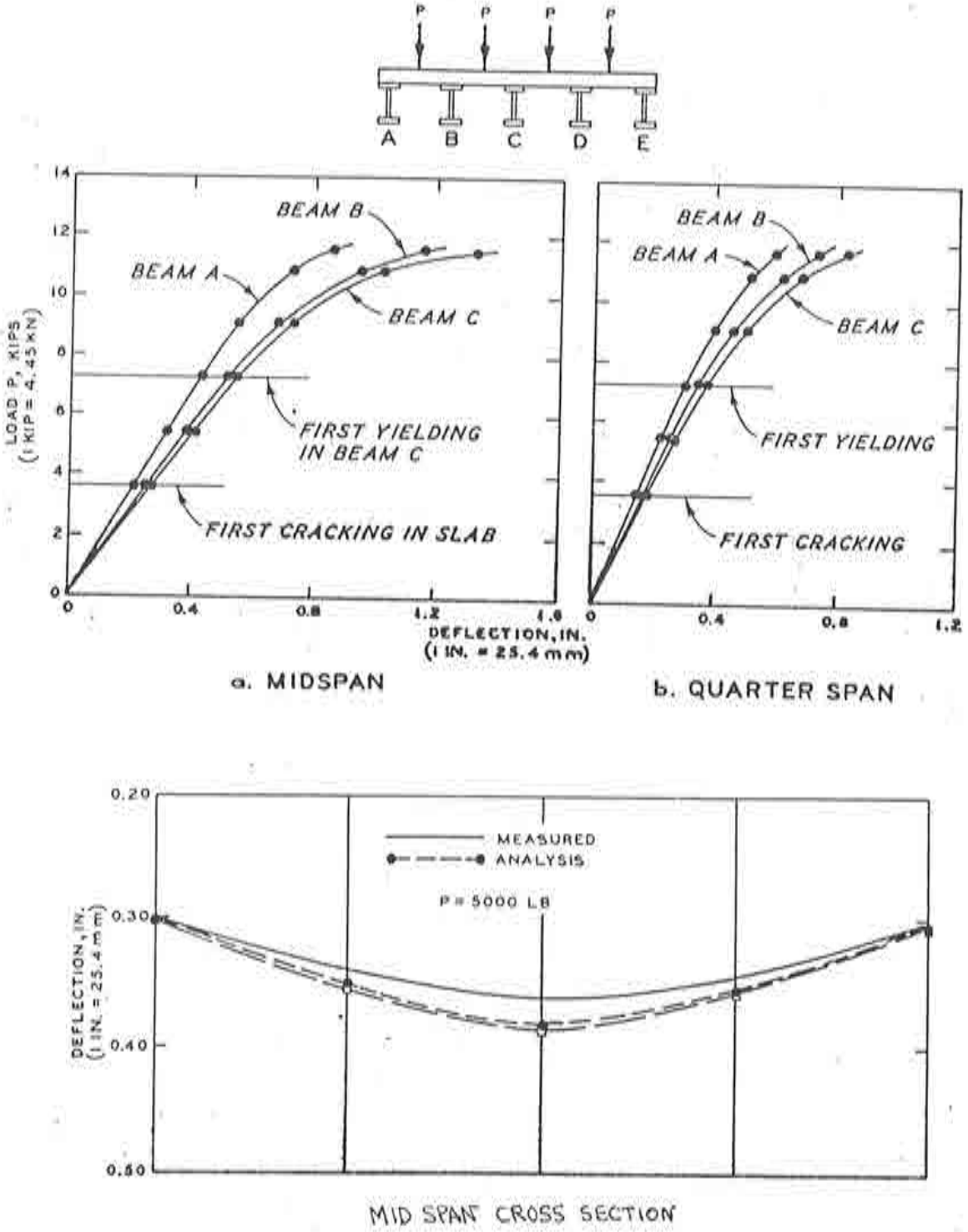

Figure 4.16 Simply supported mixed steel-concrete bridge. Load-deflection and midspan deflection curves for four central load case.

EXAMPLE 5. CYLINDRICAL CONCRETE SHELL WITH EDGE BEAMS

We present next the analysis of two reinforced and prestressed cylindrical shells studied by Roca [9]. The first analysis considers the shell and beam composed of reinforced concrete with geometrical and material properties given in Figure 4.17. The elasto-plastic-brittle model of Lecture 2 has again been used. The loading is the following: *Shell*: normal uniform pressure of 7 KPa. *Edge beams*: normal uniform loading of 1.41 KN/m.

Six degenerate shell elements and six Timoshenko beam elements have been used as shown in Figure 4.18. The load-deflection curve obtained is shown in Figure 4.19.

Figure 4.20 shows the crack distributions in the shell and beam with and without taking into account the effect of prestressing in the beam.

Finally, Figures 4.21 and 4.22 show results for a similar problem considering now the prestressing of both the shell and edge beams. Further information can be obtained from [9].

EXAMPLE 6. PARABOLIC CYLINDRICAL REINFORCED CONCRETE SHELL

A parabolic cylindrical reinforced concrete shell with variable thickness, subjected to uniformly distributed pressure, which was tested by Hedgren [12], was analysed by Owen and Figueiras [13] using degenerate layered shell elements and the elasto–plastic–brittle concrete model described in the first part of Lecture 2. The shell was tested with end support diaphragms and free edges. The shell geometry, finite element mesh, and the zones with different layer patterns are shown in Figure 4.23a. Thirty six degenerate shell elements are used to model one quarter of the shell, each of which is divided into 8 equal concrete layers.

The boundary conditions assumed to represent the effects of the end support diaphragms are free displacements in the x-direction and free rotations normal to the shell plane. The steel and concrete properties and the reinforcement characteristics for each layer pattern can be found in [13]. In Figure 4.23b the experimental load-vertical deflection curve at midspan of the free edge is compared with the present results using a linear and a nonlinear geometrical model. Geometric nonlinear analysis has an important effect in this shell problem as noted by Hedgren [12]. An increase of the shell stiffness and its load carrying capacity, due to the vertical uplift of the shell crown and the downward displacement of the free edges, is observed. An increase of the lever arm of the internal forces is consequently obtained, when the deformed geometry is taken into account.

The vertical deflections of the transverse section at midspan of the shell are presented in Figure 4.24 for load factors of 0.8 and 2.4. In all cases

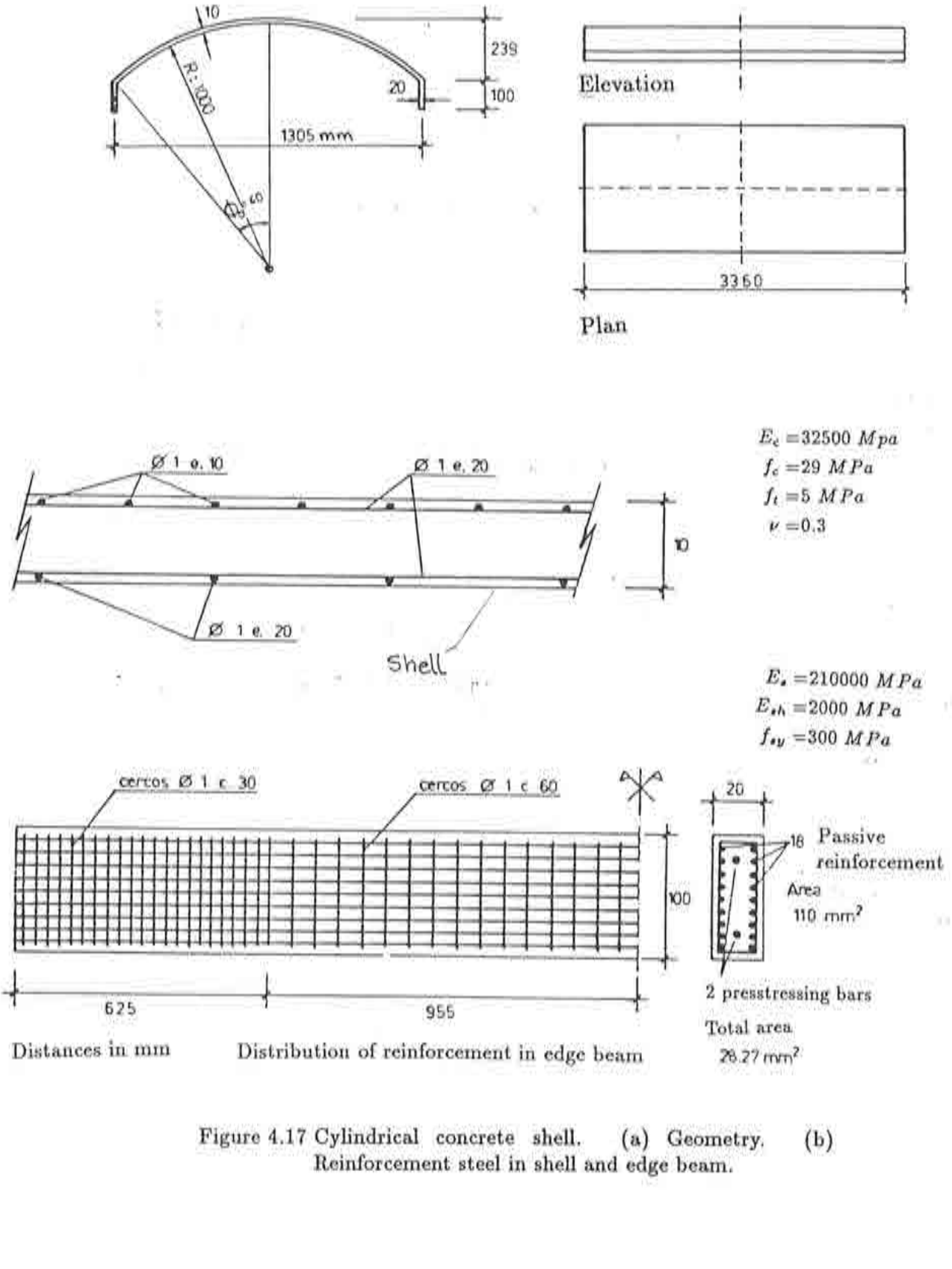

Figure 4.17 Cylindrical concrete shell. (a) Geometry. (b) Reinforcement steel in shell and edge beam.

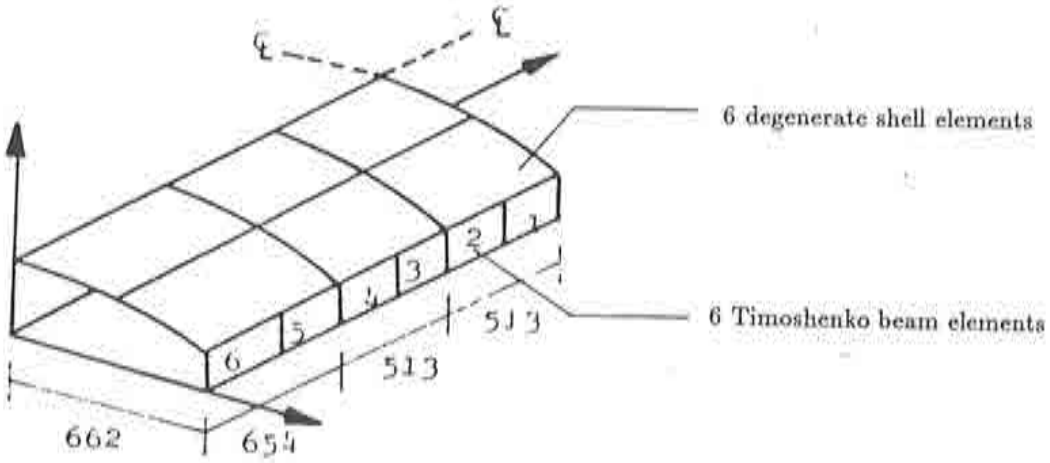

Figure 4.18 Cylindrical concrete shell. Finite element mesh of shell and edge beam elements.

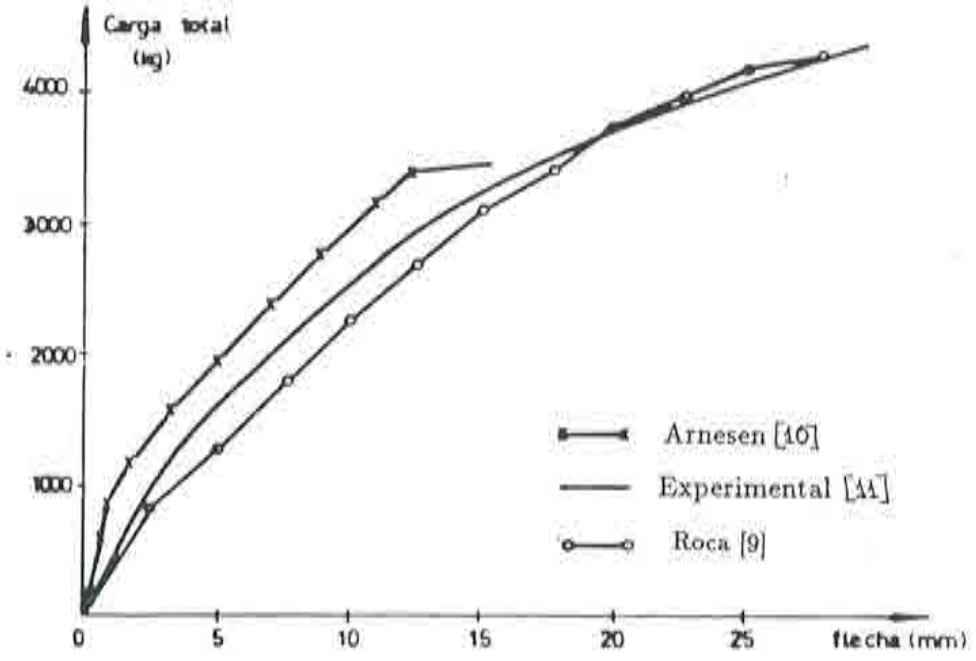

Figure 4.19 Cylindrical concrete shell. Load-displacement curve.

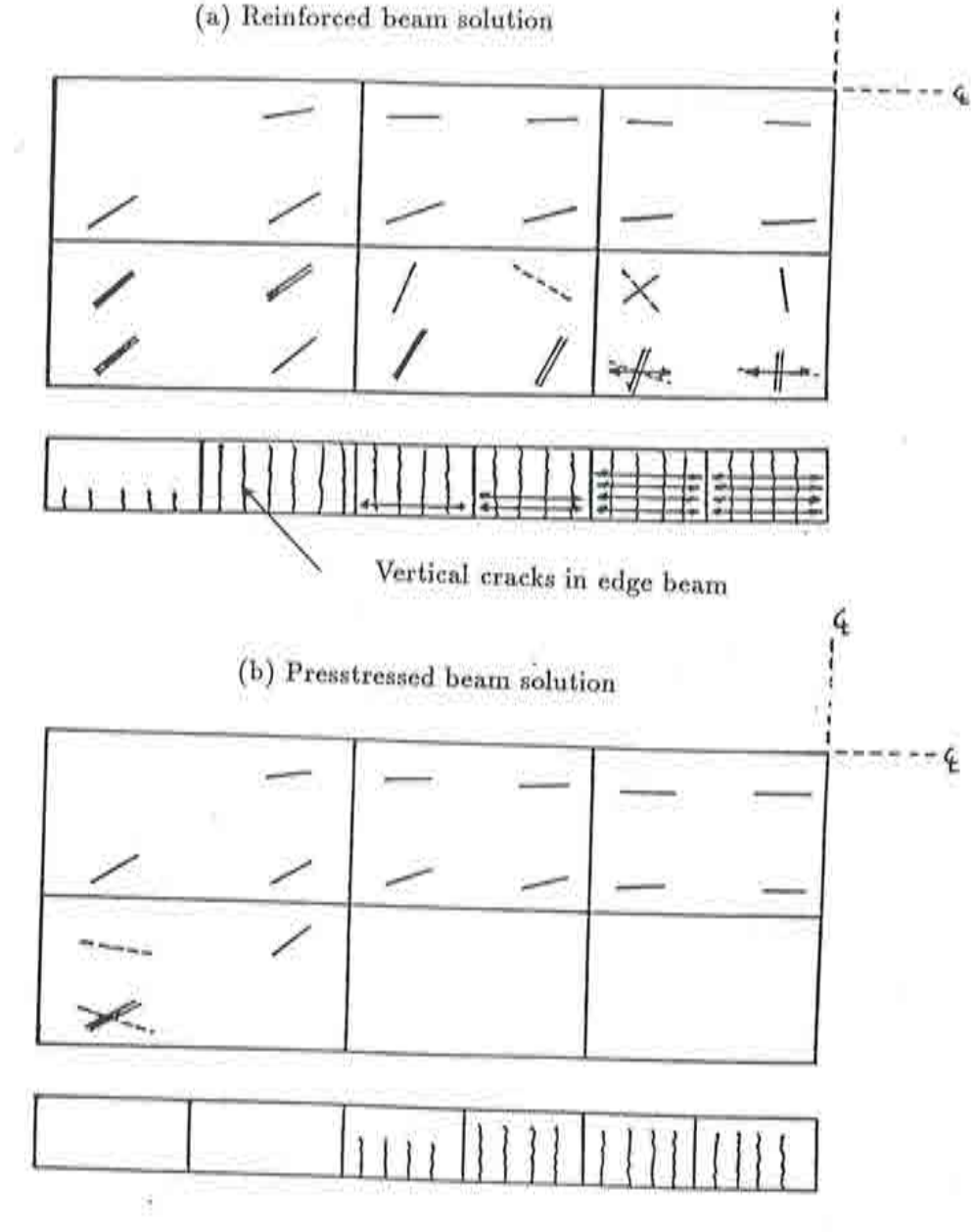

Figure 4.20 Cylindrical concrete shell. Crack patterns for reinforced steel and prestressing solutions.

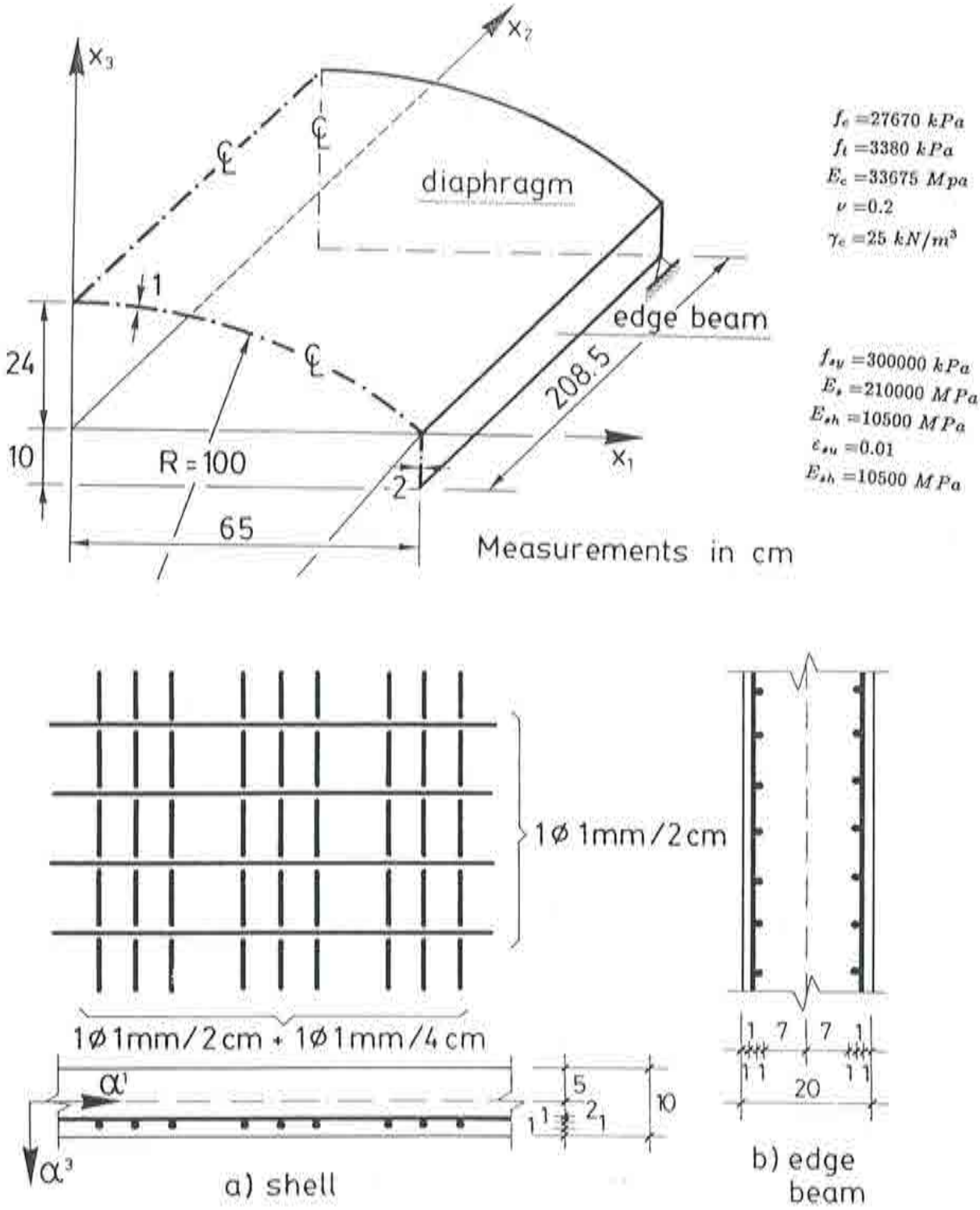

Figure 4.21 Cylindrical prestressed concrete shell. Geometry and reinforcement distribution.

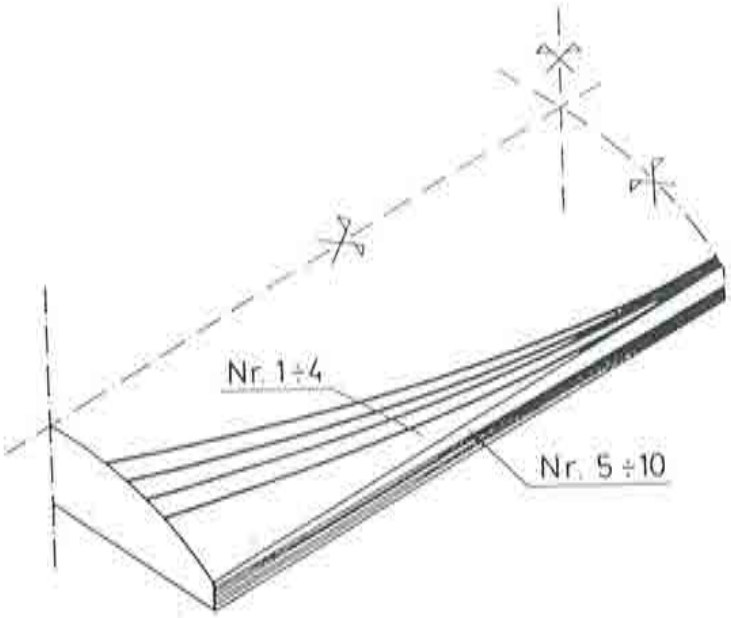

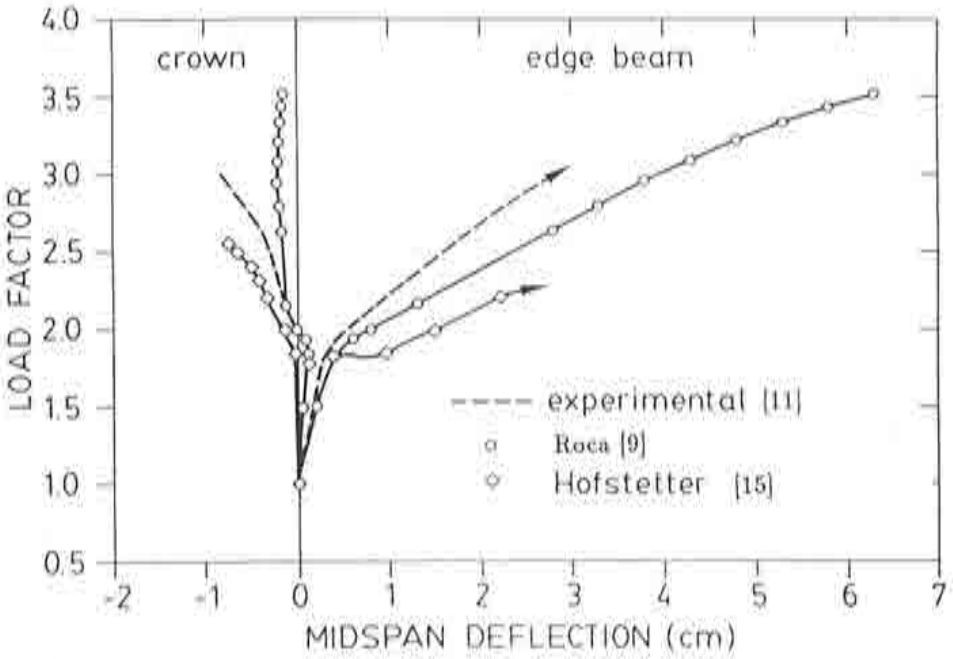

Figure 4.22 Cylindrical prestressed concrete shell. (a) Prestressing distribution. (b) Load-displacement curve.

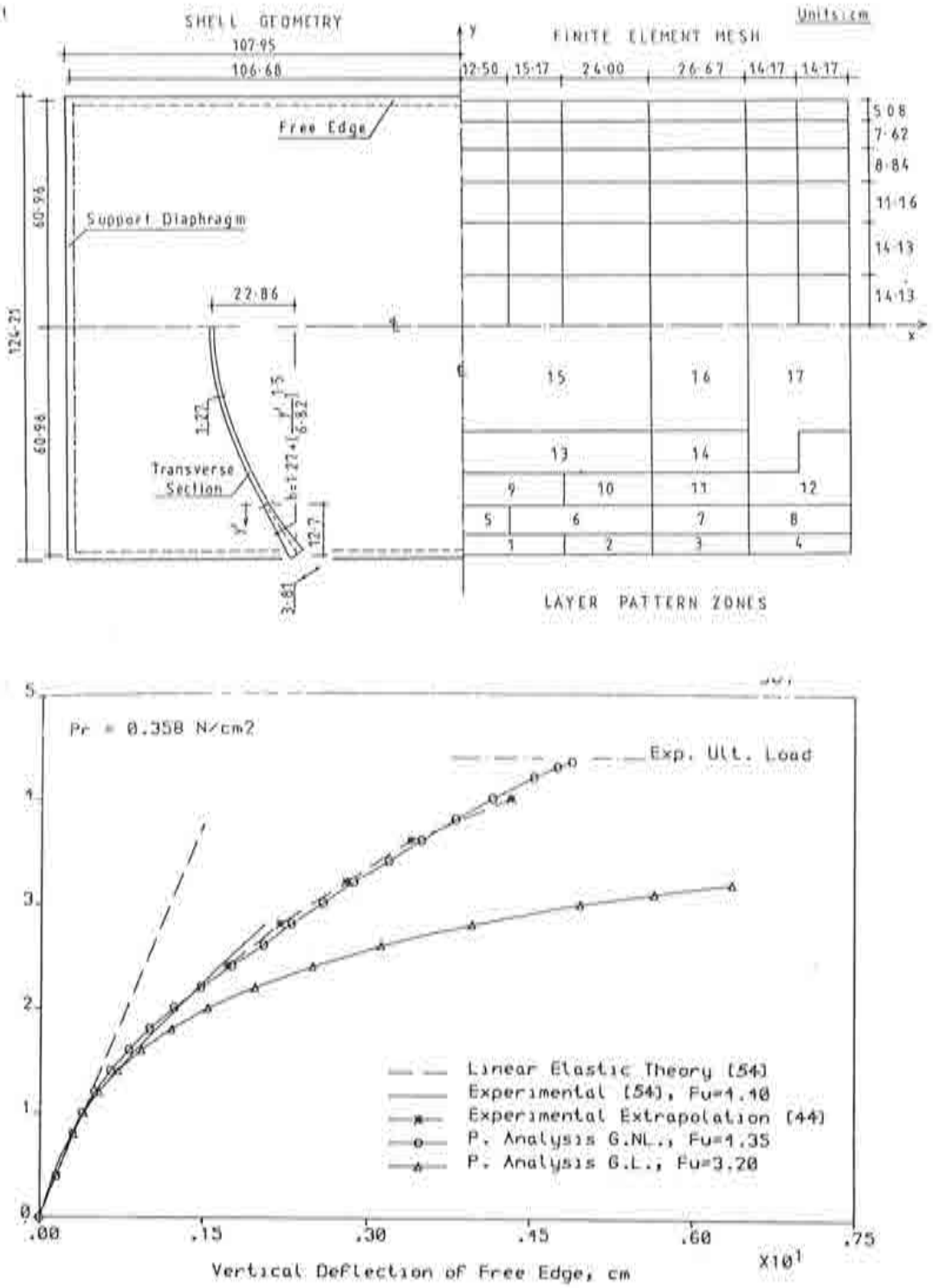

Figure 4.23 Parabolic cylindrical reinforced concrete shell. (a) Geometry. (b) Load-displacement curve.

the numerical and experimental results are seen to be in good agreement provided that geometric nonlinear effects are included in the computations.

The plastic strains in the circumferential reinforcement are represented as contour plots in Figure 4.25 for a load level, $F = 4.35$, which is close to ultimate load. Positive values correspond to the top layer and negative values refer to the bottom circumferential layer. The negative yield line (positive plastic strains) is completely formed, whereas the two positive yield lines are not yet completely developed along the edges.

EXAMPLE 7. CYLINDRICAL CRYOGENIC REINFORCED CONCRETE TANK

The last example is the analysis of a cylindrical cryogenic reinforced concrete tank with an spherical dome for liquid gas storage [14]. The tank has been assumed to be fully clamped at the base, for simplicity. The geometry of the tank, material properties and the meshes of axisymetric solid and degenerate shell finite elements used for the thermal and structural problems can be seen in Figure 4.26. The tank has been analyzed for two different thermal conditions. The first one corresponds to the case of the tank filled with liquid gas at $-160°C$ (due to the breakage of an internal container). This problem has been studied in two steps. In the first step the non linear structural response of the tank for external loads such as vertical and circumferential presstressing and self weight has been analyzed. Then the non linear thermal structural behaviour for various temperature distributions obtained at different times has been studied. Results for the temperature contours and for radial and circumferential cracking zones in the tank at various times have been plotted in Figure 4.27. It can be seen that the initial external loads give place to very localized cracking zones only. The thermal loads, on the other hand, have an special effect on the amount of cracking in the upper part of the dome. The rest of the tank is not severely altered.

The second thermal condition corresponds to the case of an internal fire in the liquid gas partially filling the tank. Temperature of the air over the gas is assumed from a value of $1300°C$ at the gas surface to a value of $1000°C$ at the top of the dome. The liquid gas is assumed to be at $-160°C$. This is a severe loading condition for which the part of the structure in contact with the fire is almost instantaneously completely colapsed, as it can be seen in the numerical results plotted in Figure 4.28. (Again, external loads have been assumed to act prior to the fire). However, it is noticeable that the part of the structure in contact with the liquid gas, is not severely damaged and the tank can still be considered "safe", with regard to avoiding the spilling of the liquid gas. Further details can be found in [14].

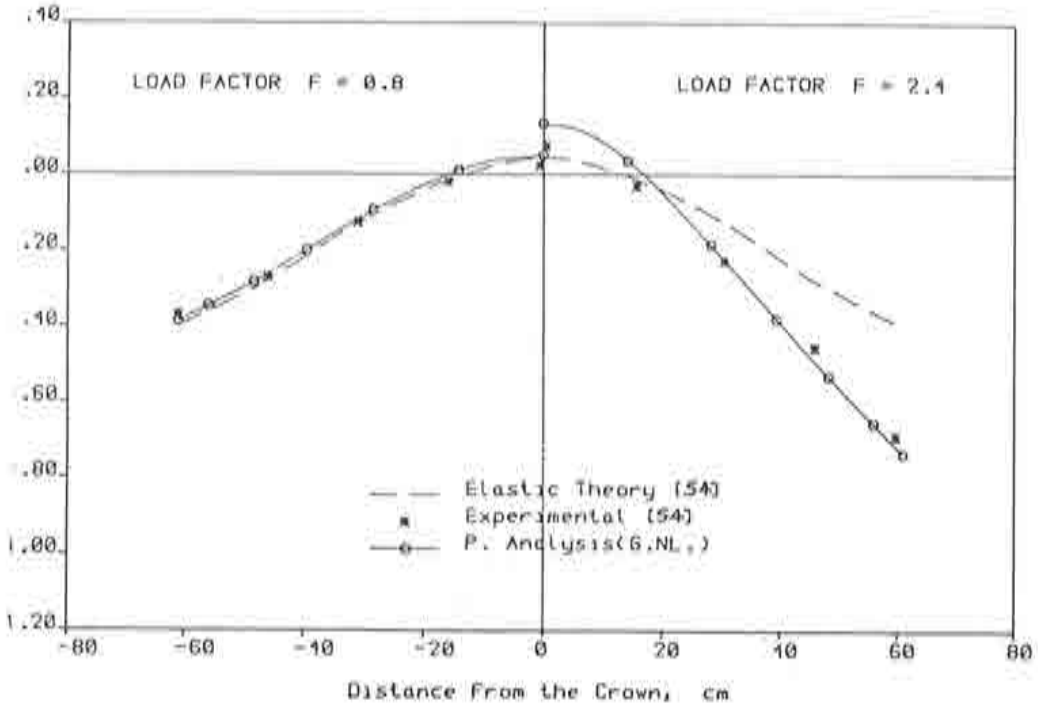

Figure 4.24 Parabolic cylindrical shell. Vertical deflections of the transverse section at mid-span ($x = 0$).

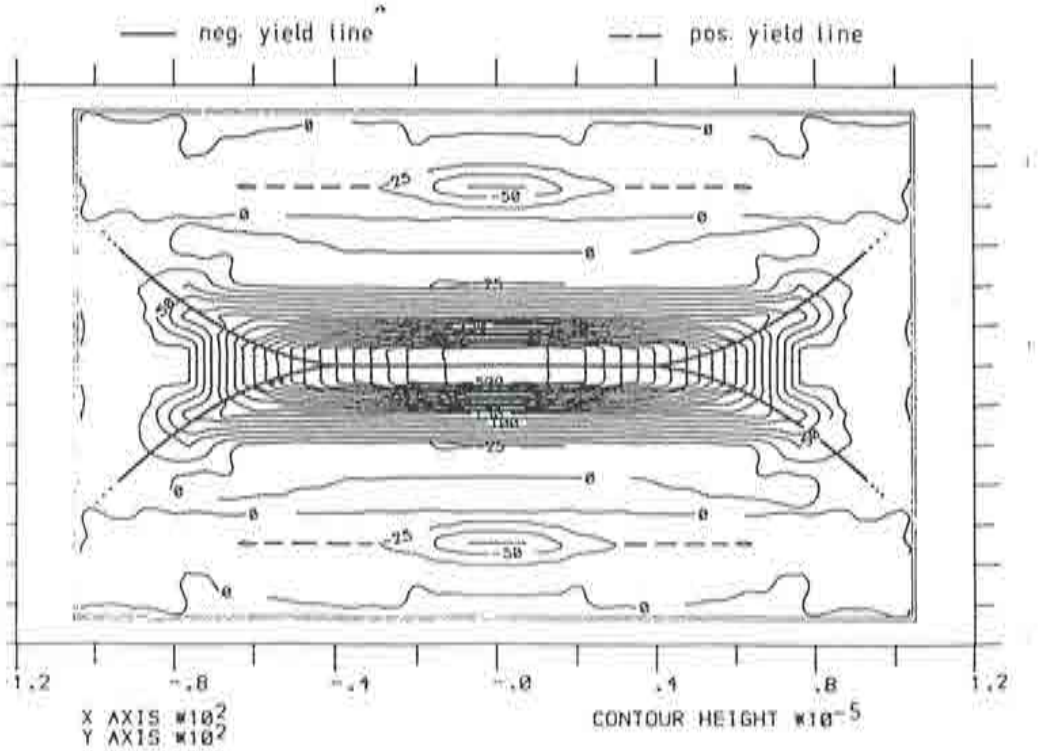

Figure 4.25 Parabolic cylindrical shell. Plastic strains in the circumferential reinforcement at failure.

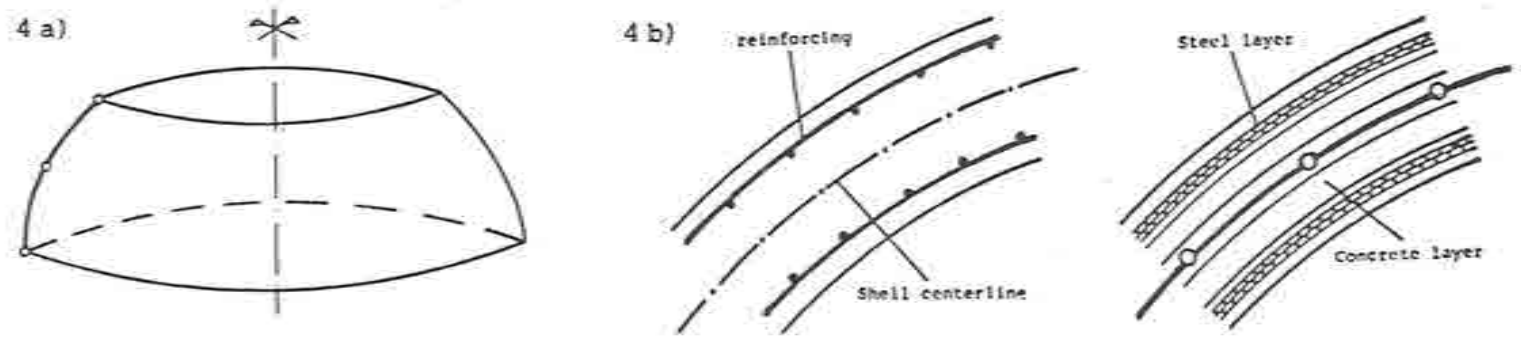

Fig. 4. a) 3 noded curved unidimensional axisymmetric shell element.
b) Layered model for concrete and steel.

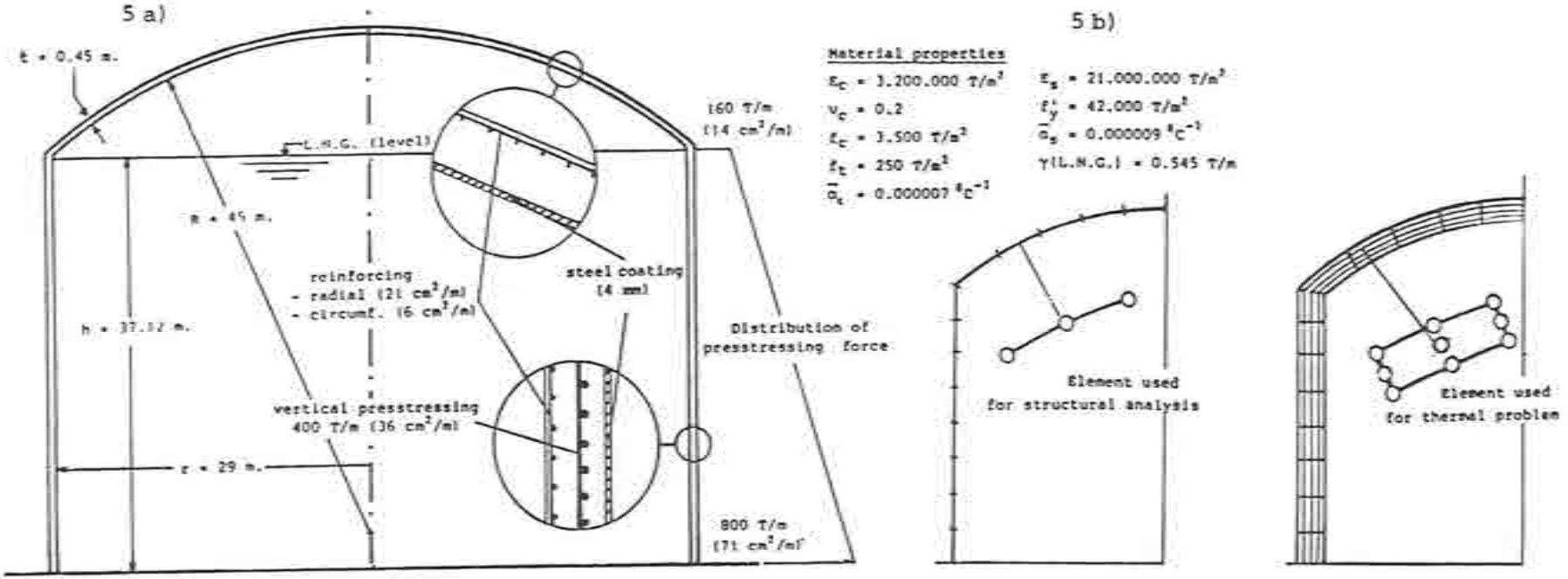

Figure 4.26 Cylindrical cryogenic concrete tank. Geometry, reinforcement distribution and layer discretization.

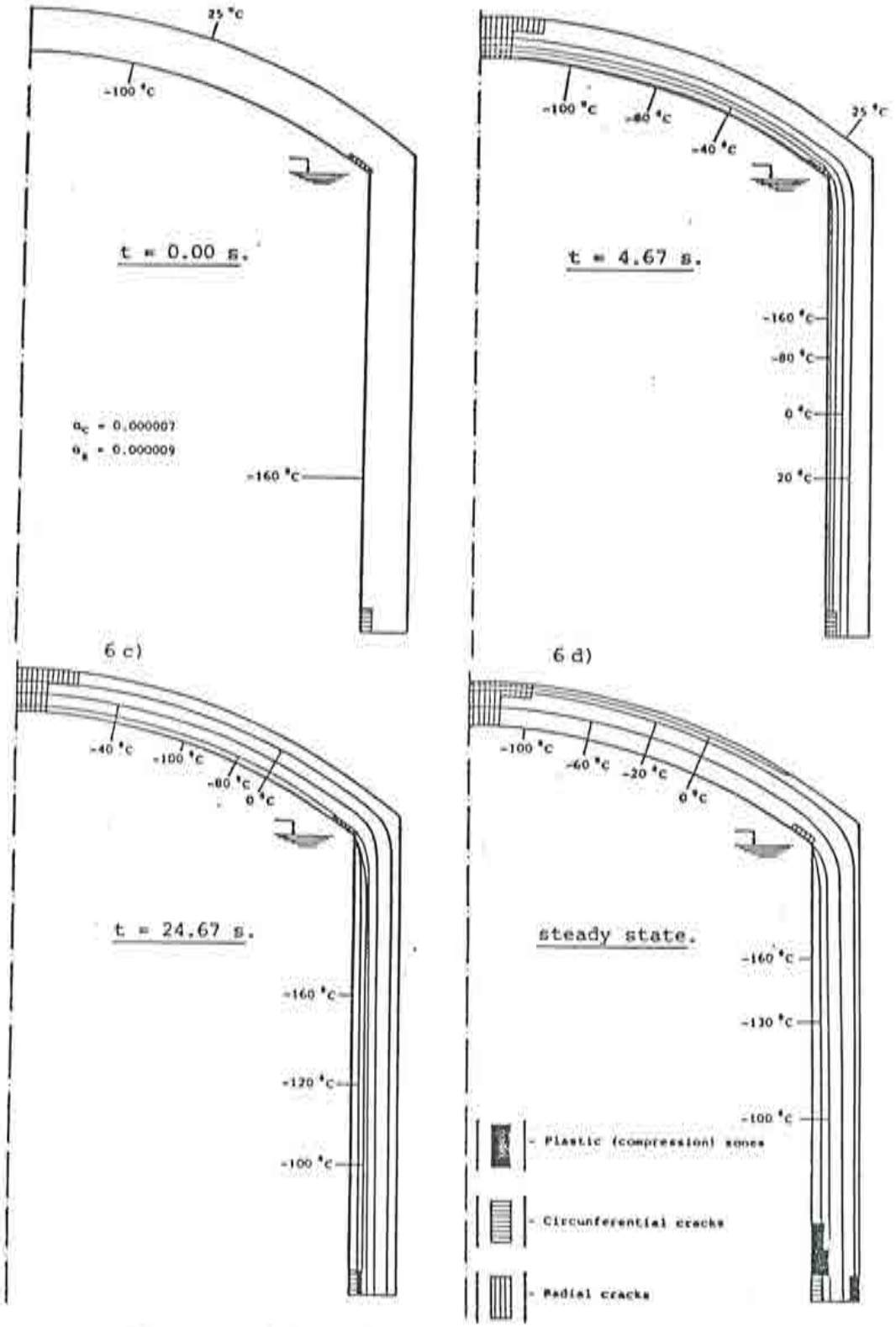

Figure 4.27 Cylindrical cryogenic concrete tank filled with liquid gas at −160°C. Evolution of temperature and cracks for different times.

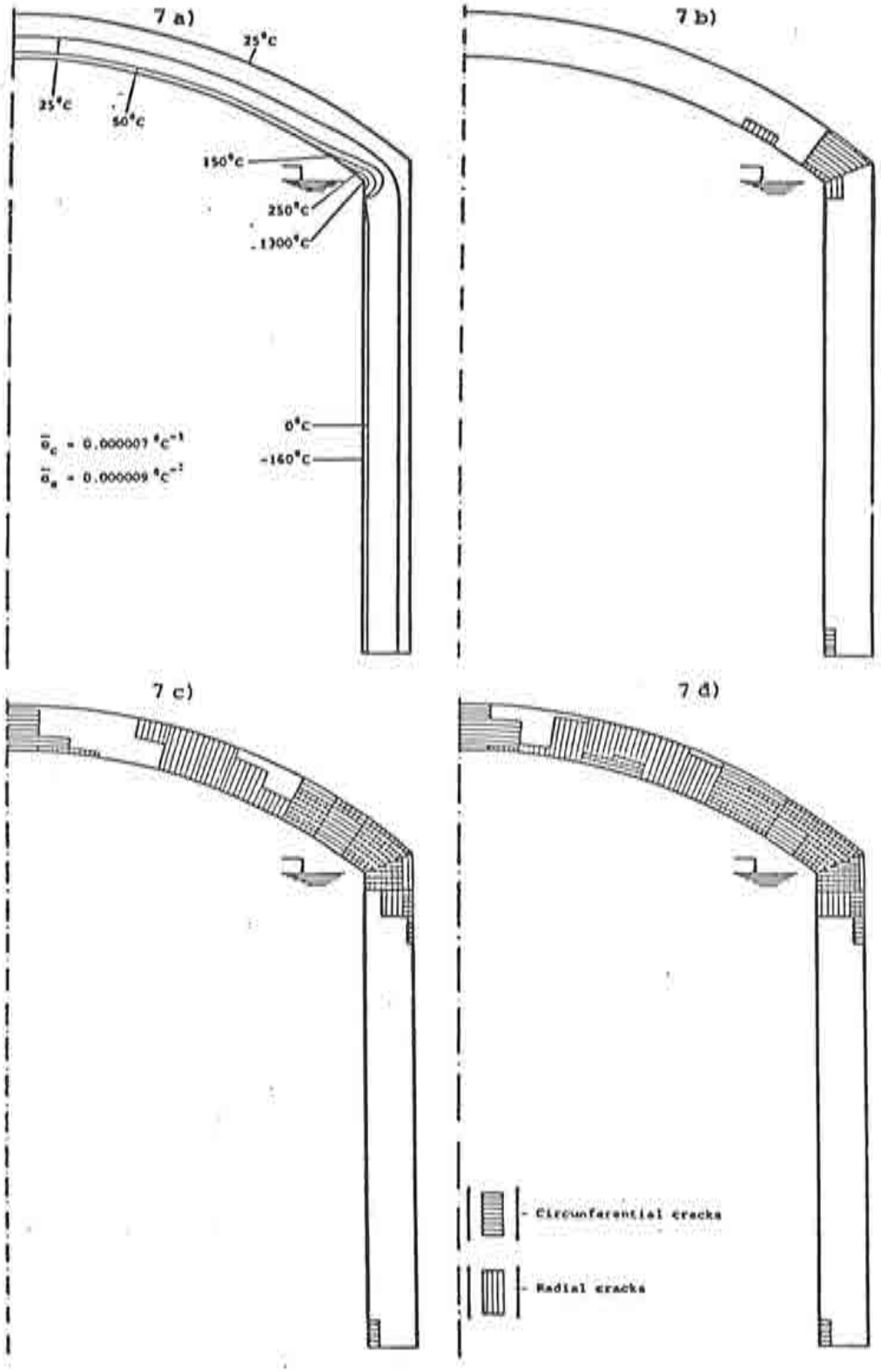

Figure 4.28 Cylindrical cryogenic concrete tank. Crack pattarn for internal fire of liquid gas.

REFERENCES

1. O.C. Zienkiewicz, and R.L. Taylor, "*The Finite Element Method*", Fourth Edtion, Mc.Graw Hill, Vol. I (1989), Vol II (1991).
2. J.G. Rots, P. Nauta, G. Kusters and J. Blaauwendraad, "Smeared crack approach and fracture localization in concrete", Heron, Univ. Delft, The Netherlands, Vol. **30**, 1985.
3. M. Arrea and A.R. Ingraffea, "Mixed mode crack propagation in mortar and concrete", *Cornell Univ., Dept. Struct. Engng Report 81-13*, Ithaka, New York, 1981.
4. M.A. Crisfeld, "A fast incremental iterative solution procedure that handles snap-through", *Comp. and Struct.*, Vol. **13**, pp. 55-62, 1981.
5. S. Oller, E. Oñate y J. Oliver, "Un modelo de fisuración del hormigón basado en la teoría incremental de la plasticidad", *II Simposium sobre Aplicaciones del Método de los Elementos Finitos en Ingeniería*, Universidad Politécnica de Cataluña, June 1986.
6. J. Lubliner, J. Oliver, S. Oller and E. Oñate, "A plastic damage model for concrete", *Int. J. Solids Structures*, Vol. **25**, 3, pp. 299-36, 1989.
7. S. Oller, E. Oñate, J. Oliver and J. Lubliner, "Finite element non linear anaylisis of concrete structures using a plastic damage model", *Engineering Fracture Mechanics*, Vol. **35**, pp. 219-31, 1990.
8. A. W. Wegmuller, "Overload behaviour of composite steel-concrete highway girder bridges", School of Engineering, University of Alabama, Birmingham, October 1986.
9. P. Roca, "Un modelo de análisis no lineal para el estudio del comportamiento de estructuras laminares de hormigón pretensado", *Ph. D. Thesis*, Universidad Politécnica de Cataluña, September 1988.
10. A. Arnesen, "Analysis of reinforced shells considering material and geometric non linearities", Report No. 79-1, *Division Struct. Mech.*, University Trandheim, Norway, July 1979.
11. A.L. Bouma, A.C. Van Riel, H. Van Koten and W.J. Beramek, "Investigations on models of eleven cylindrical shells mode on reinforced and prestressed concrete", *Proc. Symposium on Shell Research*, Delft, North Holland Pub. Co., 79-101, 1961.
12. A.W. Hedgren and D.P. Billington, "Motor model test on a cylindrical shell of varying curvature and thickness", *ACI Journal*, February, 1967.
13. D.R.J. Owen and J.A. Figueiras, "Ultimate load analysis of reinforced concrete plates and shells including geometric non linear effects" in *Finite Element Software for Plates and Shells*, Eds. and E. Hinton and D.R.J. Owen (Eds.). Pineridge Press, 1984.
14. E. Oñate, J. Oliver, R. Chueca, J. Peraire and R. Albareda, "Non linear finite element analysis of cryogenic concrete tanks under thermal actions", *II Int. Conf. on Cryogenic Concrete*, Amsterdam, 1983.
15. Hofstetter, G., "Physikalisch und geometrisch nitchlineare Traglastanalysen von Spannbetonscheiben, -Platten, und - Schalen mittels der Methode der Finiten Elemente", **Technischen Universität Wien, Fakultät für Bauingenieurwesen**, Marzo, 1987.